830-H-15

NAS1.60:1396

MAR 1979

NASA
Technical Paper 1396

AVRADCOM
Technical Report 79-11

COMPLETED
ORIGINAL

Experimental Investigation of Three Helicopter Rotor Airfoils Designed Analytically

Gene J. Bingham and Kevin W. Noonan

APRIL 1979

NASA

U.S. ARMY AVRADCOM

95

NASA
Technical Paper 1396

AVRADCOM
Technical Report 79-11

Experimental Investigation of Three Helicopter Rotor Airfoils Designed Analytically

Gene J. Bingham and Kevin W. Noonan
Structures Laboratory, AVRADCOM Research and Technology Laboratories
Langley Research Center
Hampton, Virginia

National Aeronautics
and Space Administration

**Scientific and Technical
Information Office**

1979

SUMMARY

Three helicopter rotor airfoils designed analytically have been investigated in a wind tunnel at Mach numbers from about 0.30 to 0.90 and Reynolds numbers from about 0.8 to 2.3 × 10^6. The airfoils had thickness-to-chord ratios of 0.08, 0.10, and 0.12 with maximum thickness at 40 percent chord. The camber distribution of each section was the same with maximum camber at 35 percent chord. The 10-percent-thick airfoil was also investigated at Reynolds numbers from 4.8 to 9.4 × 10^6.

The drag divergence Mach number of the 10-percent-thick airfoil is about 0.83 at a normal-force coefficient of 0 and about 0.72 at a normal-force coefficient of 0.6 at Reynolds numbers near 9 × 10^6. The maximum normal-force coefficient is slightly less than that of the NACA 0012 airfoil tested in the same facility. At the lower Reynolds numbers, the drag divergence Mach number for separation free flow showed the usual increases with decreases in thickness-to-chord ratio, and the usual increases in maximum normal-force coefficient with increases in thickness-to-chord ratio.

The results indicate that a qualitative evaluation of the drag divergence can be made at normal-force coefficients up to the onset of boundary-layer separation by analytically predicting the onset of sonic flow at the airfoil crest. The qualitative results are conservative with respect to experimental values with the experimental drag divergence Mach number up to 0.05 higher than that indicated by analysis. The differences between experiment and analysis can be related primarily to the definition of drag divergence applied. At present, the available aerodynamic computing tools do not permit accurate prediction of pressure distributions in cases where boundary-layer separation exists; therefore, a valid comparison between experiment and analysis cannot be made for these conditions.

INTRODUCTION

An analytical technique was used in reference 1 to evaluate airfoils for helicopter rotor application. The analysis permitted assessment of the influences of airfoil geometric variations on the drag divergence Mach number at lift coefficients from near zero to near maximum lift. The analytical results indicated the compromises in drag divergence Mach number which result from changes in (1) thickness ratio, (2) location of maximum thickness, (3) leading-edge radius, (4) camber addition, and (5) location of maximum camber for NACA four- and five-digit-series airfoils and some six-digit-series airfoils of potential interest for helicopters.

In reference 1, three airfoil sections which combined several of the geometric changes favorable to both advancing and retreating section drag divergence were defined. These airfoils were the 08-64C, the 10-64C, and the 12-64C. These sections had thicknesses of 8, 10, and 12 percent chord with the maximum

thickness of each at 40 percent chord; they had the standard NACA four- and five-digit-series airfoil leading-edge radius; and their maximum camber was at 35 percent chord. The 12-percent-thick section indicated a higher drag divergence Mach number than the classic NACA 0012 airfoil at lift coefficients greater than zero. The thinner sections appeared to have even higher drag divergence at lift coefficients below 1.0.

An experimental investigation has been conducted (1) to determine the aerodynamic characteristics of these three airfoils which were not covered by analysis (in particular the maximum normal-force coefficients, the normal-force—drag ratios, and the pitching moment as a function of Mach number), and (2) to evaluate the analytical approach described in reference 1. The three airfoils were tested in the Langley 6- by 19-inch transonic tunnel at Mach numbers from about 0.30 to 0.90. The Reynolds numbers varied from about 0.8 to 2.3×10^6 based on airfoil chord. After these tests, the Langley 6- by 28-inch transonic tunnel became available and the 10-percent-thick airfoil was tested over a similar Mach number range with Reynolds numbers varied from 4.8 to 9.4×10^6. The models were tested smooth and with fixed transition. Normal-force and pitching-moment coefficients were determined from measurements of airfoil-surface static pressures; drag coefficients were determined from measurements of wake total and static pressures.

SYMBOLS

The units used for the physical quantities in this paper are given both in the International System of Units (SI) and in U.S. Customary Units. The measurements and calculations were made in U.S. Customary Units.

b width of tunnel at airfoil location, cm (in.)

c airfoil chord, cm (in.)

c_d section profile-drag coefficient, $\sum_{\text{wake}} c_d' \left(\frac{\Delta h}{c}\right)$

c_d' point-drag coefficient,

$$2\left(\frac{p}{p_\infty}\right)^{6/7}\left[\frac{(p_t/p)^{2/7} - 1}{(p_{t,\infty}/p_\infty)^{2/7} - 1}\right]^{1/2}\left\{\left(\frac{p_t}{p_{t,\infty}}\right)^{1/7} - \left[\frac{(p_t/p_\infty)^{2/7} - 1}{(p_{t,\infty}/p_\infty)^{2/7} - 1}\right]^{1/2}\right\}$$

c_m section pitching-moment coefficient about quarter chord,

$$\sum_{\text{U.S.}} c_p\left(0.25 - \frac{x}{c}\right)\left(\frac{\Delta x}{c}\right) + \sum_{\text{L.S.}} c_p\left(0.25 - \frac{x}{c}\right)\left(\frac{\Delta x}{c}\right)$$

c_n section normal-force coefficient, $\sum_{U.S.} c_p\left(\frac{\Delta x}{c}\right) + \sum_{L.S.} c_p\left(\frac{\Delta x}{c}\right)$

C_p static-pressure coefficient, $\frac{p_l - p_\infty}{q_\infty}$

h height of wake-survey probe tubes from given reference plane, cm (in.)

M Mach number

M_{dd} Mach number for drag divergence

p static pressure, Pa (psi)

q dynamic pressure, $\frac{1}{2}\rho V^2$, Pa (psi)

R Reynolds number based on airfoil chord and free-stream conditions

t airfoil thickness, cm (in.)

V velocity, m/sec (ft/sec)

x airfoil abcissa, cm (in.)

z_c ordinate of airfoil mean line, cm (in.)

α angle of attack, angle between airfoil chord line and airstream direction, deg

α_c angle of attack corrected for lift-interference effects, deg

δ^* wind-tunnel wall boundary-layer displacement thickness measured at airfoil model leading-edge station (model removed from tunnel)

ρ density, kg/m^3 ($slugs/ft^3$)

Subscripts:

l local

t total

∞ free stream

Abbreviations:

U.S. upper surface

L.S. lower surface

APPARATUS AND METHODS

Airfoils

The airfoil profiles (fig. 1) were defined in reference 1 and were designated as the 08-64C, 10-64C, and 12-64C airfoils. The first two digits indicate the thickness-to-chord ratio; in 64C, the 6 indicates use of a standard leading-edge radius for the NACA four- and five-digit-series airfoils (ref. 2), the 4 indicates a maximum thickness location at 40 percent chord, and the C indicates that camber has been added to the thickness distribution. The thickness distribution is that of the NACA airfoil equations of reference 2. The maximum camber (fig. 2) is located at 35 percent chord and was obtained by extrapolating the NACA five-digit-series airfoil camber-line geometry (ref. 3) from the maximum specified value of 25 percent chord. As indicated in reference 1, the amount of camber was limited to provide a maximum pitching moment about the aerodynamic center at low subsonic velocities of no more than -0.02. The airfoil profile design coordinates are presented in tables I to III.

A model of each airfoil shape was machined from a stainless steel block and had a surface finish of 0.813 μm (32 μin.) (root mean square). The models had a 10.16-cm (4.00-in.) chord and a span of 15.24 cm (6.00 in.) with 22 orifices (tables IV to VI) located on each surface in chordwise rows; the rows are positioned 12.5 percent span on either side of the midspan. Slots were milled in the airfoil surface, and tubes were placed in the slots and covered with epoxy. The orifices were then drilled from the opposite sides of the model so there are no surface irregularities near the orifice row. The orifices had diameters of 0.0243 cm (0.0135 in.) and were drilled perpendicular to the local surface. The models were mounted to circular end plates which were flush with the walls.

A second model of the 10-64C airfoil was fabricated for tests at higher Reynolds numbers in the Langley 6- by 28-inch transonic tunnel (ref. 4). This model was identical to the 10-percent-thick model used in the Langley 6- by 19-inch transonic tunnel, except for the addition of mounting tangs which were inserted into the circular end plates; this arrangement permitted tests at the loads corresponding to the higher Reynolds numbers.

Wind Tunnels

Tunnel description.- The Langley 6- by 28-inch transonic tunnel (ref. 4) is a blowdown wind tunnel with a 0.125-open-slotted floor and ceiling and is generally operated at stagnation pressures from about 207 Pa (30 psia) to 620 Pa (90 psia) and at Mach numbers from 0.35 to 0.90. At a stagnation pressure of 620 Pa, the maximum Reynolds number, based on a 10.16-cm (4.00-in.)

chord, varies from 4.8×10^6 at a Mach number of 0.35 to 9.4×10^6 at a Mach number of 0.90. Mach number is controlled by hydraulically actuated choker doors located downstream of the test section. The airfoil model spans the 15.24-cm (6.00-in.) width of the tunnel (fig. 3) and is rigidly attached by mounting tangs to two circular end plates which are driven by a hydraulic actuator to position the airfoil at the desired angle of attack. A test run usually consists of an angle-of-attack sweep at a constant Mach number and Reynolds number.

The Langley 6- by 19-inch transonic tunnel (ref. 5) is also a blowdown wind tunnel with a 0.125-open-slotted floor and ceiling. This tunnel can be operated at Mach numbers from about 0.30 to 0.90, but it does not have independent control of Mach number and stagnation pressure. The Reynolds numbers, based on a 10.16-cm (4.00-in.) chord, range from about 0.9 to 2.2×10^6 at Mach numbers of 0.35 and 0.90, respectively. The airfoil model is rigidly supported by dowel pins in circular end plates which are manually rotated to vary the angle of attack. A test run usually consists of a Mach number sweep at a constant angle of attack. The Mach number control consists of decreasing the tunnel stagnation pressure to bring about a decrease in Mach number.

Two-dimensionality of flow.- The results of an earlier investigation of rotorcraft airfoils in the Langley 6- by 28-inch transonic tunnel (ref. 6) have shown that the indicated maximum normal-force coefficient is reduced by tunnel wall boundary-layer influences. This is characteristic of two-dimensional wind tunnels without proper sidewall boundary-layer control and occurs because the tunnel wall boundary layer is thicker than that of the airfoil; therefore, initial separation begins at the tunnel wall. Efforts are under way to correct this difficulty, but the solution was not available for the investigation described in this report.

Although it is not possible to determine precisely the affected Mach number range or the loss in maximum normal-force coefficient of the airfoils reported herein, a comparison of the NACA 0012 data measured in this facility (ref. 6) with unpublished data from two other facilities has been useful in indicating the magnitude of these losses. The maximum normal-force coefficients measured in the Langley low-turbulence pressure tunnel and the United Technologies Research Center 8 foot tunnel at similar Reynolds numbers and at a Mach number of 0.36 are higher than that from the Langley 6- by 28-inch transonic tunnel by about 0.15. The difference between the data from the Langley 6- by 28-inch transonic tunnel and the United Technologies data decreased to 0.10 at a Mach number of about 0.55. Incremental values for other airfoils may vary slightly due to specific configuration influences.

Reference 6 also reports that the maximum normal-force coefficients from the Langley 6- by 19-inch transonic tunnel are limited by premature separation of the tunnel sidewall boundary layer. The incremental influence of the walls on maximum normal-force coefficient would not necessarily be the same as that of the Langley 6- by 28-inch transonic tunnel because of the difference in Reynolds number and in specific wind-tunnel geometry.

An investigation conducted in the ONERA R1 Ch wind tunnel (ref. 7) has shown that the tunnel sidewall boundary layer can affect the normal-force

coefficients at all angles of attack (that is, with either attached or separated boundary layers). In this investigation, the sidewall boundary-layer thickness was varied by applying sidewall suction upstream of the model while the Mach number and Reynolds number were held constant. Generally, an increase in sidewall boundary-layer thickness resulted in a decrease in the normal-force coefficient at a given angle of attack; the trend reversed at Mach numbers greater than 0.85 with a supercritical airfoil. At a Mach number of 0.30 and with the ratio of sidewall boundary-layer displacement thickness to tunnel width δ^*/b equal to that measured in the Langley 6- by 28-inch transonic tunnel, the lift-curve slope in the ONERA facility was about 3 percent less than that for zero boundary-layer thickness.

Although some progress has been made toward an understanding of the influences of tunnel sidewall boundary layer on airfoil test results, the state of the art does not permit a general correction of two-dimensional wind-tunnel data to account for these influences. Because of this, test results in this report are compared (as appropriate) to those for the NACA 0012 airfoil tested in the same wind tunnel (ref. 6) at comparable Reynolds numbers.

Apparatus

Wake-survey probe.- A traversing wake-survey probe is cantilevered from one tunnel sidewall to measure the profile drag of the airfoils. The probe vertical sweep rate, which was selected after experimental determination of acceptable lag time in the pressure measurements, was about 2.54 cm/sec (1.00 in/sec).

The probe used in the Langley 6- by 28-inch transonic tunnel (fig. 3) was located 2.75 chords (based on the 10.16-cm (4.00-in.) chord model) downstream of the airfoil trailing edge. Data are acquired with four total pressure tubes which are made of stainless steel tubing with a 1.53-mm outside diameter, a 1.02-mm inside diameter (0.060 in. by 0.040 in.), and lateral spacing. (See fig. 4.)

The probe used in the Langley 6- by 19-inch transonic tunnel was similar to the one used in the Langley 6- by 28-inch transonic tunnel except that it had three total pressure tubes: one located on the tunnel center line, one 0.76 cm (0.259 in.) to the left of the center line, and one 0.64 cm (0.252 in.) to the right of the center line. The tubes were made with a 1.27-mm outside diameter and a 1.02-mm inside diameter (0.050 in. and 0.040 in.) stainless steel tubing. The probe was located 1.77 chords (based on 10.16-cm (4.00-in.) chord model) downstream of the airfoil trailing edge.

Instrumentation.- All measurements made during the test program carried out in the Langley 6- by 28-inch transonic tunnel were obtained with the use of a high-speed, computer-controlled digital data acquisition system and were recorded by a high-speed tape recording unit (ref. 4). All free-stream conditions were determined from stagnation and static pressures. All airfoil surface pressures and all wake pressures were measured with precision capacitive potentiometer pressure transducers. The electrical outputs from each of these transducers were connected to individual autoranging signal conditioners which

have seven available ranges. The output signals from the four signal conditioners measuring the wake pressures were filtered with 20-Hz low-pass filters before input to the data acquisition system; the range of frequencies to be passed was experimentally determined during a previous investigation. The geometric angle of attack was determined from the output of a digital shaft encoder attached to a pinion engaging a rack on one model support end plate.

All measurements made during the Langley 6- by 19-inch transonic tunnel investigation were obtained with a "hard-wired" digital data acquisition system (ref. 5) and were recorded on a magnetic tape unit. Transducers with fixed ranges were used to measure the two basic tunnel pressures, all airfoil surface pressures, and wake pressures. The output signals from the three transducers used to measure the wake pressures were filtered with 20-Hz low-pass filters before input to the data acquisition system as a result of a previous experimental determination of acceptable signal rise time. Geometric angle of attack was determined prior to each run with the use of an inclinometer.

Tests and Methods

The tests carried out in the Langley 6- by 28-inch transonic tunnel were made at a constant stagnation pressure at Mach numbers from 0.35 to 0.90. These conditions resulted in Reynolds numbers of 4.8×10^6 and 9.4×10^6 at the lowest and highest test Mach numbers, respectively. Geometric angles of attack ranged from -4.0° to 14.0°, at 2.0° increments at the lower test Mach numbers; this range was decreased at the higher test Mach numbers. The airfoil was tested with both a smooth surface and with a narrow strip of No. 220 carborundum grit applied to the upper and lower surfaces to assure boundary-layer transition. The grit size was determined by the method of reference 8. The 1.2-mm- (0.047-in.-) wide grit strip was centered at the 0.088 chord station; the grit coverage density was about 5 to 10 percent.

The tests in the Langley 6- by 19-inch transonic tunnel were made for Mach numbers generally ranging from about 0.30 to 0.90. As previously noted, the stagnation pressure varied with Mach number so that the Reynolds numbers ranged from about 2.3 to 0.8×10^6 at the highest and lowest test Mach numbers, respectively. Geometric angles of attack were varied from -2.0° to 14.0°, at 2.0° increments. The range of Mach numbers was decreased with increased angle of attack. At selected angles of attack, test conditions were repeated with a strip of No. 220 carborundum grit applied to the upper and lower surfaces of the models. The 1.2-mm- (0.047-in.-) wide grit strip was centered at the 0.094 chord station for each airfoil and the grit coverage density was about 5 to 10 percent.

Section normal-force and pitching-moment coefficients were calculated from the airfoil surface pressures by a trapezoidal integration of the pressure coefficients. Each of the pressure coefficients represents the average of five measurements obtained in a 1.0-sec interval in the Langley 6- by 28-inch transonic tunnel, and four measurements obtained in a 0.5-sec interval in the Langley 6- by 19-inch transonic tunnel. A form of the equation described in reference 9 was used to calculate the point-drag coefficients from the measured wake pressures, and a trapezoidal integration of the point-drag coefficients

was used to calculate the drag coefficient. The static pressures used in the wake drag calculation were measured with tunnel sidewall orifices located at the same longitudinal tunnel station as the tips of the tubes on the two wake-survey probes. All of the drag coefficients presented in this report for the data from the Langley 6- by 28-inch transonic tunnel represent the mean of the measurements made with four total pressure tubes on the wake-survey probe in one sweep through a wake; in the case of the data from the Langley 6- by 19-inch transonic tunnel they represent the mean of the three measurements made in one sweep through a wake. The corrections for lift interference (ref. 10) which have been applied to the angles of attack are given by the following equations:

$$\alpha_c = \alpha + \Delta\alpha$$

where

$$\Delta\alpha = -c_n(c)(0.2744)$$

for the Langley 6- by 19-inch transonic tunnel,

$$\Delta\alpha = -c_n(c)(0.1876)$$

for the Langley 6- by 28-inch transonic tunnel, and where c is in centimeters, α is in degrees, and the constant is in degrees per centimeter.

PRESENTATION OF RESULTS

The results of this investigation have been reduced to coefficient form and are presented as follows:

Results	Airfoil	Wind tunnel	Figure
c_n plotted against α_c; c_m and c_d plotted against c_n	10-64C	Langley 6- by 28-inch transonic tunnel	5
c_n plotted against α_c; c_m and c_d plotted against c_n; c_n, c_m, and c_d plotted against M	08-64C 10-64C 12-64C	Langley 6- by 19-inch transonic tunnel	6, 7, 8, 9
$c_{n,max}$ plotted against M	10-64C	Langley 6- by 28-inch transonic tunnel	10
	08-64C 10-64C 12-64C	Langley 6- by 19-inch transonic tunnel	11

Results	Airfoil	Wind tunnel	Figure
$(c_n/c_d)_{max}$ plotted against M	10-64C	Langley 6- by 28-inch transonic tunnel	12
	08-64C 10-64C 12-64C	Langley 6- by 19-inch transonic tunnel	13
c_n plotted against M_{dd}	10-64C	Langley 6- by 28-inch transonic tunnel	14
	08-64C 10-64C 12-64C	Langley 6- by 19-inch transonic tunnel	15
C_p plotted against x/c	10-64C	Langley 6- by 28-inch transonic tunnel	16
	08-64C 10-64C 12-64C	Langley 6- by 19-inch transonic tunnel	17, 18, 19

DISCUSSION OF RESULTS

Normal Force

The maximum normal-force coefficients of the 10-64C airfoil at flight Reynolds numbers are indicated by the normal-force coefficient curves of figure 5(a) and are summarized in figure 10. Results are presented as a function of Mach number with smooth surfaces and with fixed transition along with data for the NACA 0012 airfoil measured in the same facility (ref. 6). With smooth surfaces, the indicated $c_{n,max}$ varied from about 1.08 to 0.89 at Mach numbers from 0.35 to 0.54 and was slightly less than that of the NACA 0012 airfoil. Apparently the larger leading-edge radius and thickness of the NACA 0012 airfoil had a more favorable influence on $c_{n,max}$ than did the camber of the other airfoil.

The $c_{n,max}$ values of the 10-64C airfoil at Mach numbers above 0.54 are not defined by the data of figure 5(a), but the shape of the curves suggests that the highest c_n measured is about equal to $c_{n,max}$ for Mach numbers to 0.68. That is, the slopes of the curves approach zero at the highest measured normal-force coefficients. Accordingly, the $c_{n,max}$ appears to decrease to about 0.85 as the Mach number is increased from 0.54 to 0.68.

The addition of roughness strips at 8.8 percent chord had a small influence at $c_{n,max}$ with the largest difference observed at $M = 0.34$; at $M = 0.34$ the decrease due to roughness was about 0.05. Apparently, the primary influence of the roughness at $c_{n,max}$ is to thicken the upper surface boundary layer slightly. Based on an analysis of the pressure distributions in figure 16, boundary-layer transitions on the upper surface would be expected to occur forward of the roughness at $c_{n,max}$ for Mach numbers equal to or less than 0.64; that is, transition would be expected near the minimum pressure point which does occur forward of 8.8 percent chord.

An analysis of the static-pressure distributions of the 10-64C airfoil in figure 16(a) indicates that stall results from trailing-edge separation which exists at $c_{n,max}$ at all Mach numbers of the investigation. The trailing-edge separation is indicated by the more negative pressures at the trailing edge of the airfoil. These negative pressures are caused by increasing α_c from 10.3° to 12.0° at $M = 0.35$. The static-pressure coefficient at 0.0107c also became more negative; a more positive coefficient would be expected if the separation extended to the leading-edge region.

The static-pressure distributions (fig. 16) also indicate that supercritical flow exists at $c_{n,max}$ for all Mach numbers of the investigation. Therefore, the observed decrease in $c_{n,max}$ with increased Mach number can be attributed to shock waves in the supercritical flow region which thickens the boundary layer. At Mach numbers of 0.43 and below, there is supersonic flow at 0.0107c and 0.0237c, but not as far aft as 0.049c where the third upper surface orifice is located. Because only two orifices indicated supersonic flow at these Mach numbers, it is not possible to identify the maximum local Mach number attained or the precise location of the terminal shock wave. The measured pressure coefficients do suggest local Mach numbers as great as 1.80 when boundary-layer separation is first implied by near uniform static-pressure measurements in the upper surface trailing-edge region (for example, $M = 0.40$ and $\alpha_c = 10.3^\circ$).

As the Mach number is increased to about 0.49 and above, the upper surface leading-edge supercritical flow region at angles of attack near $c_{n,max}$ extends farther aft to alter the general shape of the pressure-distribution curves (figs. 16(d) to 16(l)). For example, at a Mach number of about 0.53 ($\alpha_c = 10.7^\circ$), the minimum measured pressure is indicated at 0.0237c instead of at 0.0107c; then, at Mach numbers of 0.63 and 0.68, the minimum is at 0.0490c. At Mach numbers ranging from 0.49 to 0.69, the maximum local Mach number corresponding to the first implied boundary-layer separation (airfoil trailing edge) is near 1.50 to 1.60. These results suggest that a lower local Mach number can be sustained in the lower local curvature region at the leading edge. That is, as the terminal shock is shifted aft to where the curvature is decreased, the shock strength (or local Mach number) corresponding to subsequent trailing-edge separation is decreased. These results reflect the advantage of airfoils with leading-edge pressure peaks (at subcritical conditions) observed earlier in references 11 and 12.

A comparison of the $c_{n,max}$ data of figure 10 with data obtained at lower Reynolds numbers with the 10-64C airfoil (figs. 6(a) and 11) shows the usual trend of reduction in $c_{n,max}$ with decreasing Reynolds number. Of perhaps

greater significance is the reduction in maximum local Mach number corresponding to $c_{n,max}$. An analysis of the minimum pressure coefficients at $c_{n,max}$ shown in figure 18 suggests that the maximum measured local Mach number is about 1.20 at $c_{n,max}$ for each free-stream Mach number between 0.34 and 0.54. The specific maximum Mach number cannot be defined; however, it can be concluded that the strength of the shock wave terminating the supercritical flow region at the onset of trailing-edge separation is significantly decreased at the lower Reynolds numbers. This decrease would be expected because of the increase in boundary-layer thickness with decreases in Reynolds number.

At free-stream Mach numbers of 0.59 and 0.64, data were not measured at the precise angles of attack for $c_{n,max}$. However, local Mach numbers to about 1.50 can be determined for the pressure measurements near $c_{n,max}$ from figures 18(e) and 18(f). This value is equal to that previously discussed at the near flight Reynolds numbers. The reasons for this result are not apparent.

The comparison of $c_{n,max}$ data at the lower Reynolds numbers for the 8-, 10-, and 12-percent-thick sections presented in figure 6(a) is summarized in figure 11. The figure 6(a) data were obtained by cross plots of figures 7(a), 8(a), and 9(a) at the same Mach numbers as those of figure 5. Figure 6(a) shows that at Mach numbers below about 0.64, the $c_{n,max}$ increases with increases in thickness. An analysis of the pressure distributions at midrange angles of attack shows that the leading-edge minimum pressure coefficients become less negative and the midchord minimum pressure coefficients become more negative as the thickness is increased. This characteristic change in pressure distribution (with corresponding decreases in maximum local Mach number) results from the reduction in leading-edge curvature (increased leading-edge radius) with increasing thickness for the family of airfoils and permits higher normal-force coefficients at stall.

The Langley 6- by 19-inch transonic tunnel data indicate that the 12-64C airfoil provides a $c_{n,max}$ as much as 0.05 higher than the $c_{n,max}$ of the 10-64C airfoil (fig. 11). This difference suggests that this 12-percent-thick cambered section would produce a slightly higher $c_{n,max}$ than that for the NACA 0012 airfoil of reference 6. (See fig. 10.) As indicated previously in this report, the maximum normal-force coefficients are believed to be conservative but qualitatively correct.

Pitching Moment

The pitching-moment coefficient at zero normal force (the moment about the aerodynamic center) of the 10-64C airfoil is about -0.015 to -0.020 at subcritical Mach numbers for the near flight Reynolds numbers (fig. 5(b)). At supercritical Mach numbers (about 0.78) the pitching-moment coefficient at zero normal force increased to as much as -0.035, which is more than the desirable absolute level of 0.020 noted by some (ref. 13, for example). Except at a free-stream Mach number of 0.83, the slope of the pitching-moment coefficient curves of figure 5(b) are positive to indicate a forward movement of the center of pressure with increasing positive normal-force coefficients and an aerodynamic center forward of the quarter-chord. The slopes remain near constant until the onset of supercritical flow in the forward upper surface region

(fig. 16). Then, the slopes increase to indicate that the center of pressure moves forward even more rapidly to near the maximum normal-force coefficient. This is caused by the increase in chordwise supercritical flow as shown in figure 16(b) at $\alpha_c = 6.7^\circ$ and 8.4° ($c_n = 0.82$ and 0.94, respectively) for example. The pitching-moment results obtained with the three airfoils tested at the lower Reynolds number (fig. 6(b)) are similar to those at the flight Reynolds numbers. The range of near linear slope for c_m plotted against c_n is increased with increases in thickness due to the corresponding increase in $c_{n,max}$.

Drag Coefficient

The minimum section drag coefficient of the 10-64C airfoil with the smooth surface and near flight Reynolds numbers (fig. 5(c)) is constant at about 0.0065 for subcritical free-stream Mach numbers ($M < 0.78$) and is about equal to that of the NACA 0012 section tested in the same tunnel (ref. 6). Supercritical flow began to develop at a Mach number of about 0.78 (fig. 16(j), $\alpha_c = 0^\circ$), and as indicated in later discussion, drag divergence at near zero normal-force coefficient occurred at a Mach number of about 0.83.

The addition of a fixed transition strip tended to increase the minimum-drag coefficient about 0.0010 at the lower Mach numbers due to earlier transition and/or thickening of the turbulent boundary layer. At free-stream Mach numbers above about 0.64, the roughness had little effect on the minimum-drag coefficient. Apparently, the free-stream turbulence level causes boundary-layer transition on the smooth model to occur at the same location as the transition strip so the addition of roughness had little influence on the drag coefficient. An increase in free-stream turbulence level with increases in Reynolds numbers above 6×10^6 has been indicated by unpublished drag-coefficient data from the Langley 6- by 28-inch transonic tunnel.

At the lower Reynolds numbers (Langley 6- by 19-inch transonic tunnel), the minimum-drag coefficient of the 10-64C airfoil was near 0.0050 at the subcritical Mach numbers (fig. 6(c)), apparently due to more extensive laminar flow. The addition of roughness (fig. 8(c)) eliminated the laminar flow behind the roughness and caused the minimum drag to increase substantially. Similar results were obtained with the 8- and 12-percent-thick airfoils (figs. 7(c) and 9(c)).

The maximum ratios of normal force to drag of the 10-64C airfoil at near full-scale Reynolds numbers as determined from the data of figure 5(c) are presented in figure 12. An evaluation of these results can be made by comparison of NACA 0012 airfoil data obtained with the same facility and test techniques (ref. 6). At Mach numbers from about 0.35 to 0.43, the 10-64C airfoil provides a maximum indicated normal-force—drag ratio of about 101 compared to about 85 to 93 for the NACA 0012 airfoil. An analysis of the pressure distributions has been made (figs. 16(a) to 16(c), and ref. 6) at the respective $(c_n/c_d)_{max}$. It was determined that supercritical flow exists for the 10-64C airfoil at Mach numbers from 0.35 to 0.43; for the NACA 0012 airfoil, supercritical flow exists at a test Mach number of 0.44 but not at 0.35 or 0.40. It appears that the addition of camber has a more significant influence on the c_n/c_d ratio than

does the supercritical flow, so the 10-64C section provides the greater $(c_n/c_d)_{max}$ at these Mach numbers. At Mach numbers of 0.49 and 0.54, this relationship between camber and supercritical flow apparently reverses so the NACA 0012 airfoil provides the higher ratio. At a Mach number of about 0.59 and above, the camber increases the loading in the midchord region (compared to the NACA 0012 airfoil) sufficient to cause the 10-64C airfoil to again provide a greater $(c_n/c_d)_{max}$ than the NACA 0012 airfoil, although the corresponding local Mach numbers are greater for the cambered airfoil. The same trends were observed when transition had been fixed (fig. 12). The curve for the cambered airfoil with fixed transition is not extended beyond $M = 0.6$ because fewer data points were recorded with fixed transition. However, the data of figure 5(c) suggest that the c_n/c_d relationship between the smooth and fixed transition configurations is not significantly changed at Mach numbers above 0.6. At the lower Reynolds numbers, the thicker boundary layer caused a general reduction in $(c_n/c_d)_{max}$ for the 10-64C airfoil at free-stream Mach numbers below about 0.74. (Compare figs. 12 and 13.) The curves intersect at a Mach number of about 0.74; the reasons for this are unknown.

Increasing the thickness-to-chord ratio from 0.08 to 0.10 to 0.12 continuously increases $(c_n/c_d)_{max}$ except at Mach numbers of about 0.74 and 0.80. At a Mach number of about 0.80, the thinner airfoil provides the higher $(c_n/c_d)_{max}$ because the drag divergence Mach number is higher than that for the thicker airfoil.

The drag coefficients of figure 5(c) were cross-plotted as a function of Mach number at constant normal-force coefficients to determine drag divergence (fig. 14). Drag divergence is defined herein as the free-stream Mach number at which $dc_d/dM = 0.1$. Data for the analytically defined curve (ref. 1) for this airfoil are included for comparison. The figure shows that the analytical results are conservative with respect to (1) drag divergence Mach number at a constant c_n or (2) conservative with respect to c_n at a given drag divergence Mach number. The displacement of the analytical and experimental results can be explained as follows. The onset of the drag rise generally occurs immediately after the supercritical flow region moves aft of the airfoil crest; that is, immediately after the crest Mach number reaches 1.0. However, a slightly higher Mach number is required to cause the rate of change in drag with Mach number to equal 0.1; this causes the experimental curves to be shifted accordingly. For example, interpolation of the pressure coefficients for $\alpha_c = 0^\circ$ in figures 16(i) and 16(j) suggests sonic flow at the airfoil crest (definition of drag divergence for analytical approach) at a Mach number of about 0.77. This compares to $M = 0.78$ predicted analytically (fig. 14). The normal-force coefficient corresponding to $\alpha_c = 0^\circ$ is about 0.12 (fig. 5(a)), and, at $c_n = 0.12$, c_d is near constant at Mach numbers up to 0.77. Then c_d increased about 0.0030 between the Mach numbers of 0.77 and 0.83 ($\Delta c_d/\Delta M = 0.050$) to indicate the onset of the drag rise. The cross plot of c_d as a function of Mach number indicated $dc_d/dM = 0.1$ (which defines drag divergence) at $M = 0.83$ and $c_n = 0.12$.

Another factor, which is probably less significant, contributes to the difference in the experimental and analytical normal-force coefficients for drag divergence. The lift coefficient in the analysis is assumed to increase with Mach number according to the Prandtl-Glauert factor. Experimentally, the

increase can be more rapid than predicted because of the supercritical flow. For example, the results at $\alpha_c = 0^\circ$ and $M = 0.74$ to $M = 0.84$ suggest an increase in c_n about 0.03 greater than that predictable by the Prandtl-Glauert factor. This increase causes the experimental data points to be proportionally higher, and increases the differences between analysis and experiment. Data for other airfoils (ref. 11) suggest differences in Prandtl-Glauert extrapolations of low-speed data and experimental lift coefficients as great as 0.10.

The analytical and experimental curves of figure 14 intersect at a c_n of 0.78 and a Mach number of 0.65. Experimental data were not obtained at the precise point. However, the decrease in slope of the normal-force curve (fig. 5(a)) at this normal-force coefficient at $M = 0.64$ suggests separation, and the pressure distribution for $c_n = 0.83$ (fig. 16(g), $\alpha_c = 6.8^\circ$) suggests boundary-layer separation at 95 percent chord. As discussed in more detail in reference 1, the analytical model of the pressure distributions does not account for boundary-layer separation. Therefore, the predicted drag divergence Mach numbers are not valid.

The influence of boundary-layer separation is also shown in figure 15 by the lower Reynolds number data for the 10-64C airfoil. Here the analyses and experimental data curves intersect at a normal-force coefficient of about 0.60, apparently because of earlier boundary-layer separation at the lower Reynolds number. At a constant normal-force coefficient below about 0.6, the comparison between experiment and analysis for increasing drag divergence Mach number with decreases in thickness-to-chord ratios is in substantial agreement. The curves of figure 15 are displaced for the reasons previously discussed. Even with the displacement considered, it can be seen that the relative normal-force—drag-divergence-Mach-number characteristics of the airfoils can be predicted for the boundary-layer separation for free-stream conditions.

CONCLUSIONS

Three helicopter rotor airfoils designed analytically have been investigated in a wind tunnel at Mach numbers from about 0.30 to 0.90, and at Reynolds numbers from about 0.8 to 2.3×10^6. The airfoils had thickness-to-chord ratios of 0.08, 0.10, and 0.12 with maximum thickness at 40 percent chord. The camber distribution of each section was the same with maximum camber at 35 percent chord. The 10-percent-thick airfoil was also investigated at Reynolds numbers from 4.8 to 9.4×10^6. Analysis of the test data has resulted in the following conclusions:

1. The experimental drag divergence Mach number of the 10-64C airfoil is about 0.83 at a normal-force coefficient of 0 and about 0.72 at a normal-force coefficient of 0.6 at Reynolds numbers near 9×10^6.

2. The maximum normal-force coefficient of the 10-64C airfoil is slightly less than that of the NACA 0012 airfoil tested in the same facility at near flight Reynolds numbers.

3. The drag divergence Mach number for separation free flow showed the usual increase with decreases in thickness-to-chord ratio; the usual increase

in maximum normal-force coefficient was observed with increases in thickness-to-chord ratio.

4. A qualitative indication of differences in the drag divergence characteristics of airfoils at selected normal-force coefficients can be made by analytically predicting the onset of sonic flow at the airfoil crest. This approach is valid if the airfoil is free of boundary-layer separation so that the predicted pressure distributions are valid.

5. The analytical predictions of drag divergence are conservative with the experimental drag divergence Mach number up to 0.05 higher than the corresponding analytical value. This difference can be explained on the basis of the definition of drag divergence Mach number applied.

Langley Research Center
National Aeronautics and Space Administration
Hampton, VA 23665
March 2, 1979

REFERENCES

1. Bingham, Gene J.: An Analytical Evaluation of Airfoil Sections for Helicopter Rotor Applications. NASA TN D-7796, 1975.

2. Stack, John; and Von Doenhoff, Albert E.: Tests of 16 Related Airfoils at High Speeds. NACA Rep. 492, 1934.

3. Jacobs, Eastman N.; and Pinkerton, Robert M.: Tests in the Variable-Density Wind Tunnel of Related Airfoils Having the Maximum Camber Unusually Far Forward. NACA Rep. 537, 1935.

4. Ladson, Charles L.: Description and Calibration of the Langley 6- by 28-Inch Transonic Tunnel. NASA TN D-8070, 1975.

5. Ladson, Charles L.: Description and Calibration of the Langley 6- by 19-Inch Transonic Tunnel. NASA TN D-7182, 1973.

6. Noonan, Kevin W.; and Bingham, Gene J.: Two-Dimensional Aerodynamic Characteristics of Several Rotorcraft Airfoils at Mach Numbers From 0.35 to 0.90. NASA TM X-73990, 1977.

7. Bernard-Guelle, René: Influence of Wind Tunnel Wall Boundary Layers on Two-Dimensional Transonic Tests. NASA TT F-17,255, 1976.

8. Braslow, Albert L.; and Knox, Eugene C.: Simplified Method for Determination of Critical Height of Distributed Roughness Particles for Boundary-Layer Transition at Mach Numbers From 0 to 5. NACA TN 4363, 1958.

9. Baals, Donald D.; and Mourhess, Mary J.: Numerical Evaluation of the Wake-Survey Equations for Subsonic Flow Including the Effect of Energy Addition. NACA WR L-5, 1945. (Formerly NACA ARR L5H27.)

10. Davis, Don D., Jr.; and Moore, Dewey: Analytical Study of Blockage- and Lift-Interference Corrections for Slotted Tunnels Obtained by the Substitution of an Equivalent Homogeneous Boundary for the Discrete Slots. NACA RM L53E07b, 1953.

11. Graham, Donald J.; Nitzberg, Gerald E.; and Olson, Robert N.: A Systematic Investigation of Pressure Distributions at High Speeds Over Five Representative NACA Low-Drag and Conventional Airfoil Sections. NACA Rep. 832, 1945.

12. Pearcey, H. H.: The Aerodynamic Design of Section Shapes for Swept Wings. Advances in Aeronautical Sciences, Volume 3, Macmillan Co., c.1962, pp. 277-322.

13. Kemp, Larry D.: An Analytical Study for the Design of Advanced Rotor Airfoils. NASA CR-112297, 1973.

TABLE I.- DESIGN COORDINATES FOR 08-64C AIRFOIL

[Stations and ordinates given in percent airfoil chord]

Stations	Upper surface	Stations	Lower surface
0.000	0.000	0.000	0.000
.034	.700	.034	-.585
1.016	1.245	1.016	-.975
1.152	1.308	1.348	-1.088
2.391	1.830	2.609	-1.424
3.808	2.245	3.808	-1.666
4.891	2.506	5.109	-1.836
5.744	2.689	5.744	-1.912
7.386	2.993	7.614	-2.087
8.010	3.099	8.010	-2.120
9.887	3.383	10.113	-2.263
13.206	3.791	13.206	-2.424
14.904	3.968	15.096	-2.506
19.927	4.387	20.073	-2.672
22.293	4.538	22.293	-2.734
24.952	4.679	25.048	-2.801
28.937	4.838	28.937	-2.881
29.976	4.870	30.024	-2.900
32.348	4.929	32.348	-2.937
35.000	4.971	35.000	-2.971
40.002	4.986	39.980	-3.014
46.380	4.887	46.380	-3.019
50.048	4.776	49.952	-2.994
57.368	4.437	53.656	-2.946
60.058	4.278	59.941	-2.809
64.943	3.947	64.943	-2.642
70.053	3.543	69.947	-2.427
76.516	2.950	76.516	-2.065
80.040	2.590	79.960	-1.842
84.332	2.116	84.332	-1.524
90.022	1.430	89.978	-1.060
92.185	1.153	92.185	-.861
95.011	.778	94.989	-.596
96.105	.629	96.105	-.485
100.000	.080	100.000	-.080

TABLE II.- DESIGN COORDINATES FOR 10-64C AIRFOIL

[Stations and ordinates given in percent airfoil chord]

Stations	Upper surface	Stations	Lower surface
0.000	0.000	0.000	0.000
.355	.910	.355	-.737
1.128	1.611	1.373	-1.391
2.363	2.241	2.637	-1.835
3.836	2.754	3.836	-2.132
4.864	3.053	5.136	-2.383
5.766	3.282	5.766	-2.478
7.357	3.632	7.643	-2.726
8.022	3.759	8.022	-2.769
9.859	4.091	10.141	-2.971
13.226	4.569	13.226	-3.205
14.879	4.779	15.121	-3.317
16.115	4.907	16.115	-3.373
19.908	5.271	20.092	-3.356
22.385	5.448	22.385	-3.648
24.940	5.614	25.060	-3.737
29.970	5.842	30.030	-3.872
32.544	5.909	32.544	-3.925
34.999	5.964	35.001	-3.964
40.024	5.986	39.976	-4.014
46.674	5.860	46.674	-4.004
50.060	5.747	49.940	-3.965
53.964	5.551	53.964	-3.884
60.073	5.164	59.927	-3.695
65.212	4.745	65.212	-3.450
70.066	4.288	69.934	-3.172
76.700	3.556	76.700	-2.676
80.050	3.144	79.950	-2.396
84.428	2.560	84.428	-1.970
90.028	1.742	89.972	-1.372
92.202	1.045	92.202	-1.112
95.014	.949	94.986	-.767
100.000	.100	100.000	-.100

TABLE III.- DESIGN COORDINATES FOR 12-64C AIRFOIL

[Stations and ordinates given in percent airfoil chord]

Stations	Upper surface	Stations	Lower surface
0.000	0.000	0.000	0.000
.340	1.120	.340	-1.485
1.103	1.909	1.397	-1.689
2.336	2.665	2.664	-2.240
3.783	3.272	3.783	-2.591
4.837	3.595	5.163	-2.925
5.691	3.857	5.691	-3.017
7.328	4.266	7.672	-3.360
9.831	4.796	10.169	-3.676
14.855	5.588	15.144	-4.126
19.890	6.152	20.110	-4.438
24.928	6.549	25.072	-4.672
29.964	6.813	30.036	-4.843
34.999	6.957	35.001	-4.957
40.029	6.986	39.971	-5.014
46.821	6.849	46.821	-4.989
50.072	6.717	49.928	-4.936
54.138	6.492	54.138	-4.821
60.087	6.050	59.913	-4.580
65.390	5.555	65.380	-4.256
70.079	5.035	69.921	-3.919
76.819	4.166	76.819	-3.285
80.060	3.697	79.940	-2.950
84.519	2.999	84.519	-2.410
90.033	2.053	89.967	-1.683
95.017	1.121	94.983	-.939
100.000	.120	100.000	-.120

TABLE IV.- STATIC-PRESSURE ORIFICE LOCATIONS FOR 08-64C AIRFOIL

[Locations given in percent airfoil chord]

Upper surface station	Lower surface station
1.23	1.30
2.41	2.47
4.95	5.04
7.47	7.53
9.99	10.05
15.02	15.06
20.03	20.05
25.04	25.05
30.05	30.06
35.06	35.07
40.08	40.07
45.07	45.06
50.09	50.08
55.08	55.09
60.08	60.08
65.09	65.10
70.07	70.10
75.09	75.11
80.11	80.11
85.11	85.11
90.11	90.11
95.07	95.05

TABLE V.- STATIC-PRESSURE ORIFICE LOCATIONS FOR 10-64C AIRFOIL

[Locations given in percent airfoil chord]

Upper surface station	Lower surface station
1.07	1.17
2.37	2.44
4.90	4.95
7.38	7.51
9.94	10.03
14.96	15.09
19.95	20.04
24.97	25.04
30.02	30.09
35.08	35.07
39.99	40.06
44.99	45.05
50.02	50.06
55.02	55.11
59.98	60.06
65.09	65.06
70.02	70.05
75.03	75.10
80.04	80.07
85.03	85.09
90.04	90.10
95.04	95.10

TABLE VI.- STATIC-PRESSURE ORIFICE LOCATIONS FOR 12-64C AIRFOIL

[Locations given in percent airfoil chord]

Upper surface station	Lower surface station
1.23	1.11
2.39	2.41
4.85	4.92
7.41	7.45
9.92	9.95
14.95	14.99
20.00	20.02
25.04	25.02
30.05	30.07
35.07	35.09
40.08	40.10
45.10	45.11
50.13	50.20
55.15	55.15
60.18	60.18
65.20	65.20
70.23	70.23
75.23	75.09
80.26	80.24
85.27	85.26
90.20	90.30
95.34	95.31

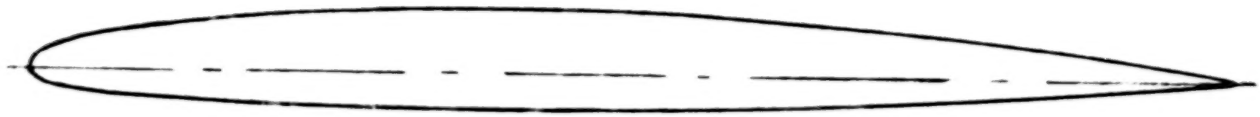

08-64C

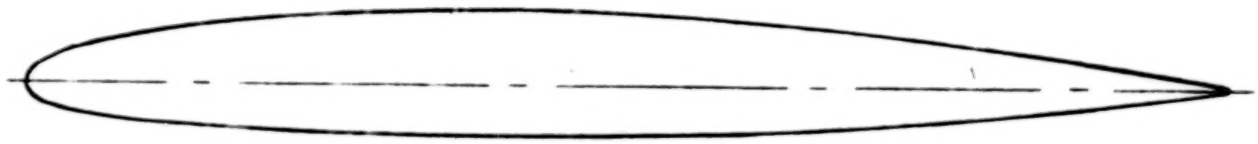

10-64C

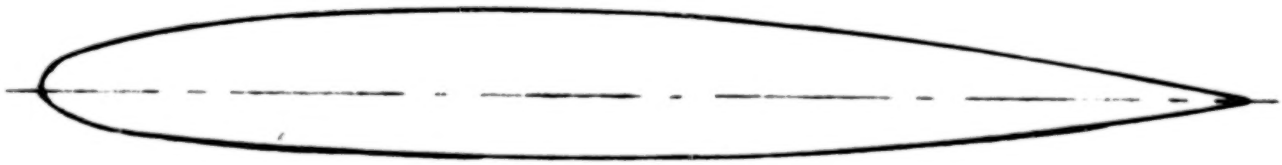

12-64C

Figure 1.- Airfoil profiles.

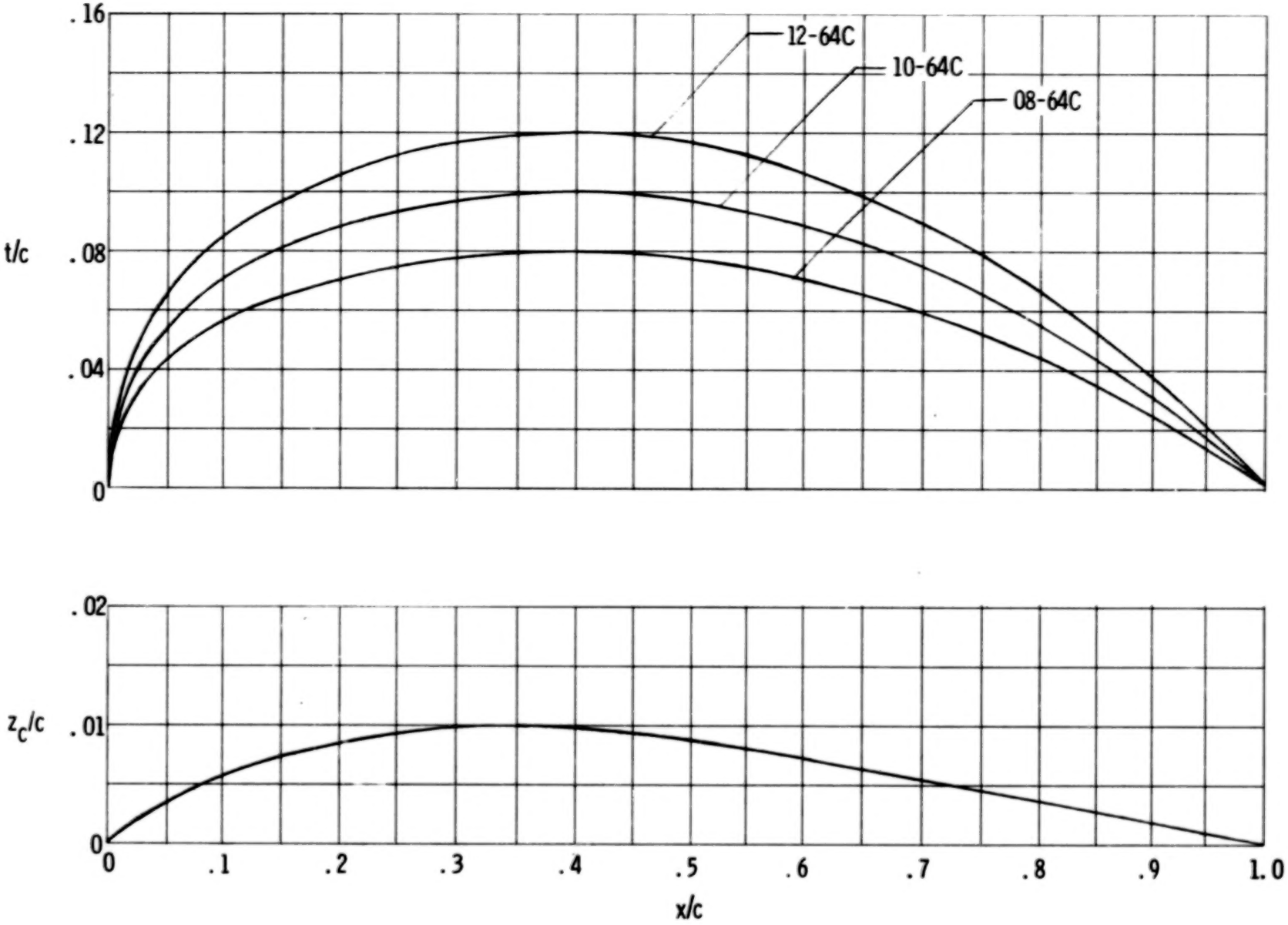

Figure 2.- Airfoil thickness distributions and mean lines.

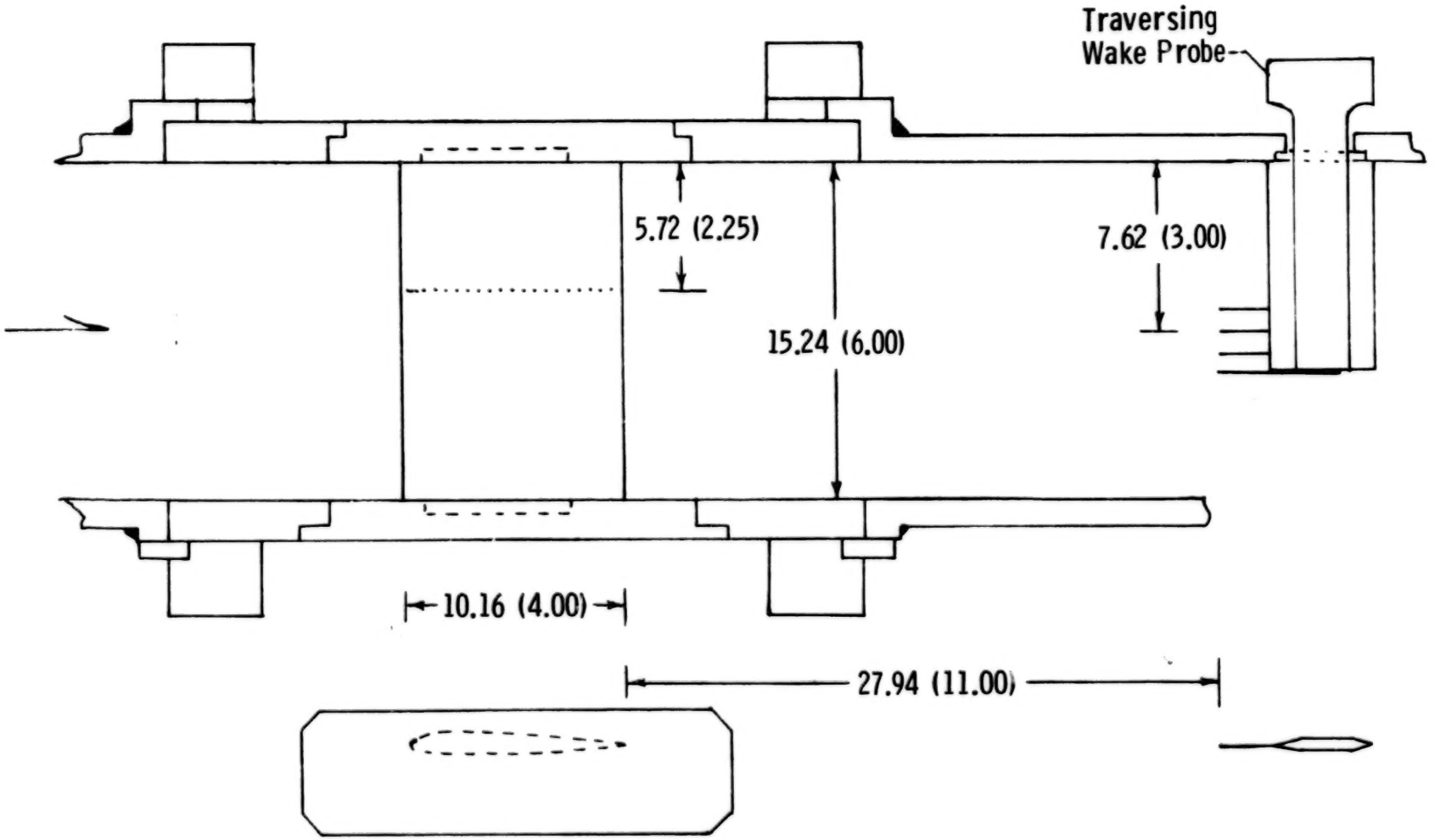

Figure 3.- Model and wake probe installation in Langley 6- by 28-inch transonic tunnel.
All dimensions are in centimeters (inches).

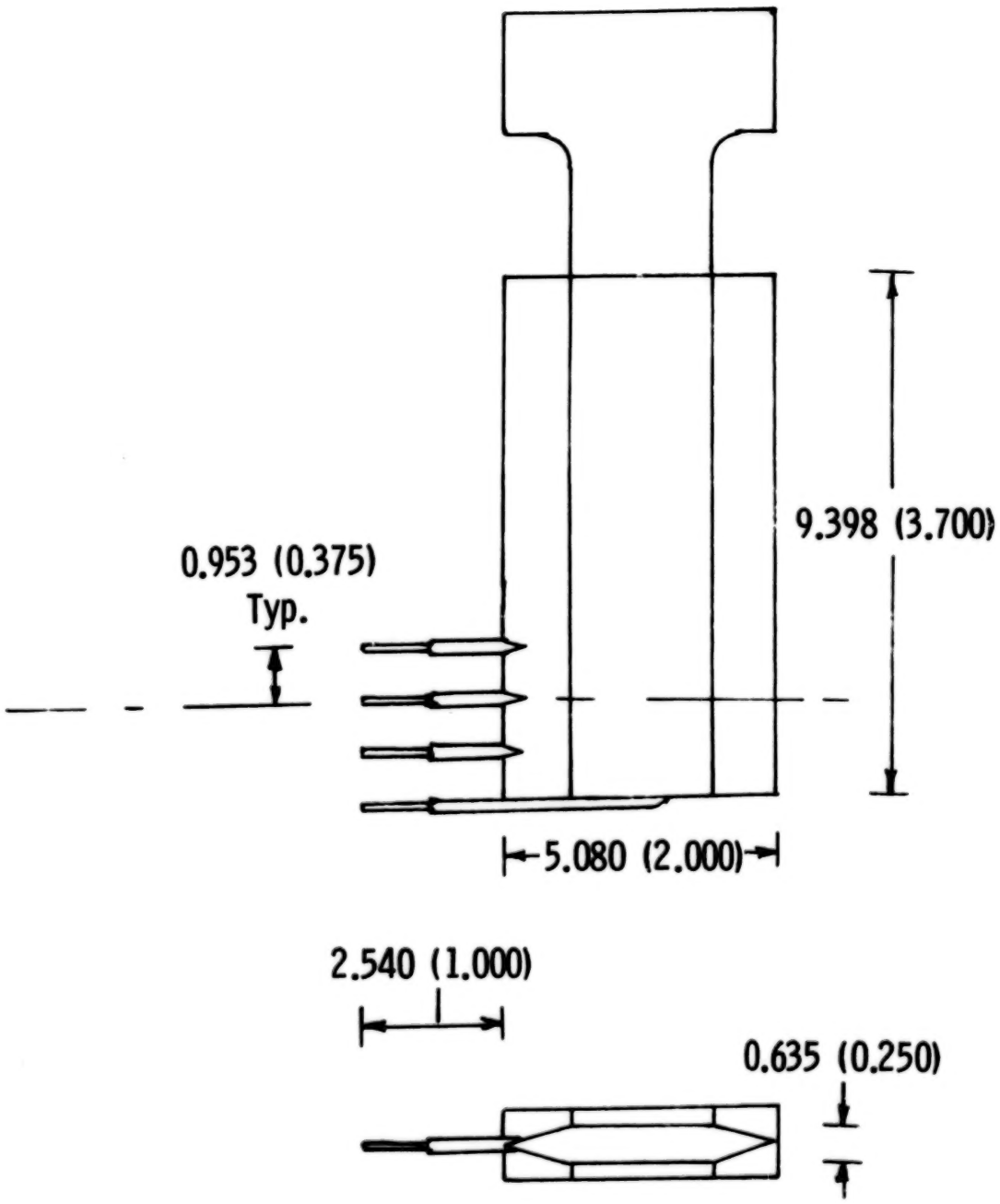

Figure 4.- Wake-survey probe used in Langley 6- by 28-inch transonic tunnel. All dimensions in centimeters (inches).

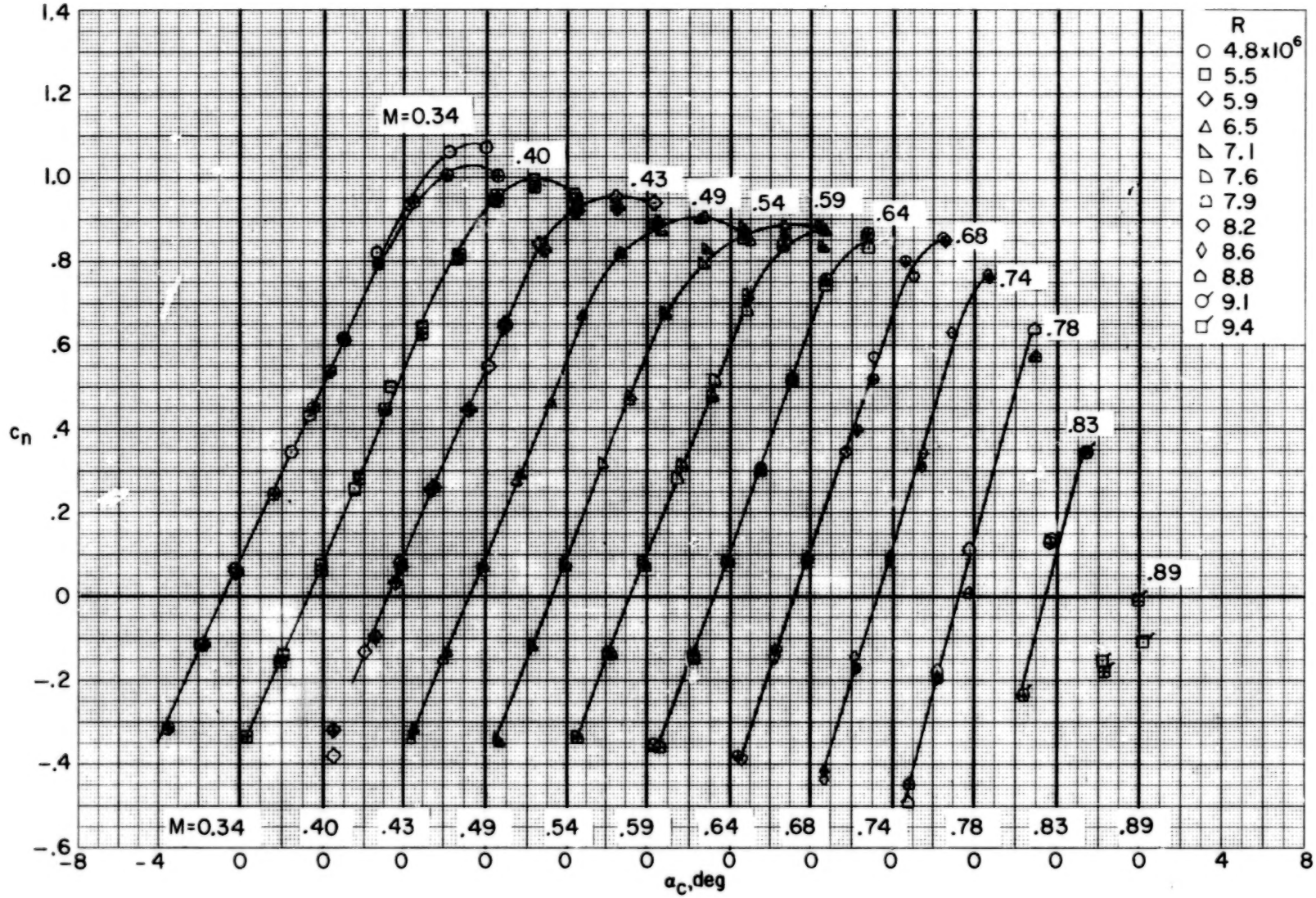

(a) Section normal-force coefficient.

Figure 5.- Aerodynamic characteristics of 10-64C airfoil measured in Langley 6- by 28-inch transonic tunnel. Open symbols indicate model surface smooth; center symbols indicate transition fixed.

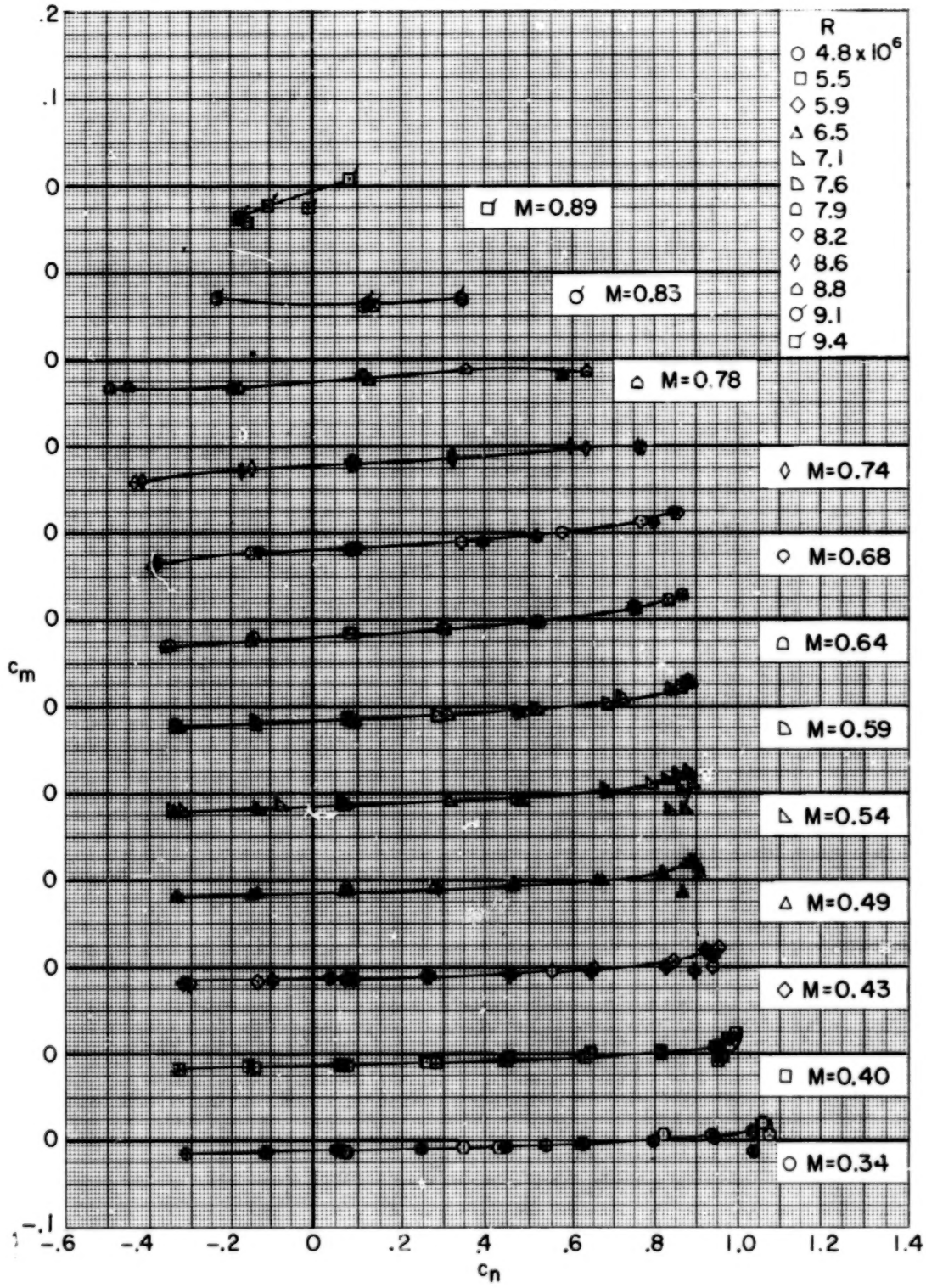

(b) Section pitching-moment coefficient.

Figure 5.- Continued.

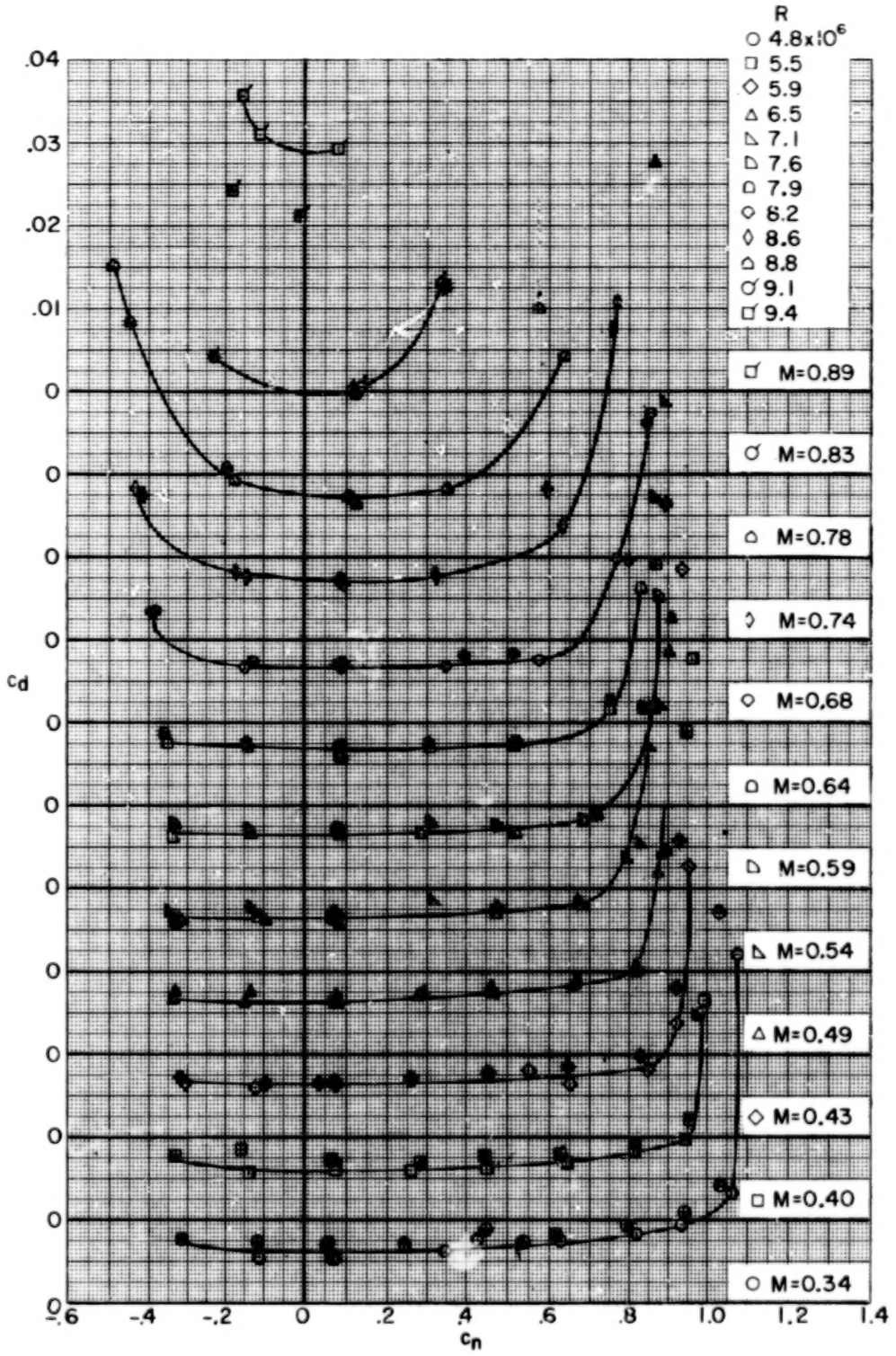

(c) Section drag coefficient.

Figure 5.- Concluded.

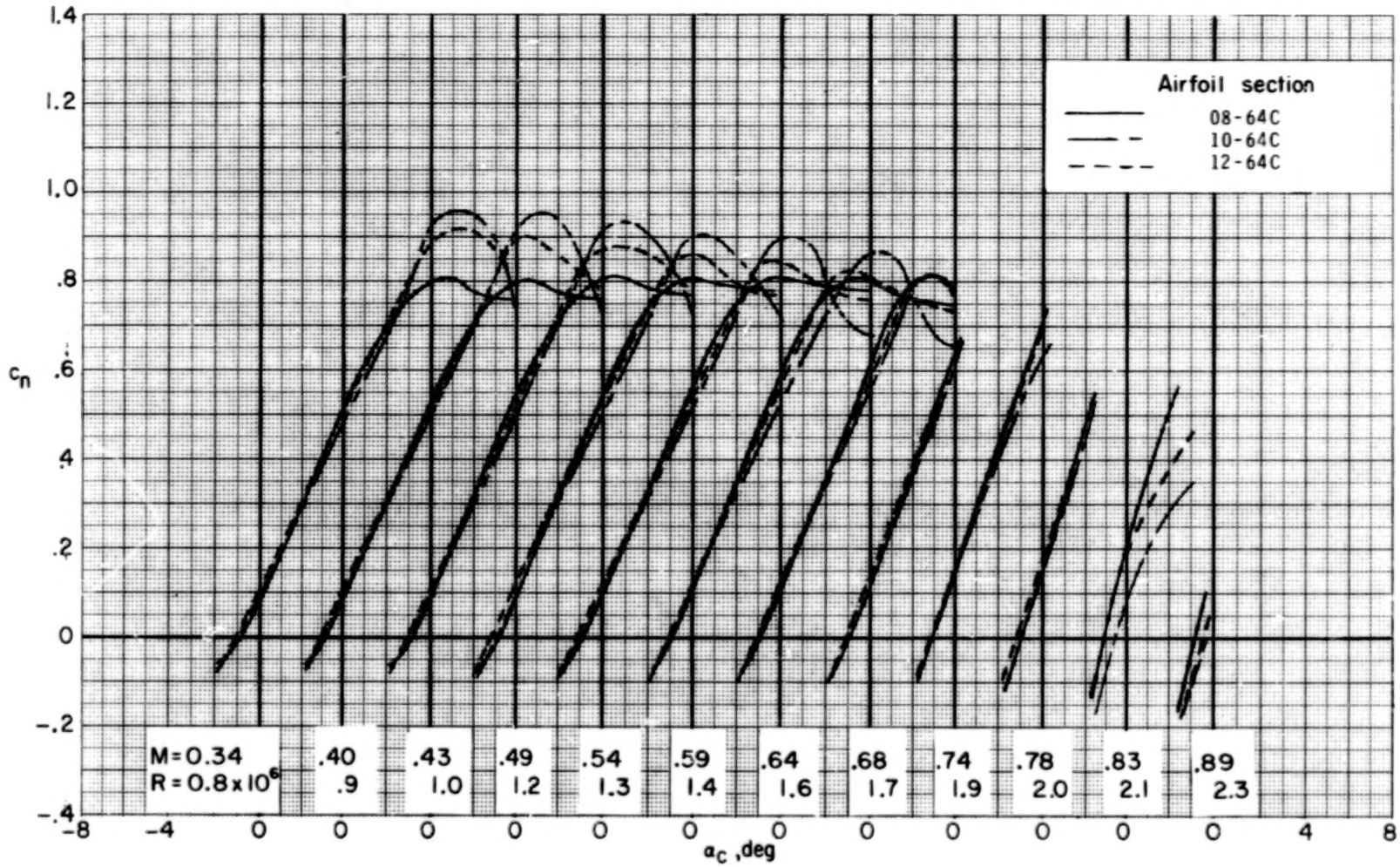

(a) Section normal-force coefficient.

Figure 6.- Aerodynamic characteristics of three airfoils measured in Langley 6- by 19-inch transonic tunnel. Model surfaces smooth.

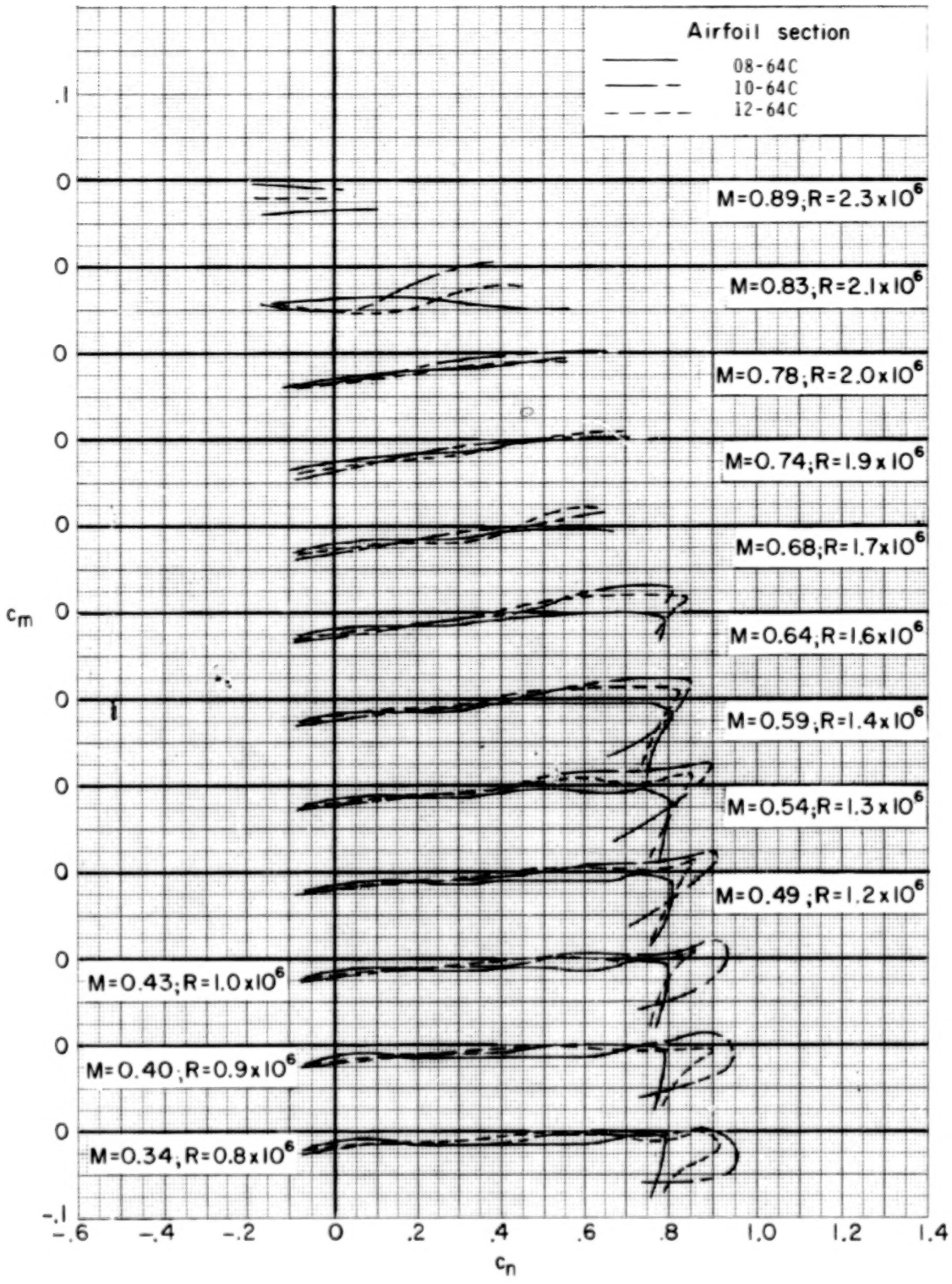

(b) Section pitching-moment coefficient.

Figure 6.- Continued.

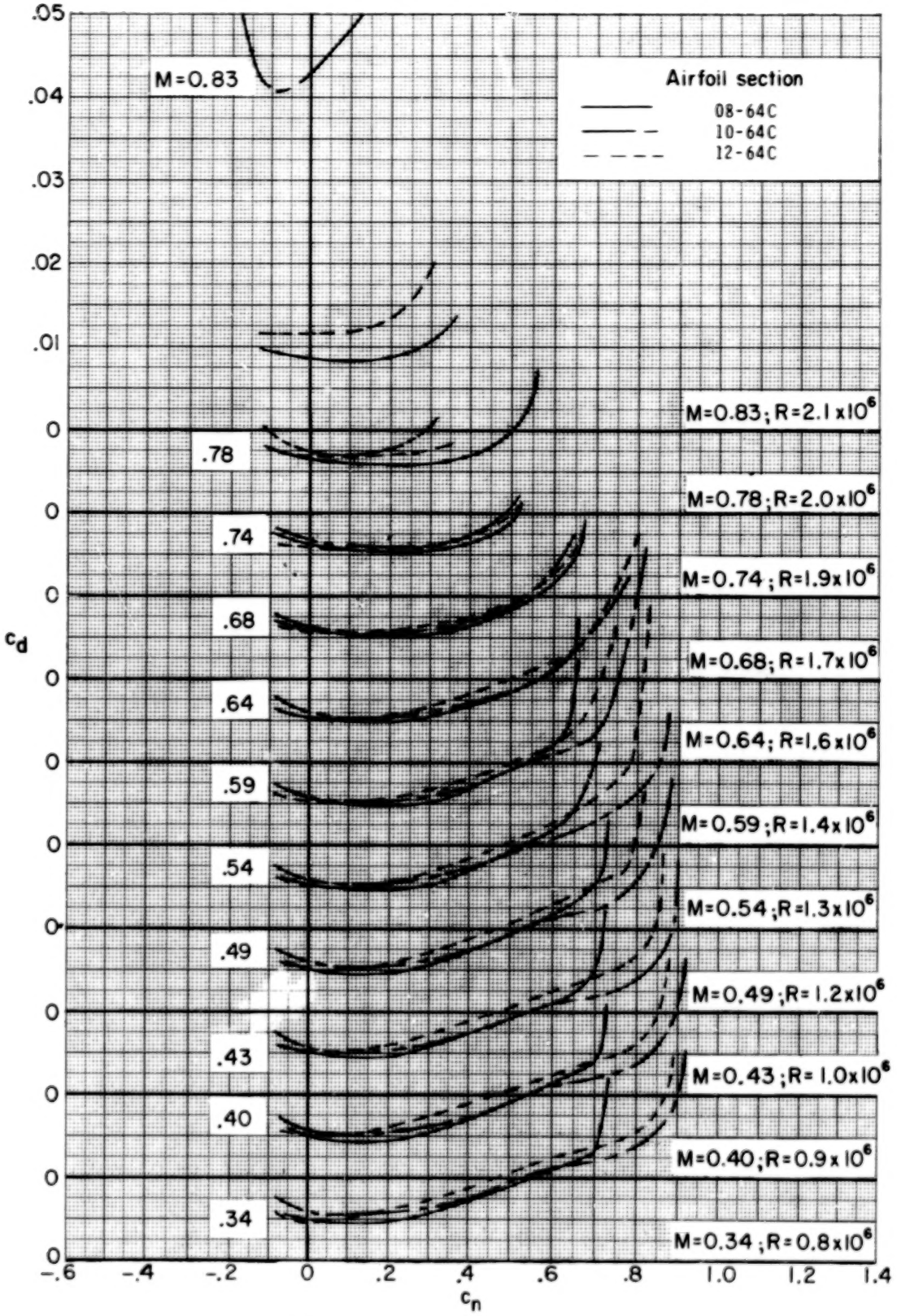

(c) Section drag coefficient.

Figure 6.- Concluded.

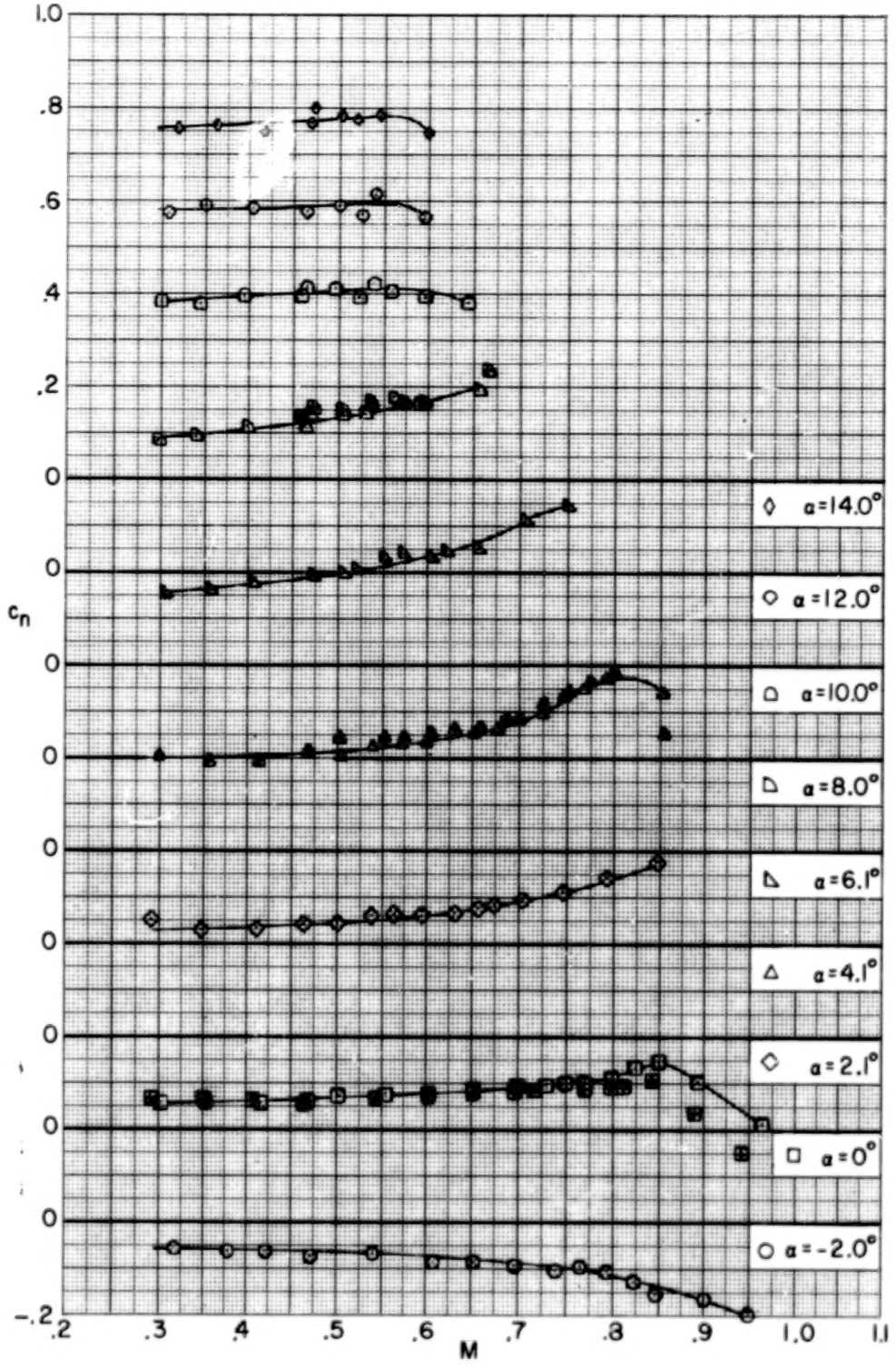

(a) Section normal-force coefficient.

Figure 7.- Aerodynamic characteristics of 08-64C airfoil measured in Langley 6- by 19-inch transonic tunnel. Open symbols indicate model surface smooth; centered symbols indicate transition fixed.

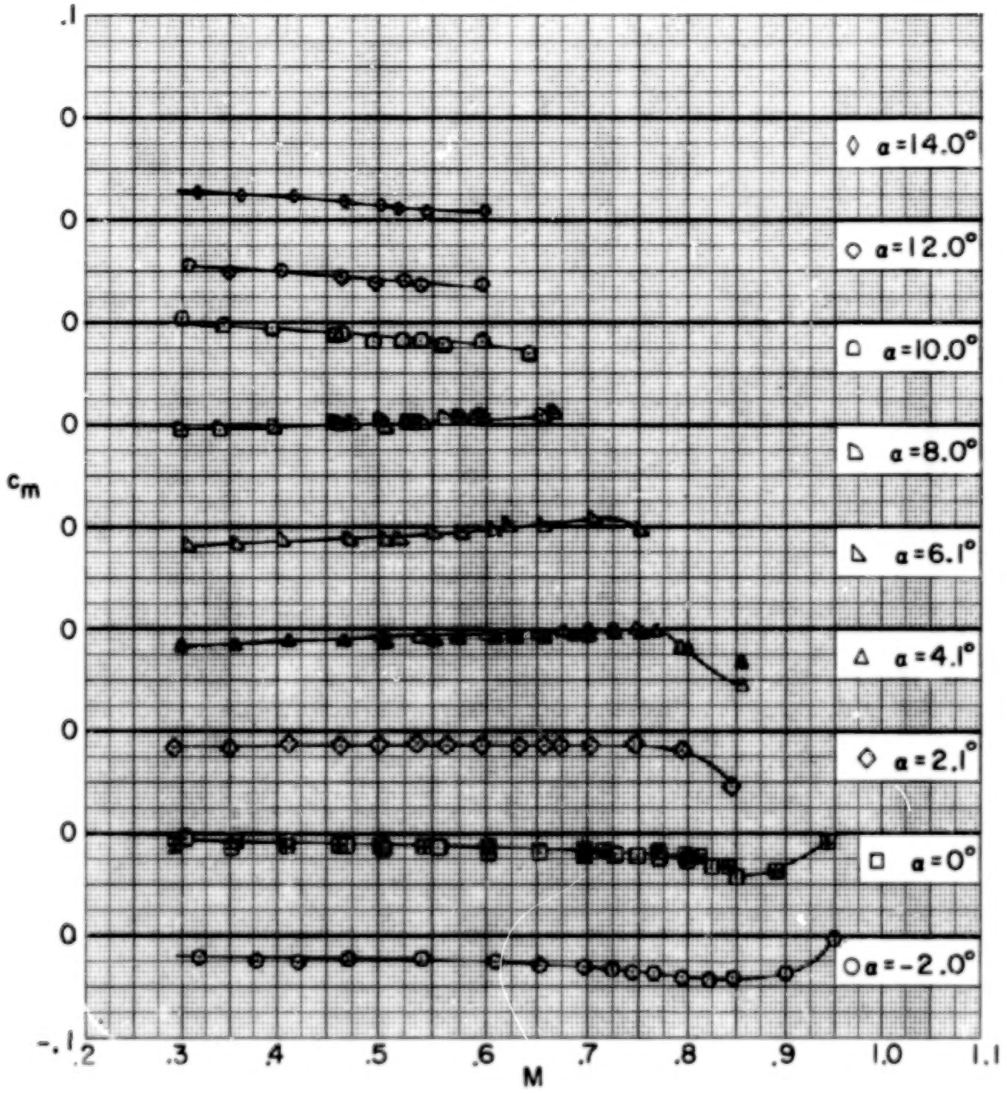

(b) Section pitching-moment coefficient.

Figure 7.- Continued.

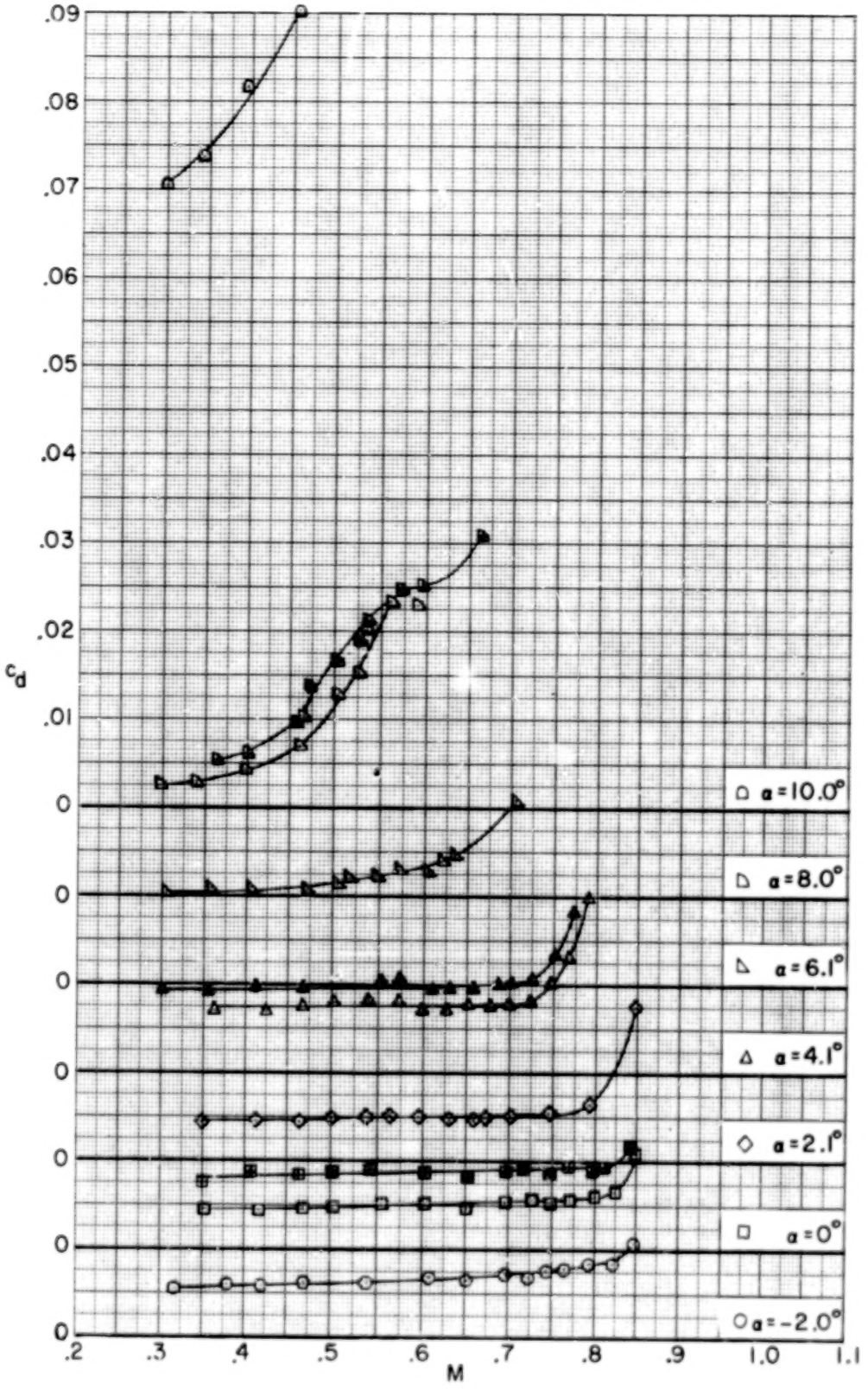

(c) Section drag coefficient.

Figure 7.- Concluded.

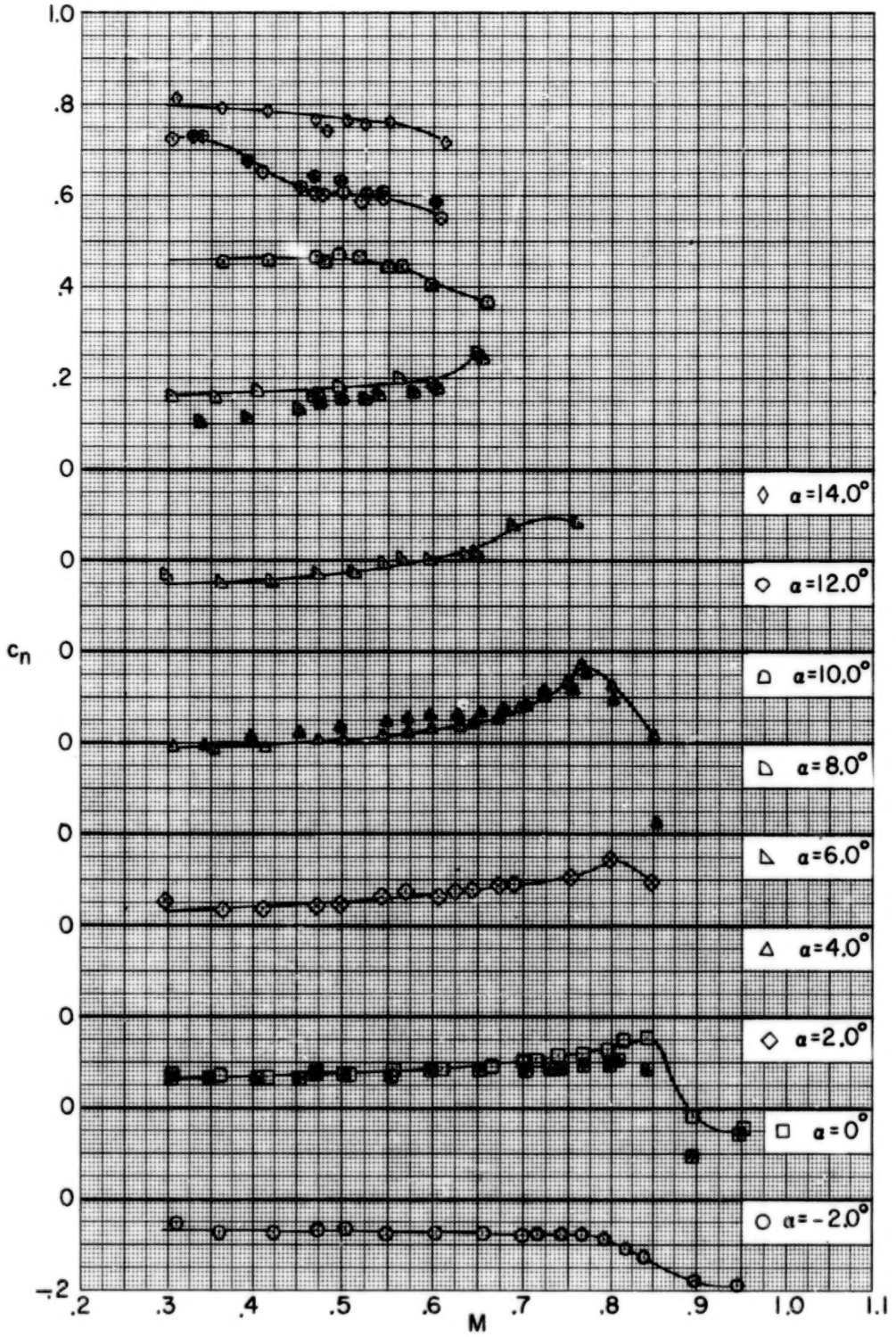

(a) Section normal-force coefficient.

Figure 8.- Aerodynamic characteristics of 10-64C airfoil measured in Langley 6- by 19-inch transonic tunnel. Open symbols indicate model surface smooth; centered symbols indicate transition fixed.

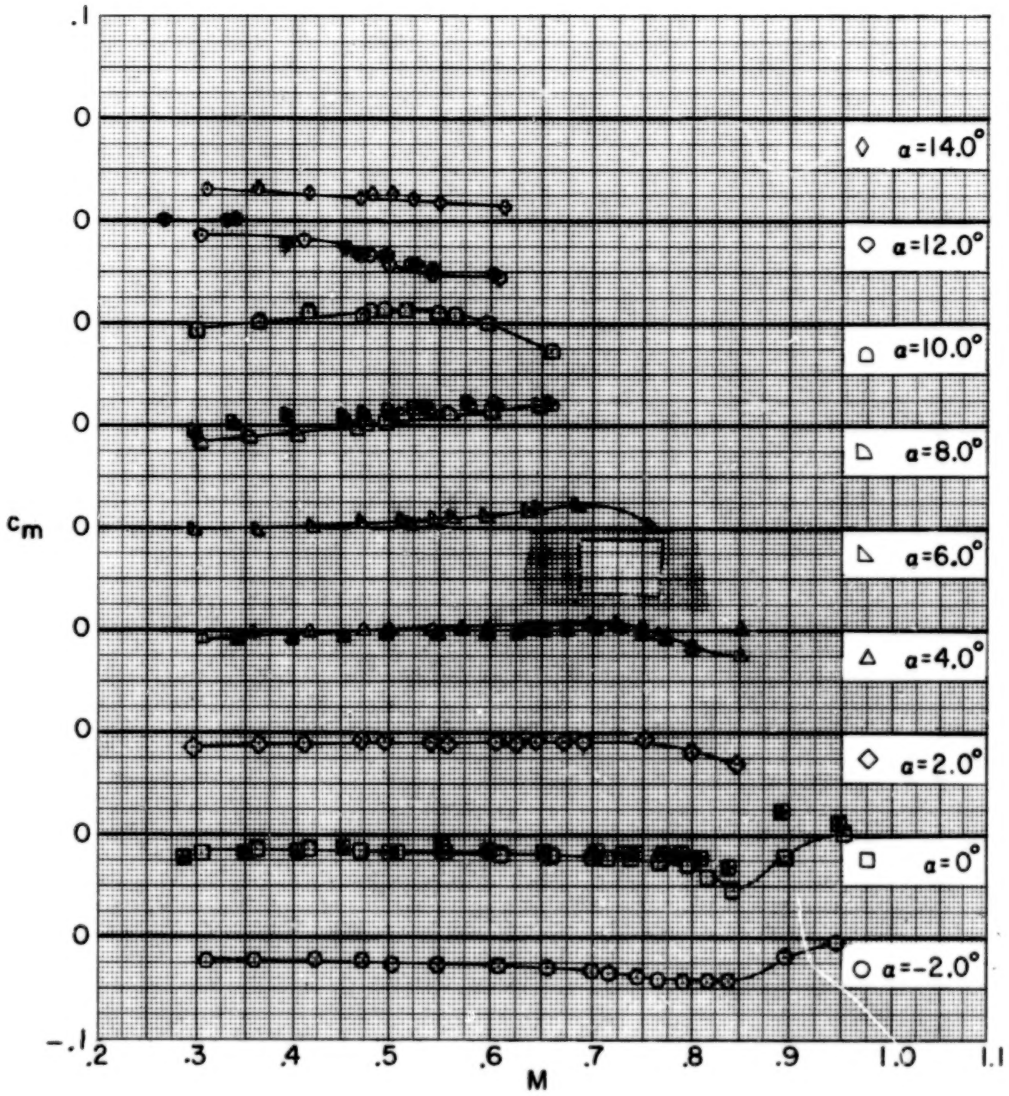

(b) Section pitching-moment coefficient.

Figure 8.- Continued.

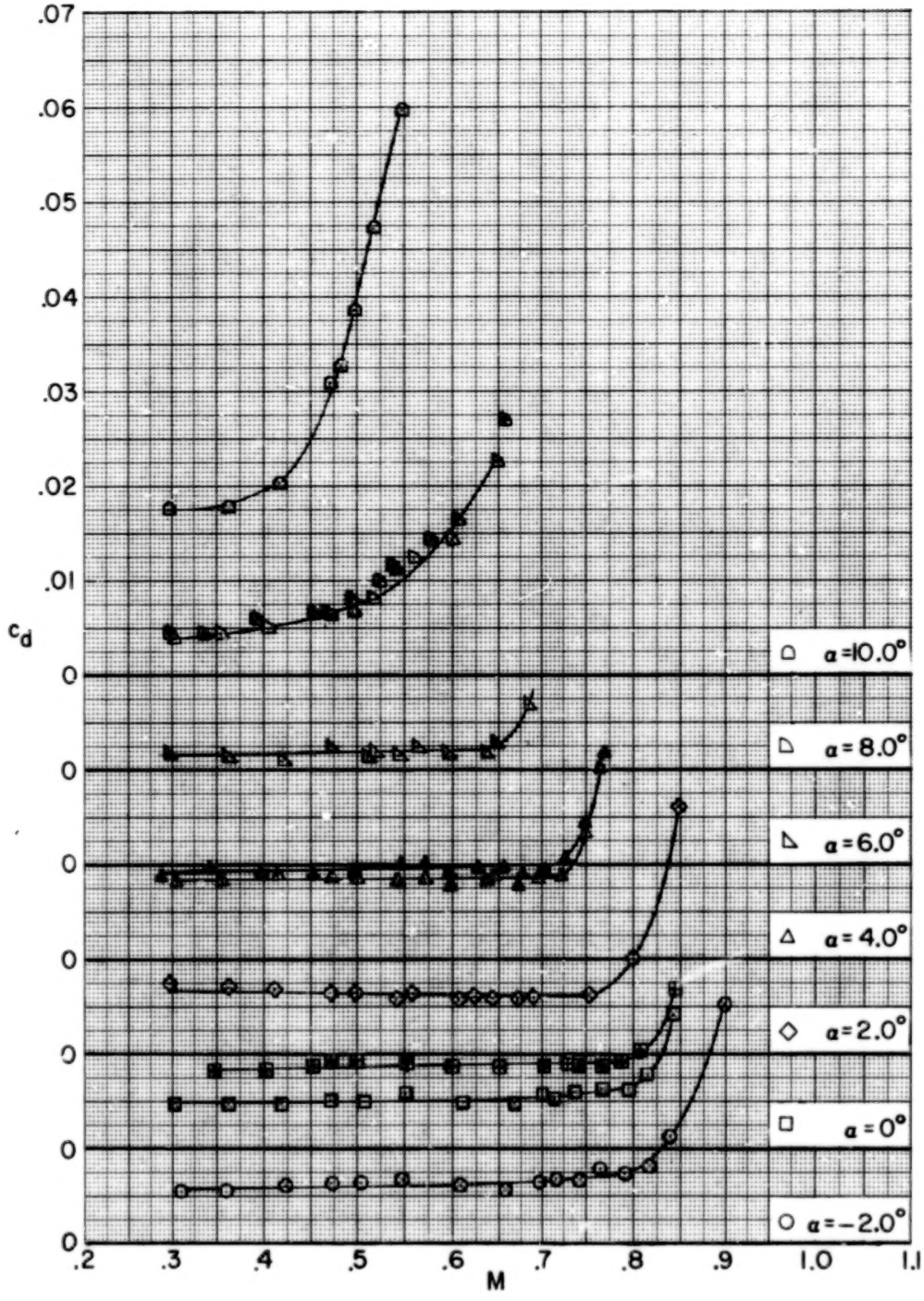

(c) Section drag coefficient.

Figure 8.- Concluded.

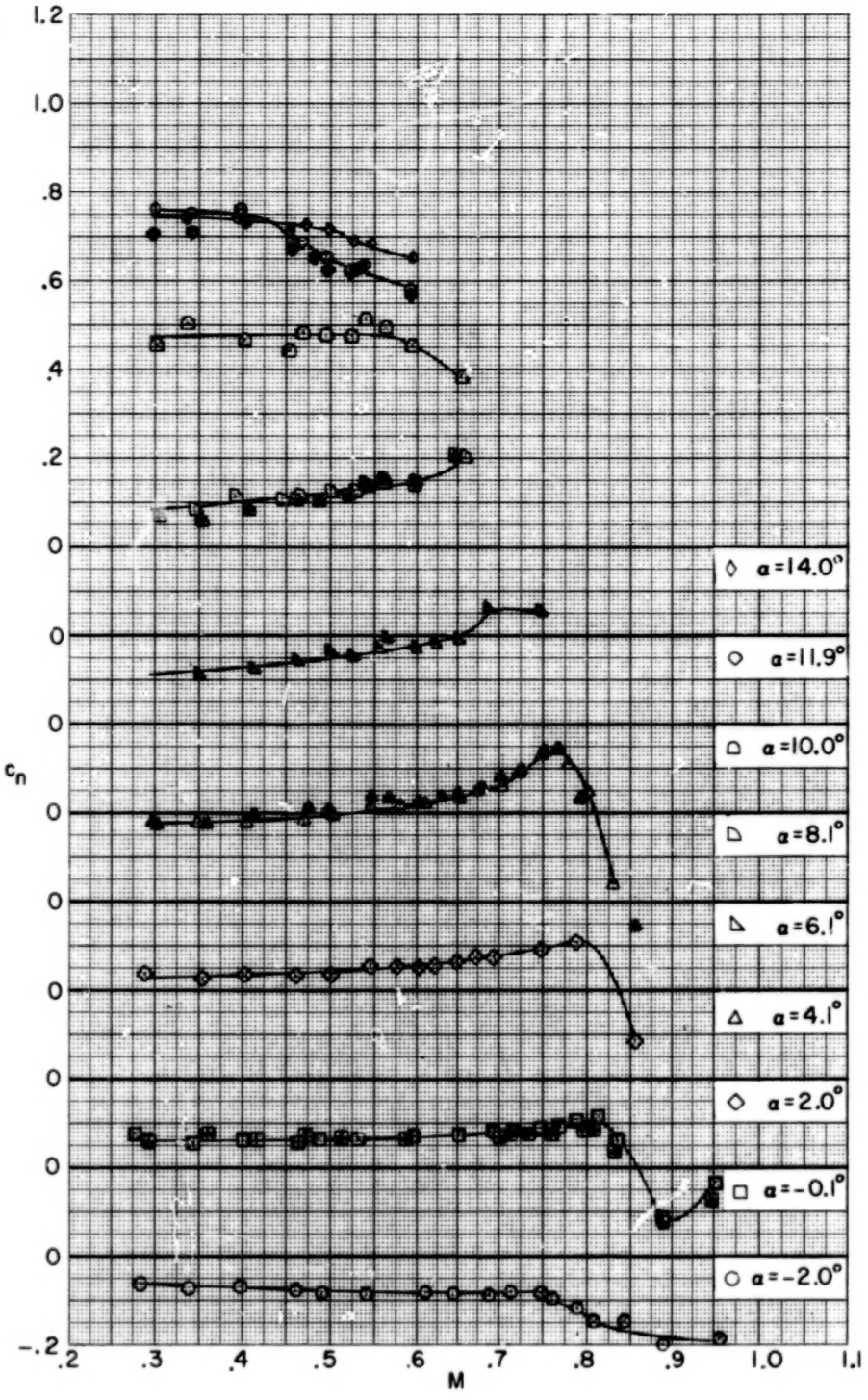

(a) Section normal-force coefficient.

Figure 9.- Aerodynamic characteristics of 12-64C airfoil measured in Langley 6- by 19-inch transonic tunnel. Open symbols indicate model surface smooth; centered symbols indicate transition fixed.

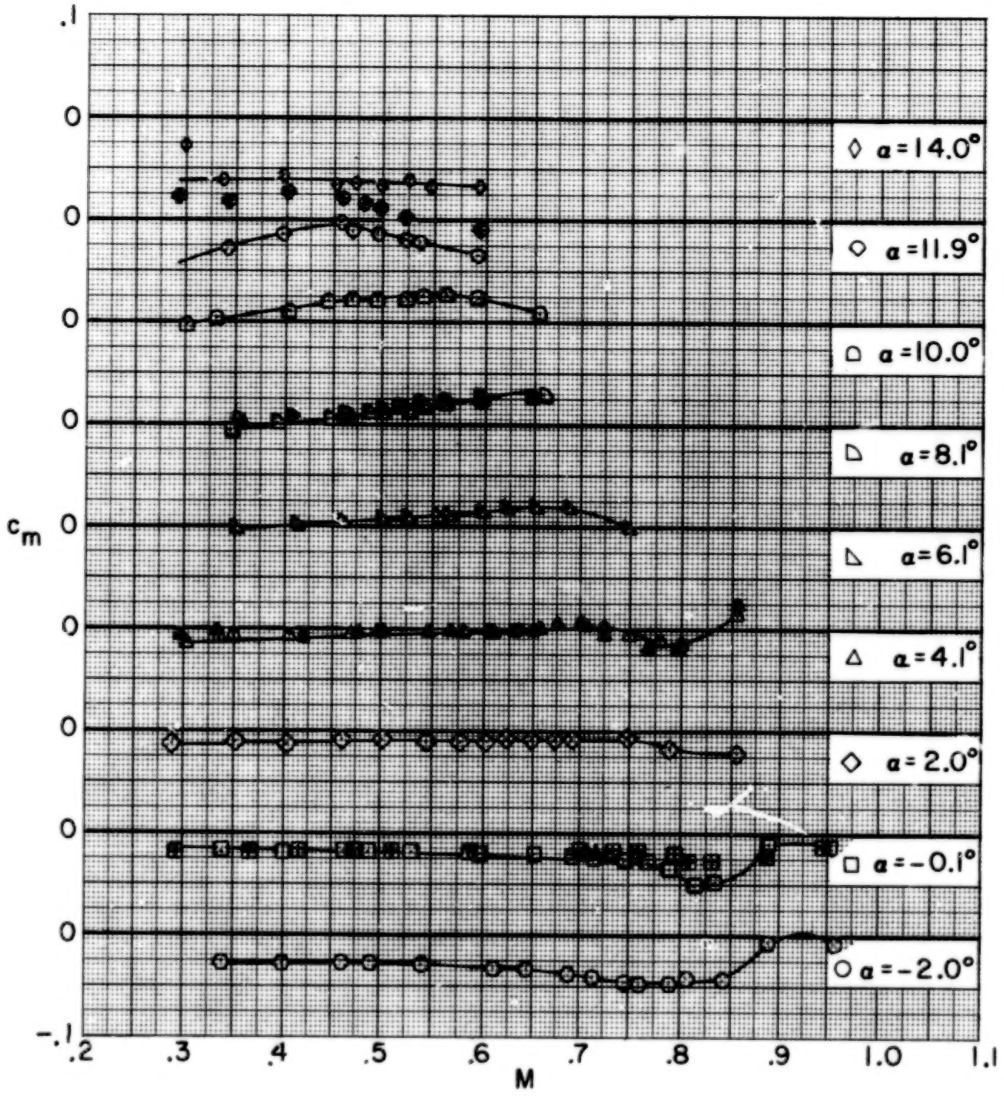

(b) Section pitching-moment coefficient.

Figure 9.- Continued.

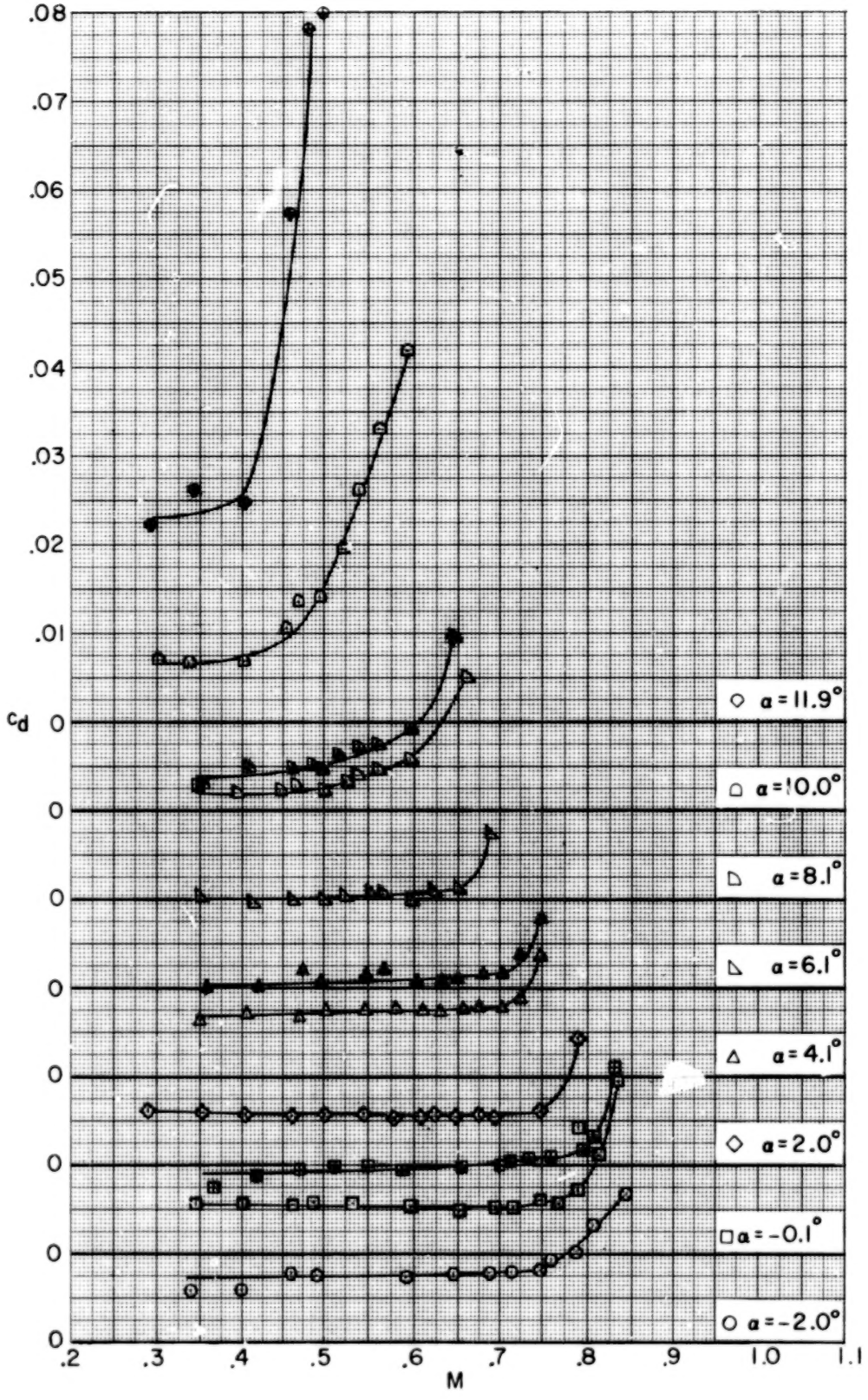

(c) Section drag coefficient.

Figure 9.- Concluded.

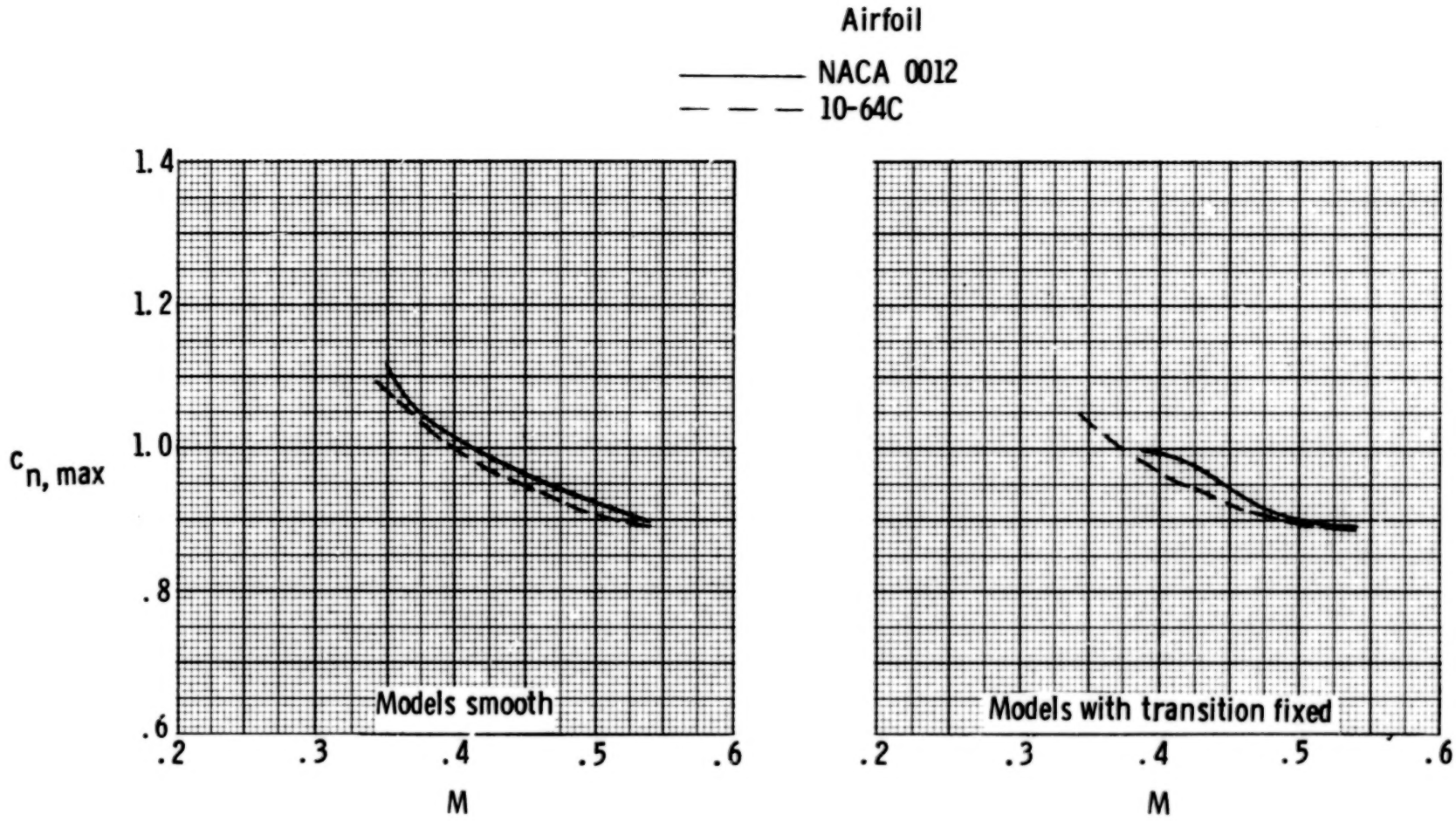

Figure 10.- Variation of maximum section normal-force coefficient with Mach number of NACA 0012 and 10-64C airfoils as measured in Langley 6- by 28-inch transonic tunnel.

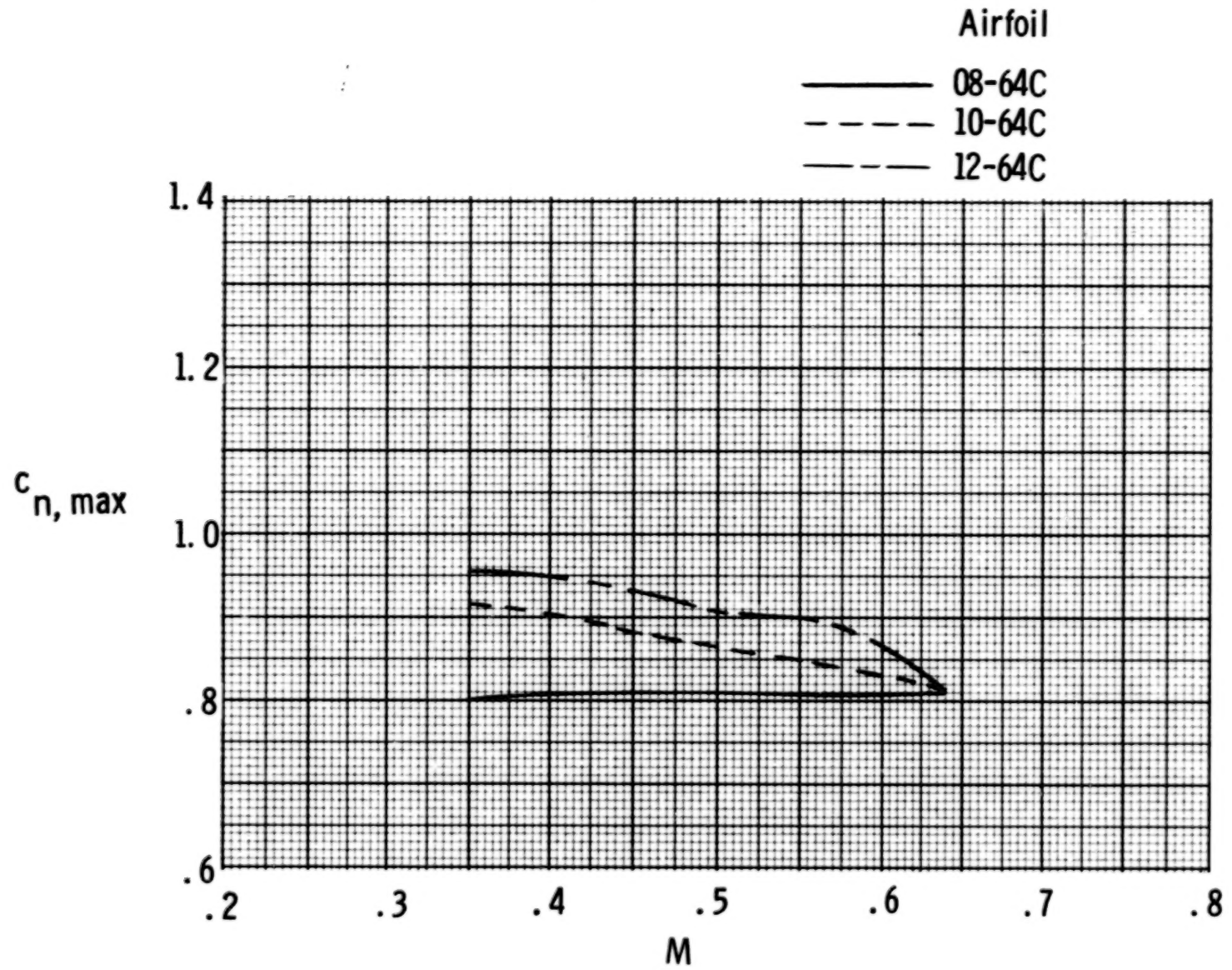

Figure 11.- Variation of maximum section normal-force coefficient with Mach number of 08-64C, 10-64C, and 12-64C airfoils as measured in Langley 6- by 19-inch transonic tunnel. Models smooth.

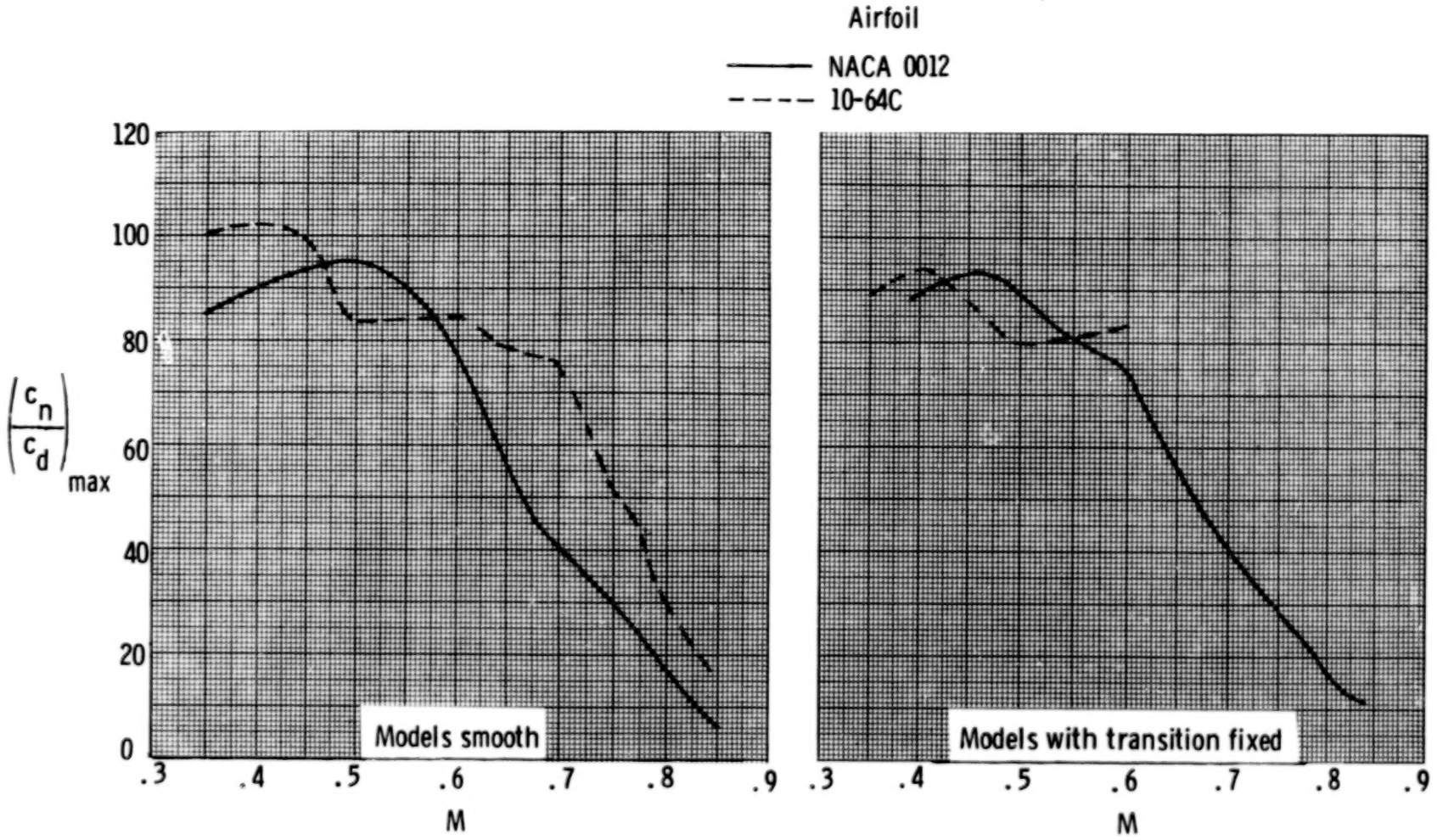

Figure 12.- Variation of maximum section normal-force—drag ratio with Mach number of NACA 0012 and 10-64C airfoils as measured in Langley 6- by 28-inch transonic tunnel.

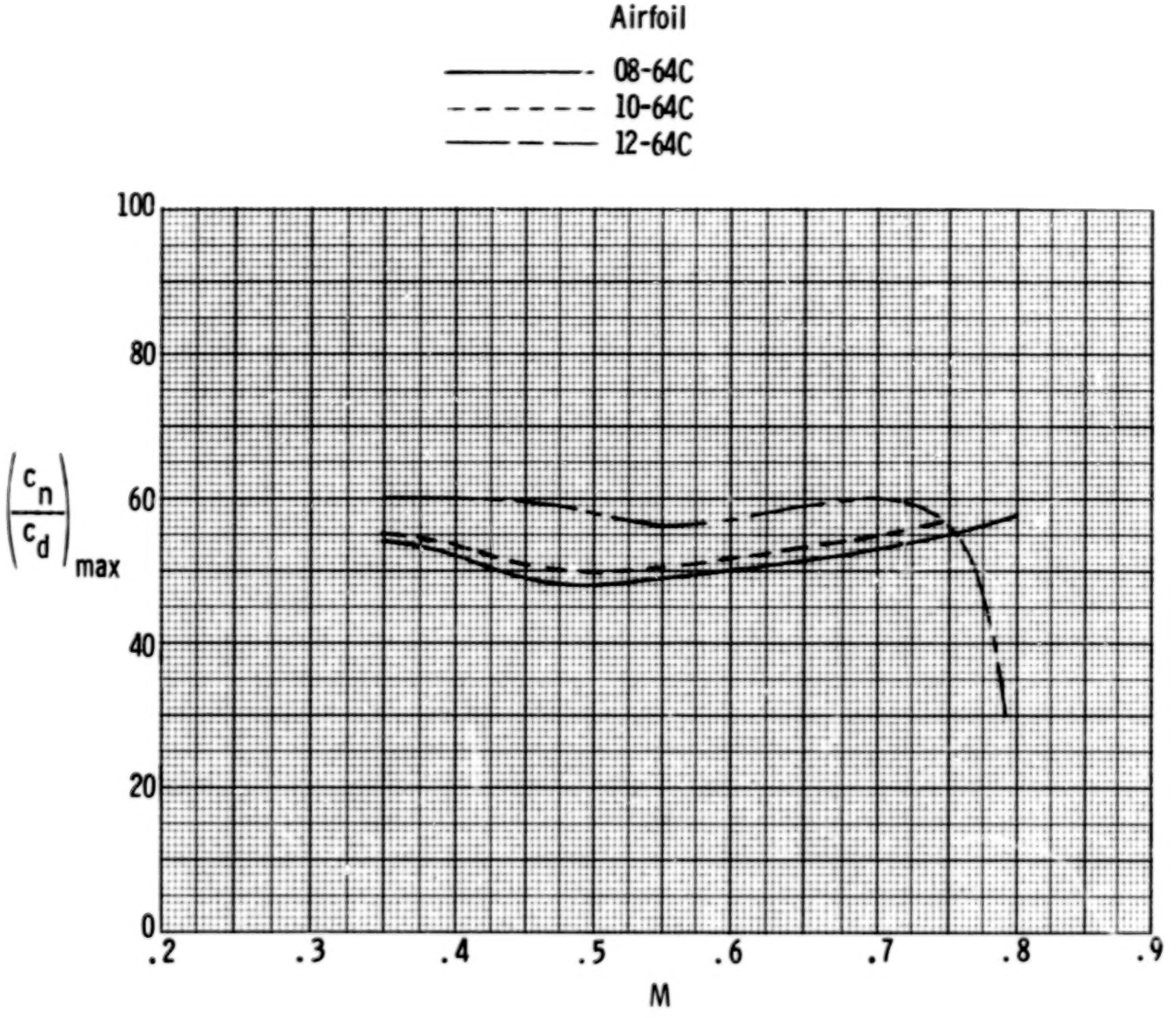

Figure 13.- Variation of maximum section normal-force—drag ratio with Mach number of 08-64C, 10-64C, and 12-64C airfoils as measured in Langley 6- by 19-inch transonic tunnel. Models smooth.

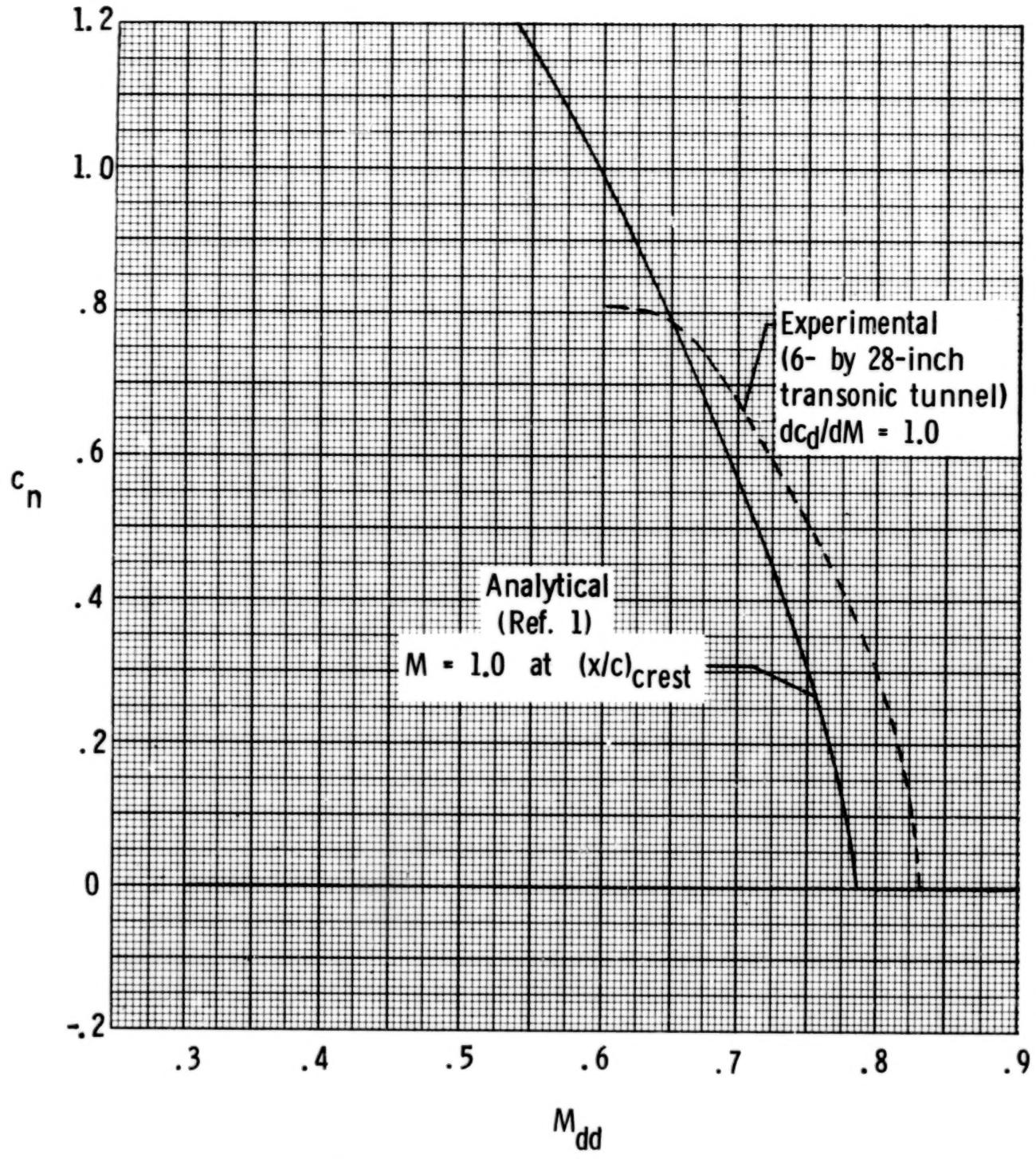

Figure 14.- Comparison of analytical and experimental variation of 10-64C airfoil section normal-force coefficient with drag divergence Mach number ($R = 4.8$ to 9.4×10^6).

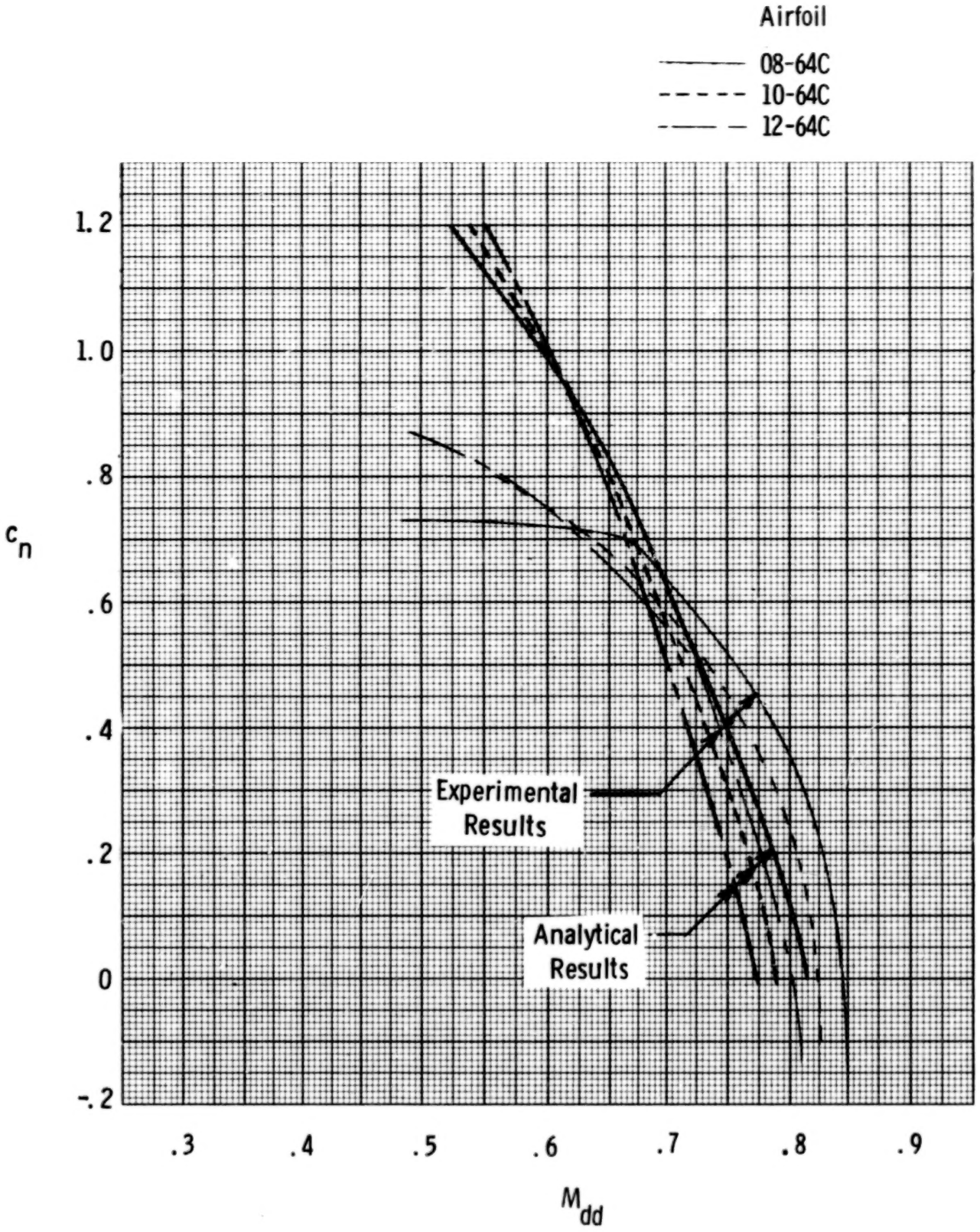

Figure 15.- Comparison of analytical and experimental variation of section normal-force coefficient with drag divergence Mach number ($R = 1.2$ to 2.3×10^6). Data obtained in Langley 6- by 19-inch transonic tunnel.

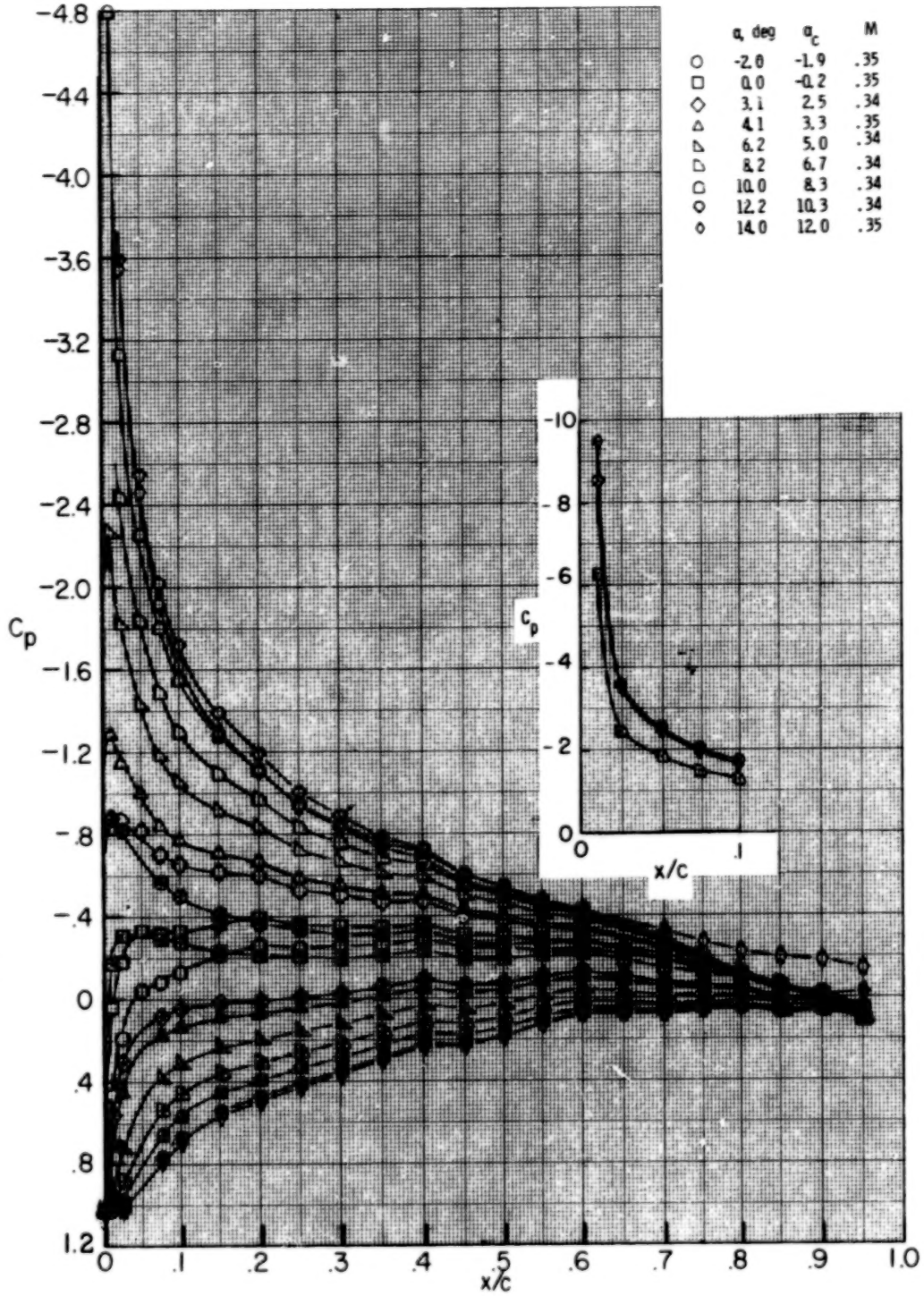

(a) $M \approx 0.34$; $R \approx 4.8 \times 10^6$.

Figure 16.- Pressure distribution over 10-64C airfoil measured in Langley 6- by 28-inch transonic tunnel. Open symbols indicate model surface smooth; centered symbols indicate lower surface.

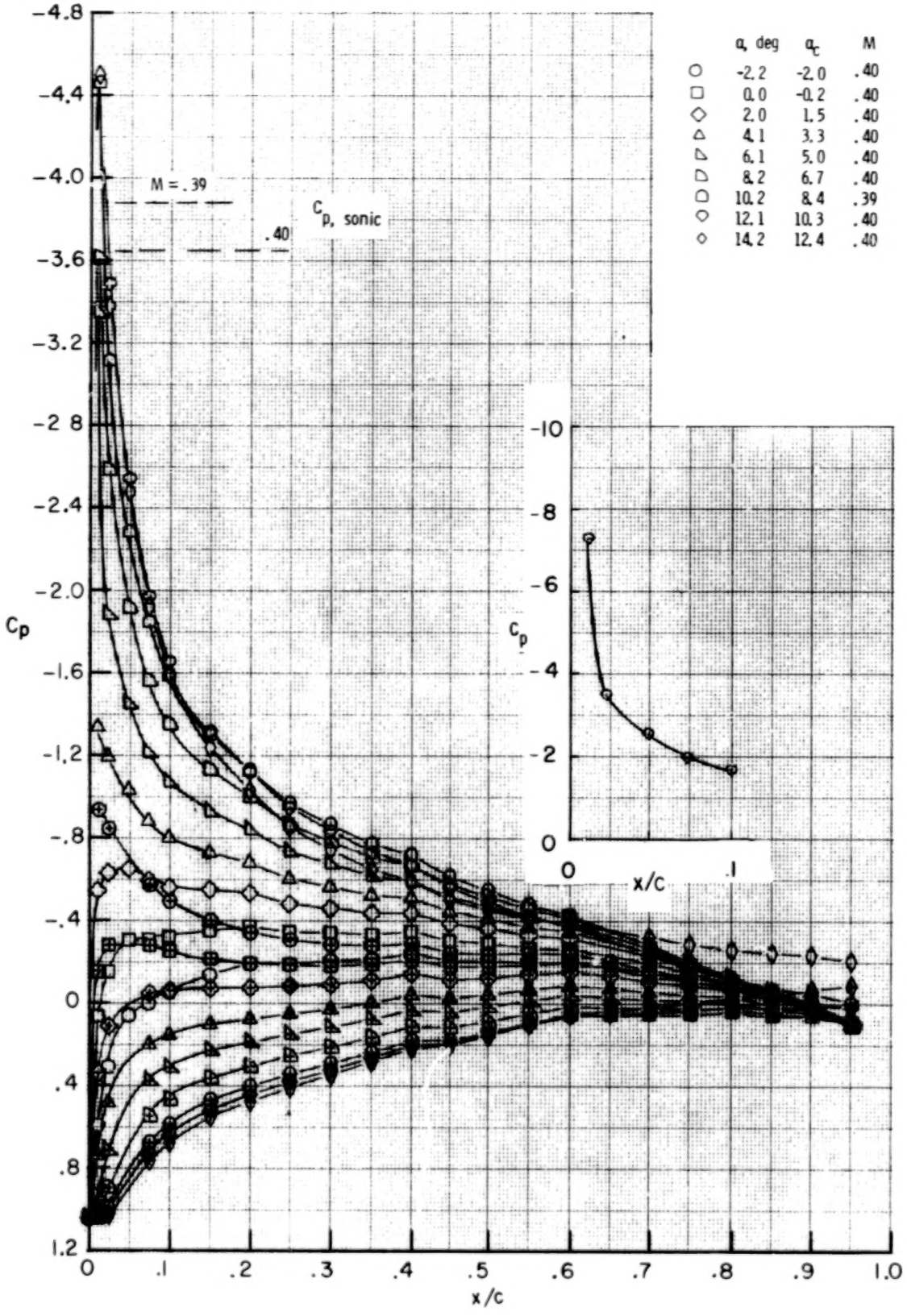

(b) M ≈ 0.40; R ≈ 5.5×10^6.

Figure 16.- Continued.

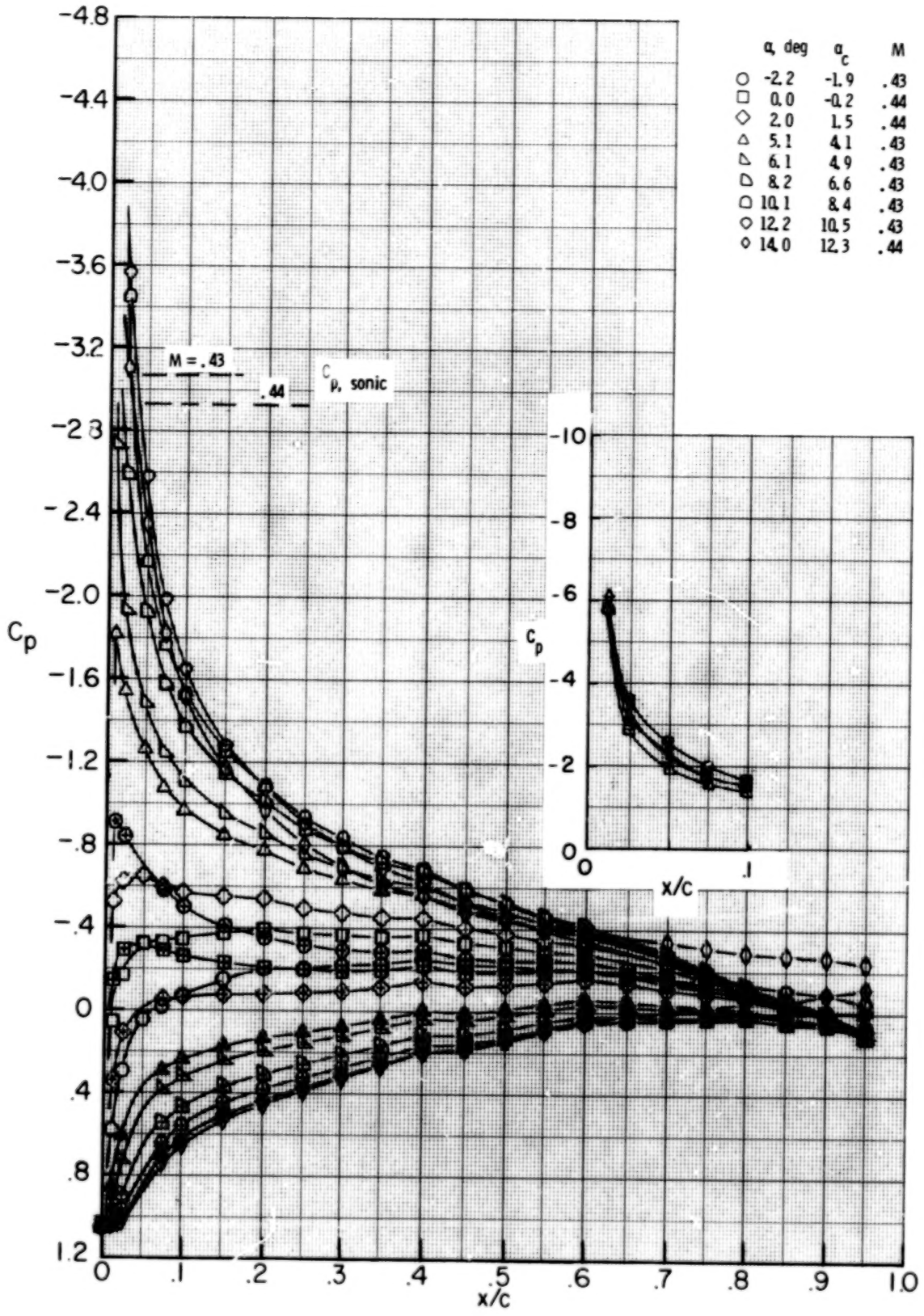

(c) M ≈ 0.43; R ≈ 5.9×10^6.

Figure 16.- Continued.

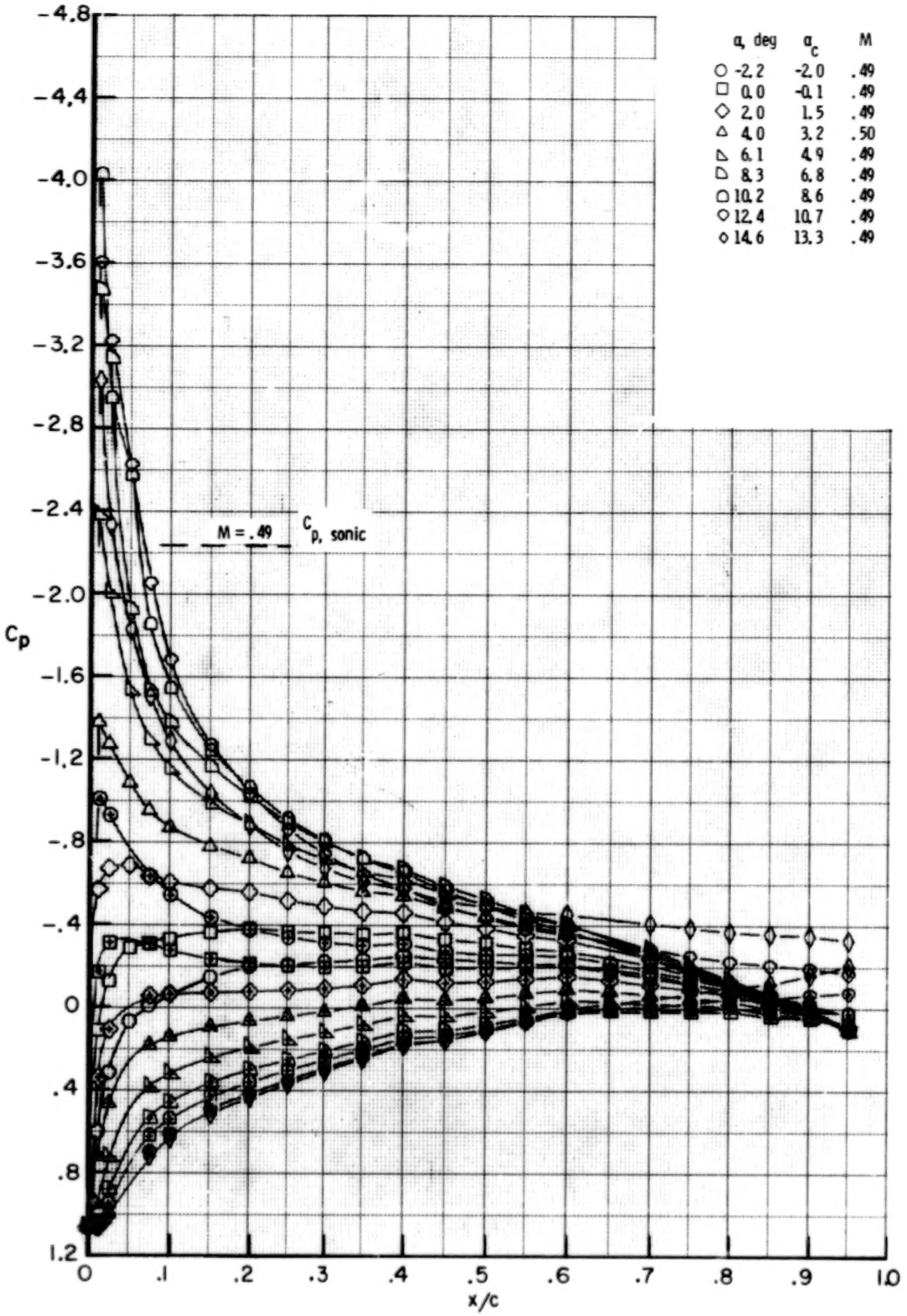

(d) M ≈ 0.49; R ≈ 6.5×10^6.

Figure 16.- Continued.

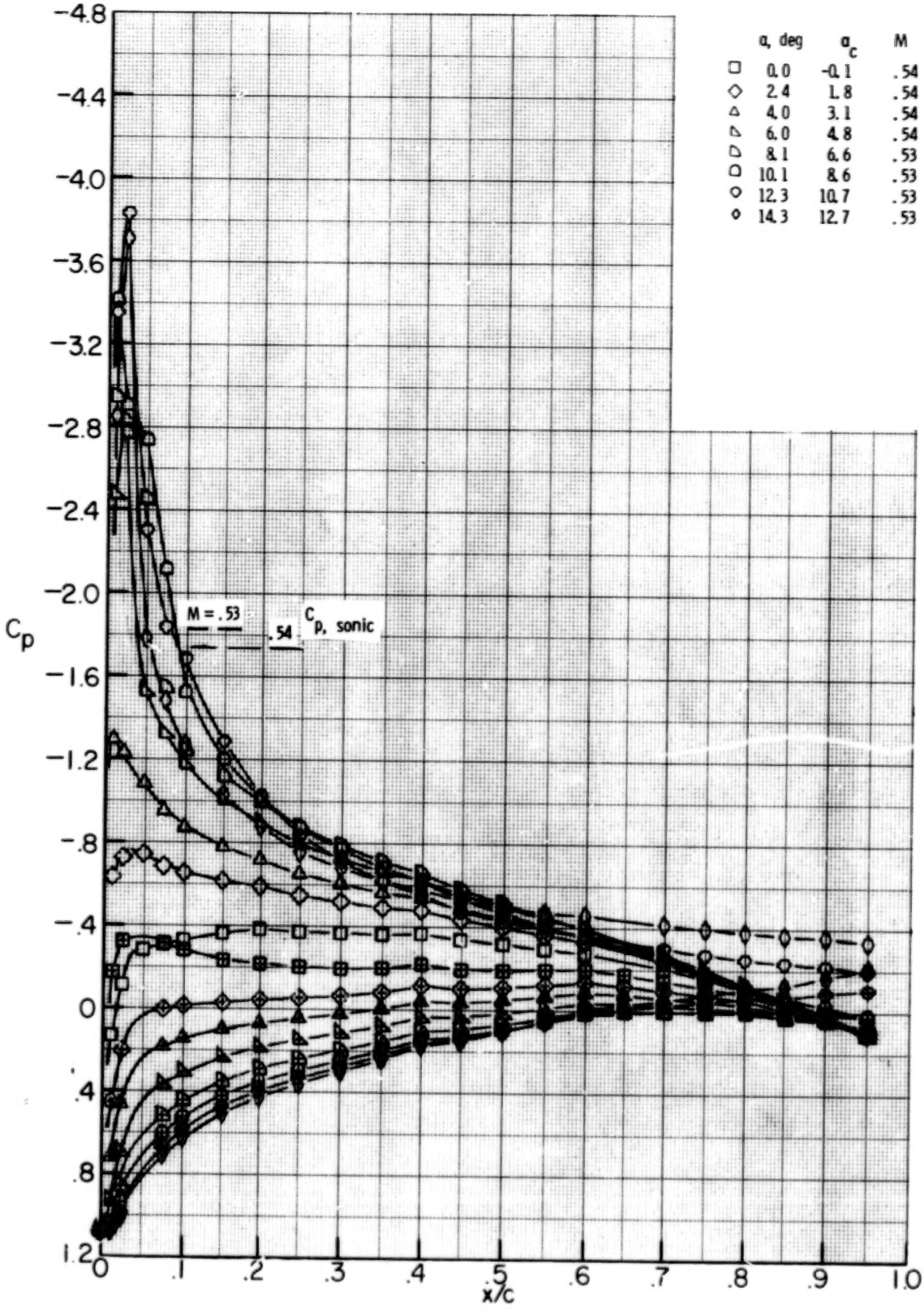

(e) M ≈ 0.54; R ≈ 7.1×10^6.

Figure 16.- Continued.

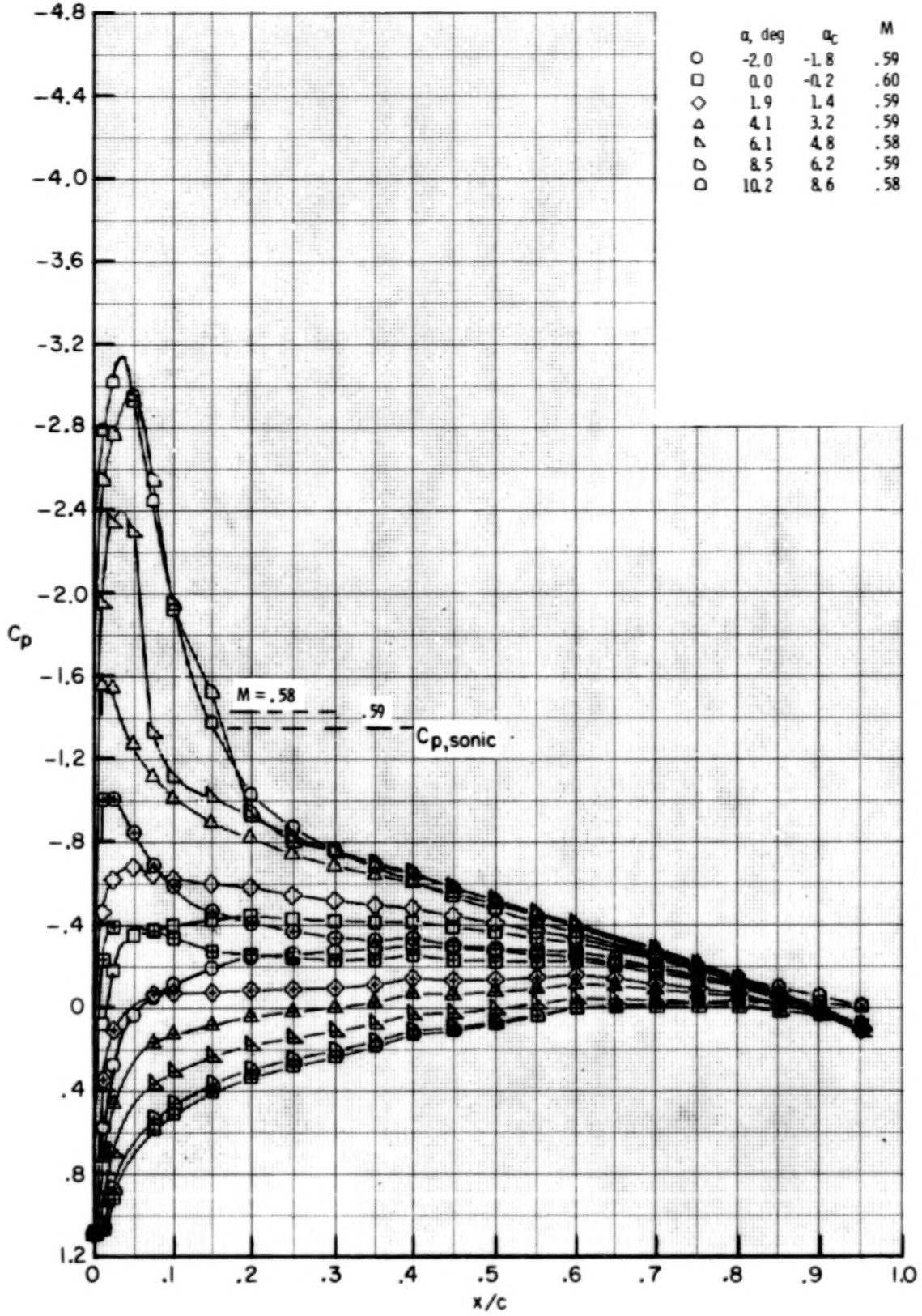

(f) M ≈ 0.59; R ≈ 7.6×10^6.

Figure 16.- Continued.

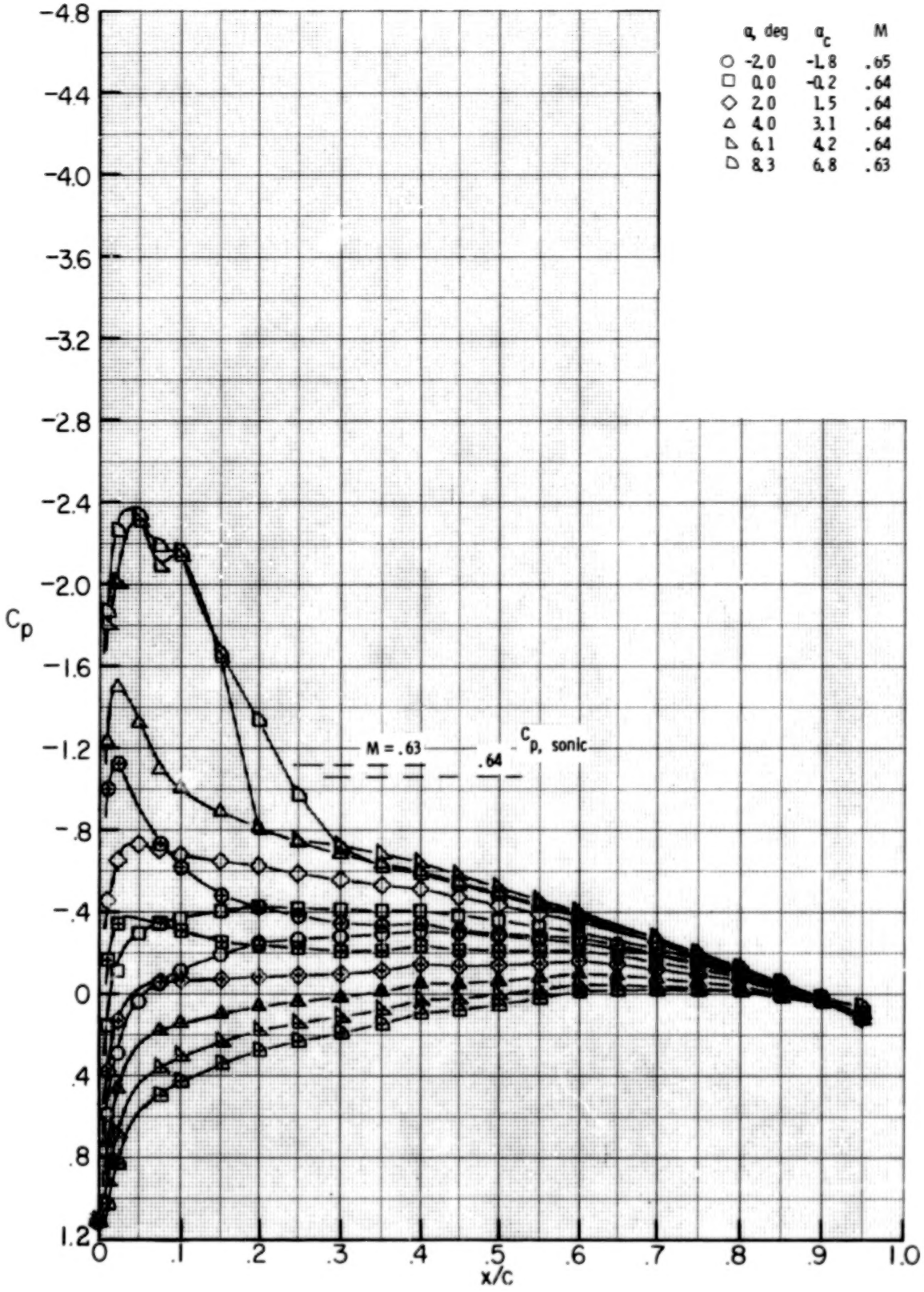

(g) M ≈ 0.64; R ≈ 7.9×10^6.

Figure 16.- Continued.

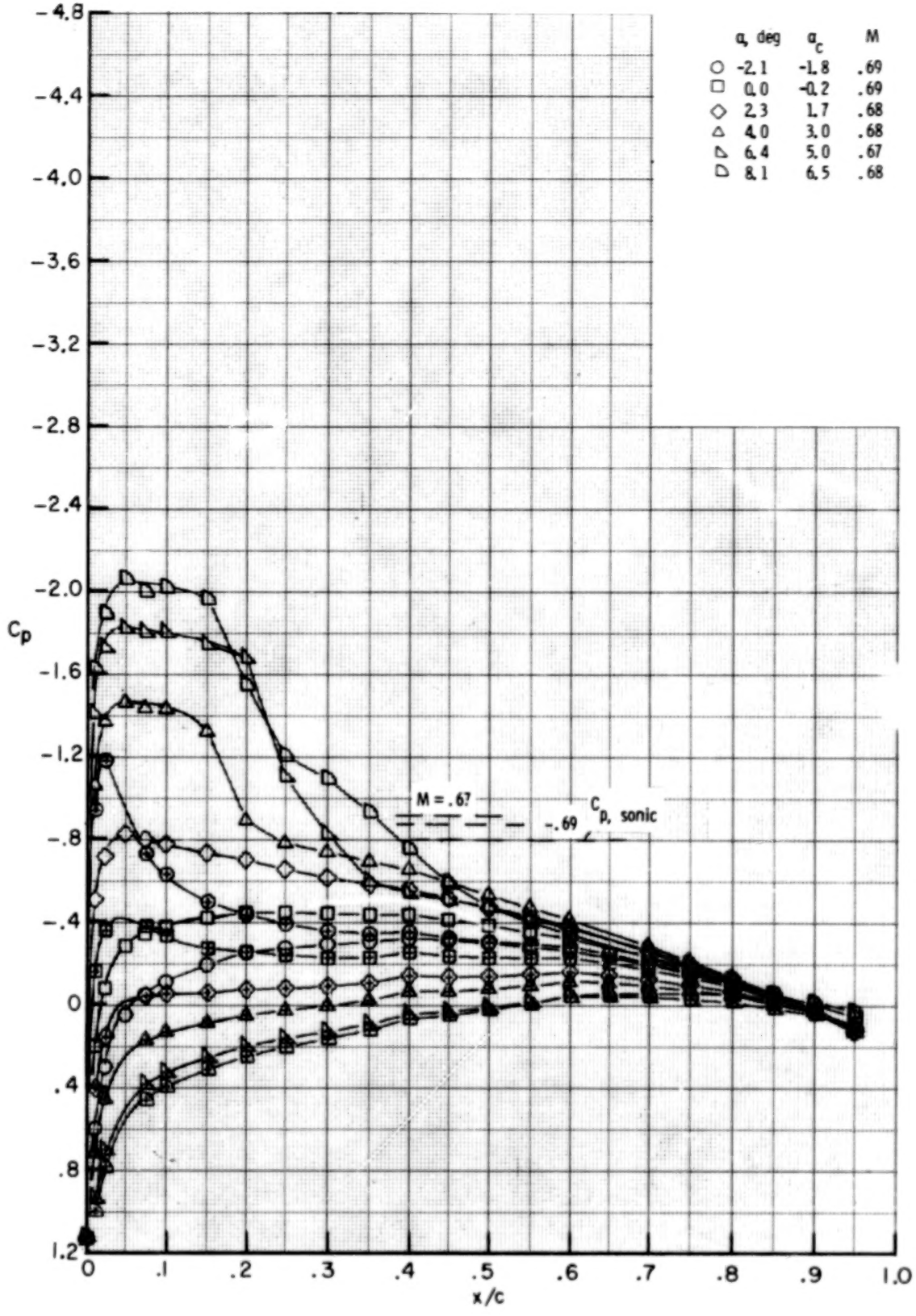

(h) M ≈ 0.68; R ≈ 8.2×10^6.

Figure 16.- Continued.

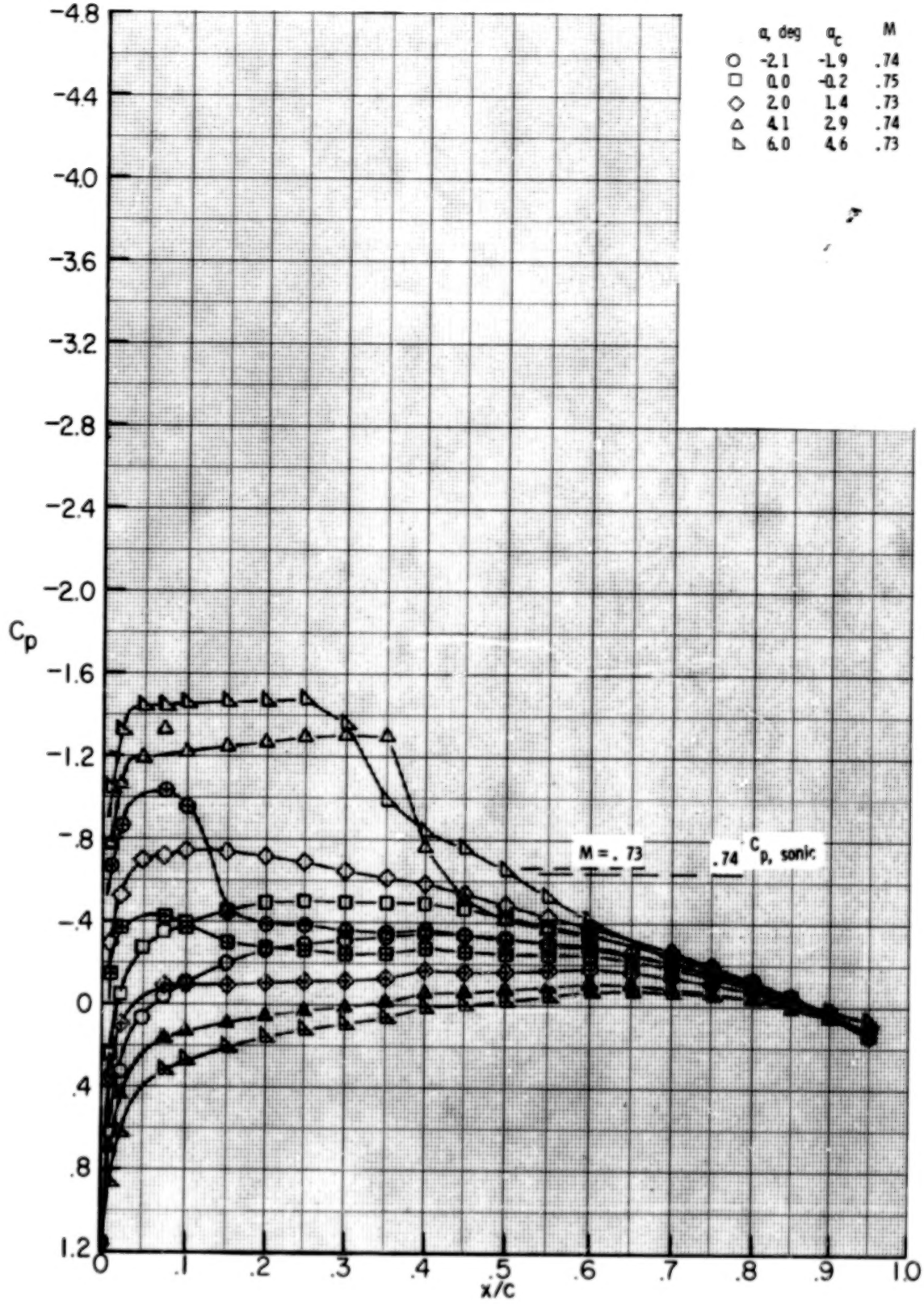

(i) M ~ 0.74; R ~ 8.6 × 10^6.

Figure 16.- Continued.

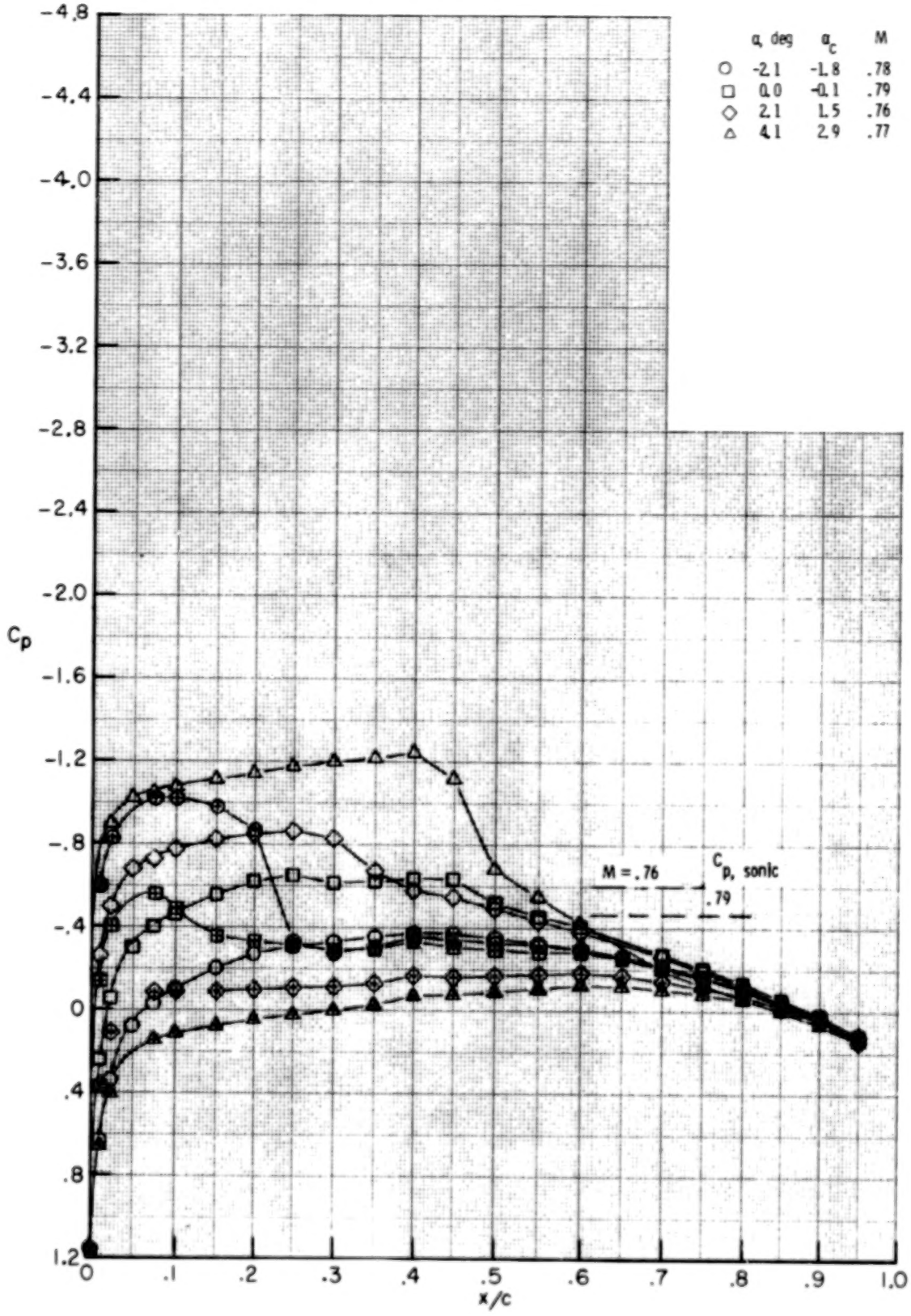

(j) $M \sim 0.78$; $R \sim 8.8 \times 10^6$.

Figure 16.- Continued.

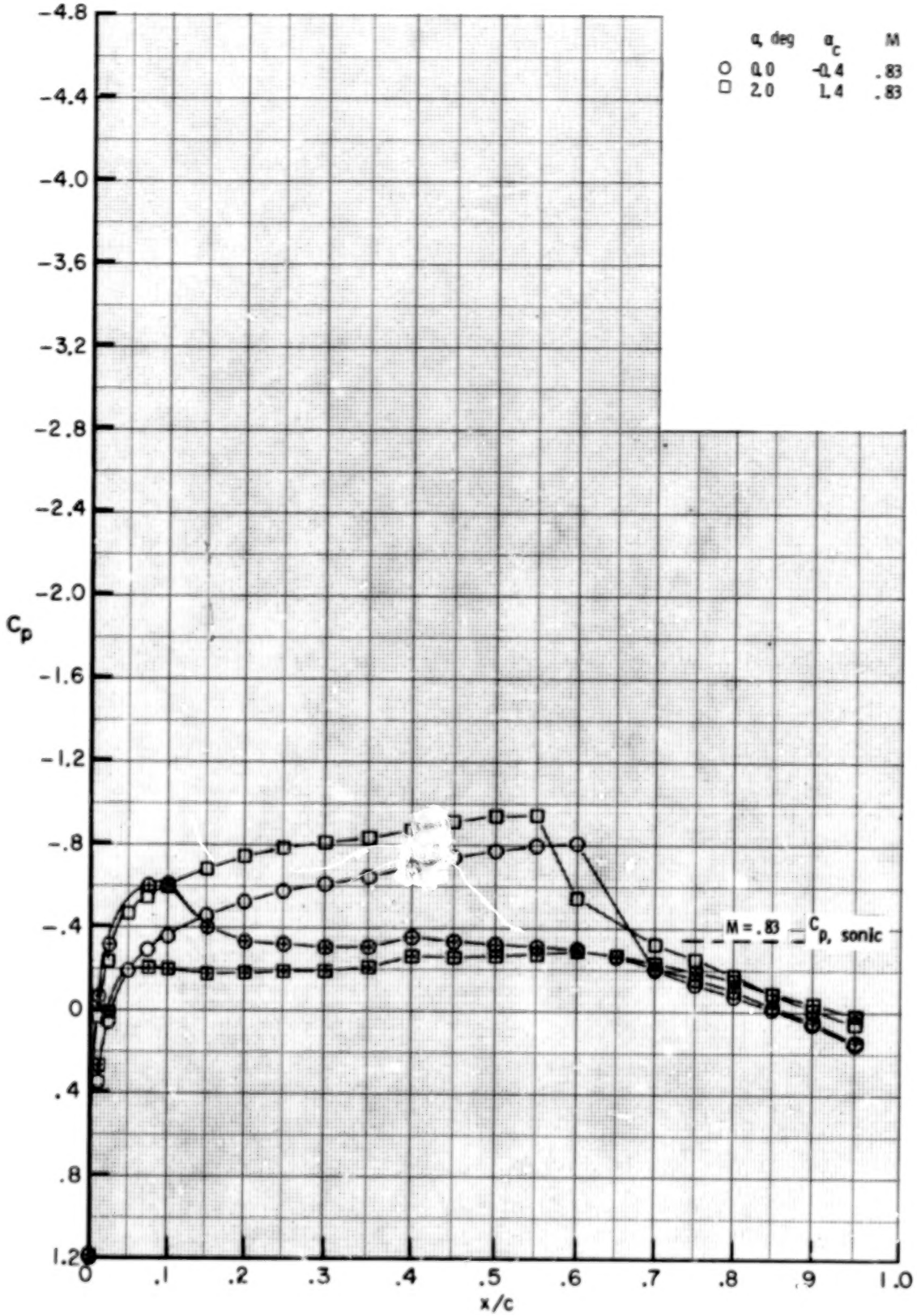

(k) M ~ 0.83; R ~ 9.1×10^6.

Figure 16.- Continued.

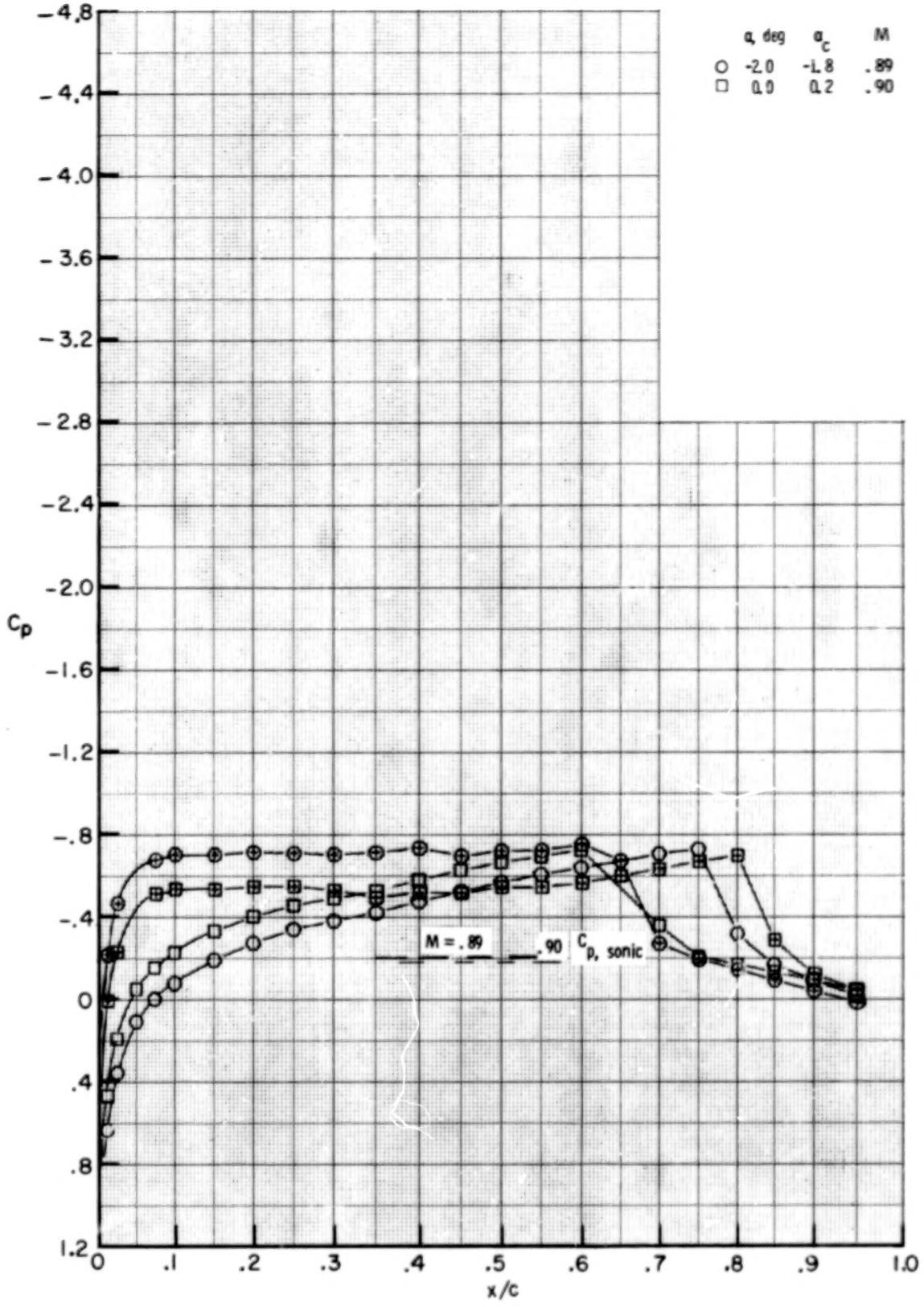

(1) M ≈ 0.90; R ≈ 9.4×10^6.

Figure 16.- Concluded.

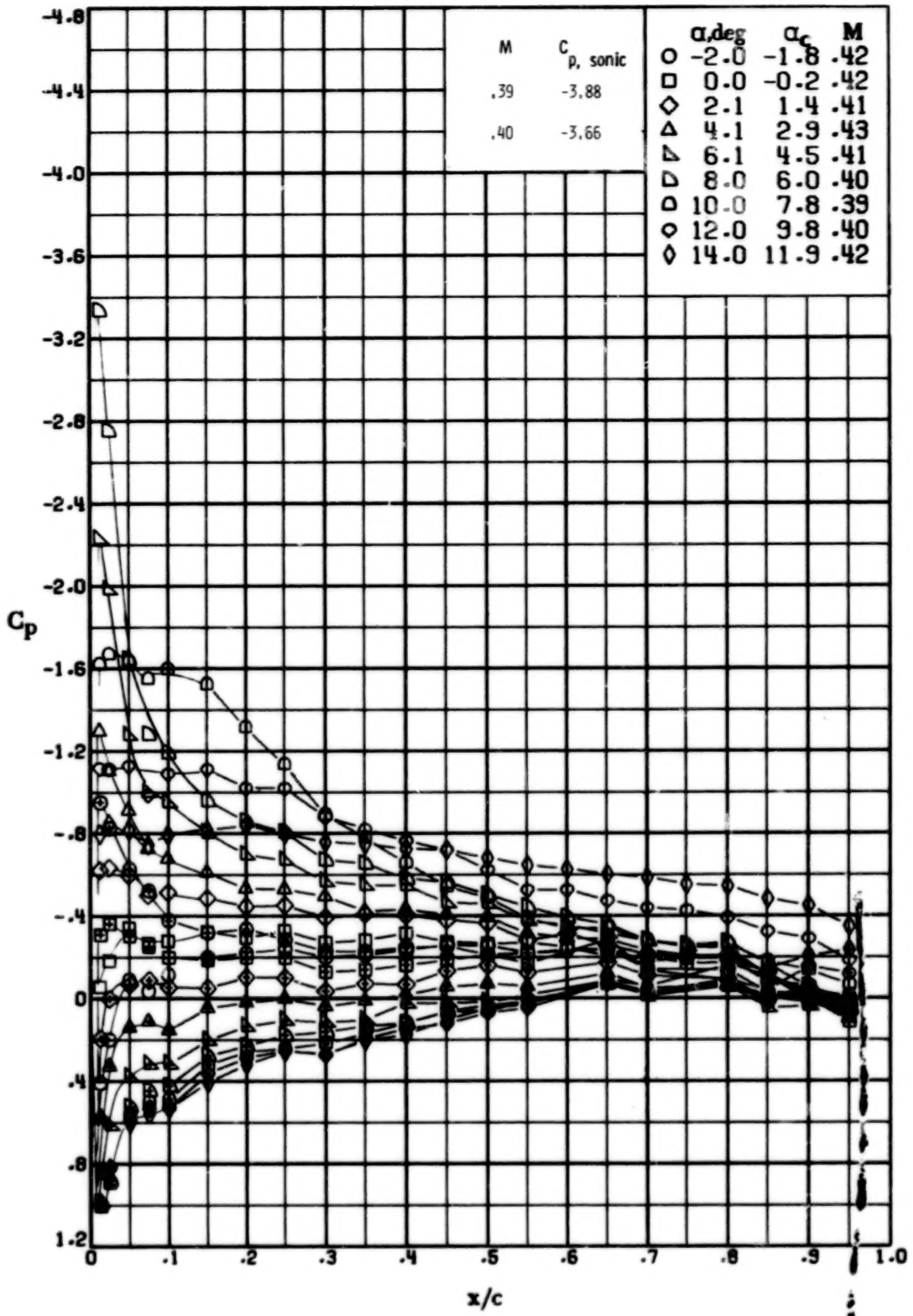

(a) M ≈ 0.40; R ≈ 1.0×10^6.

Figure 17.- Pressure distribution over 08-64C airfoil measured in Langley 6- by 19-inch transonic tunnel. Open symbols indicate model surface smooth; centered symbols indicate lower surface.

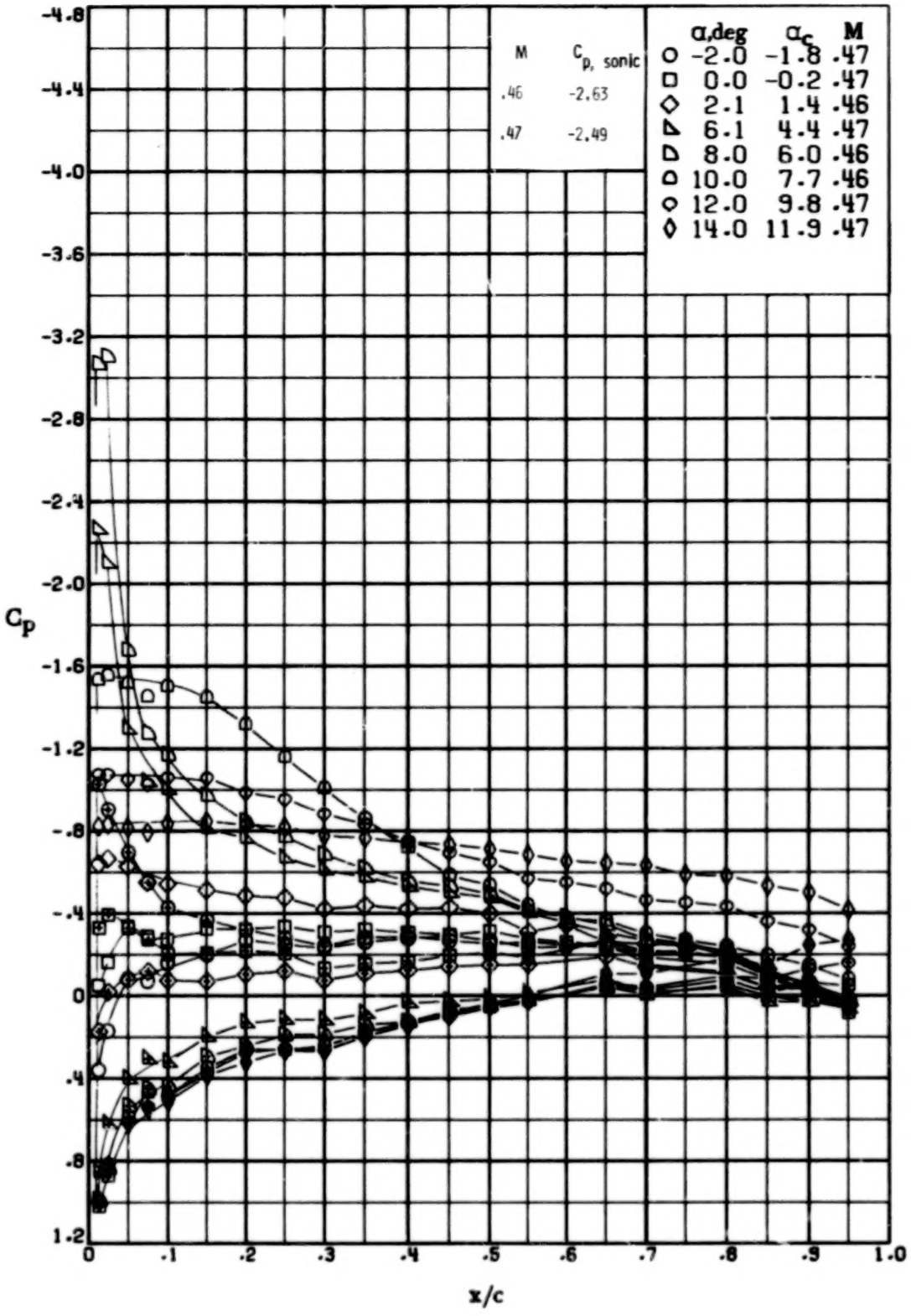

(b) $M \sim 0.47$; $R \sim 1.1 \times 10^6$.

Figure 17.- Continued.

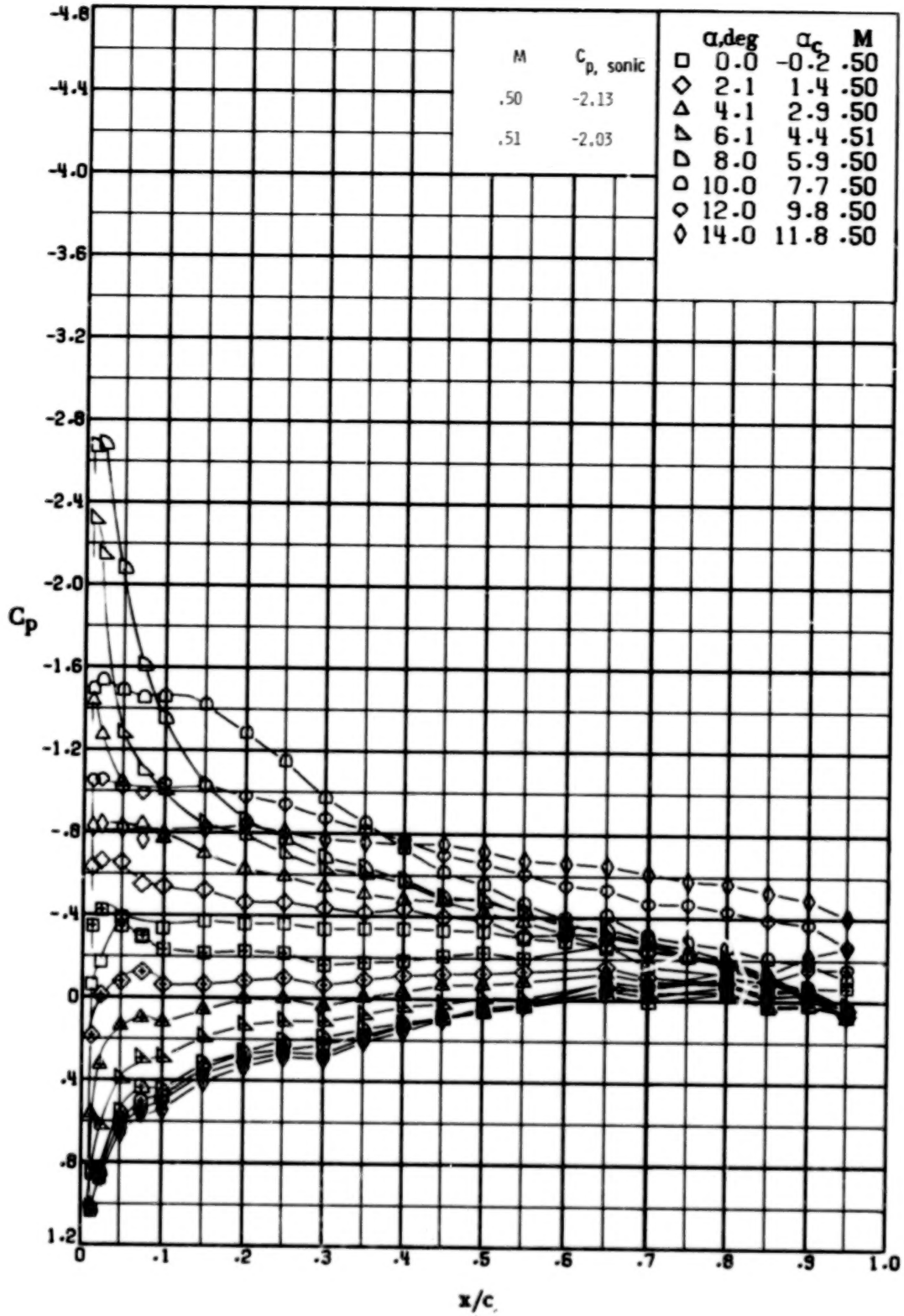

(c) M ~ 0.50; R ~ 1.2×10^6.

Figure 17.- Continued.

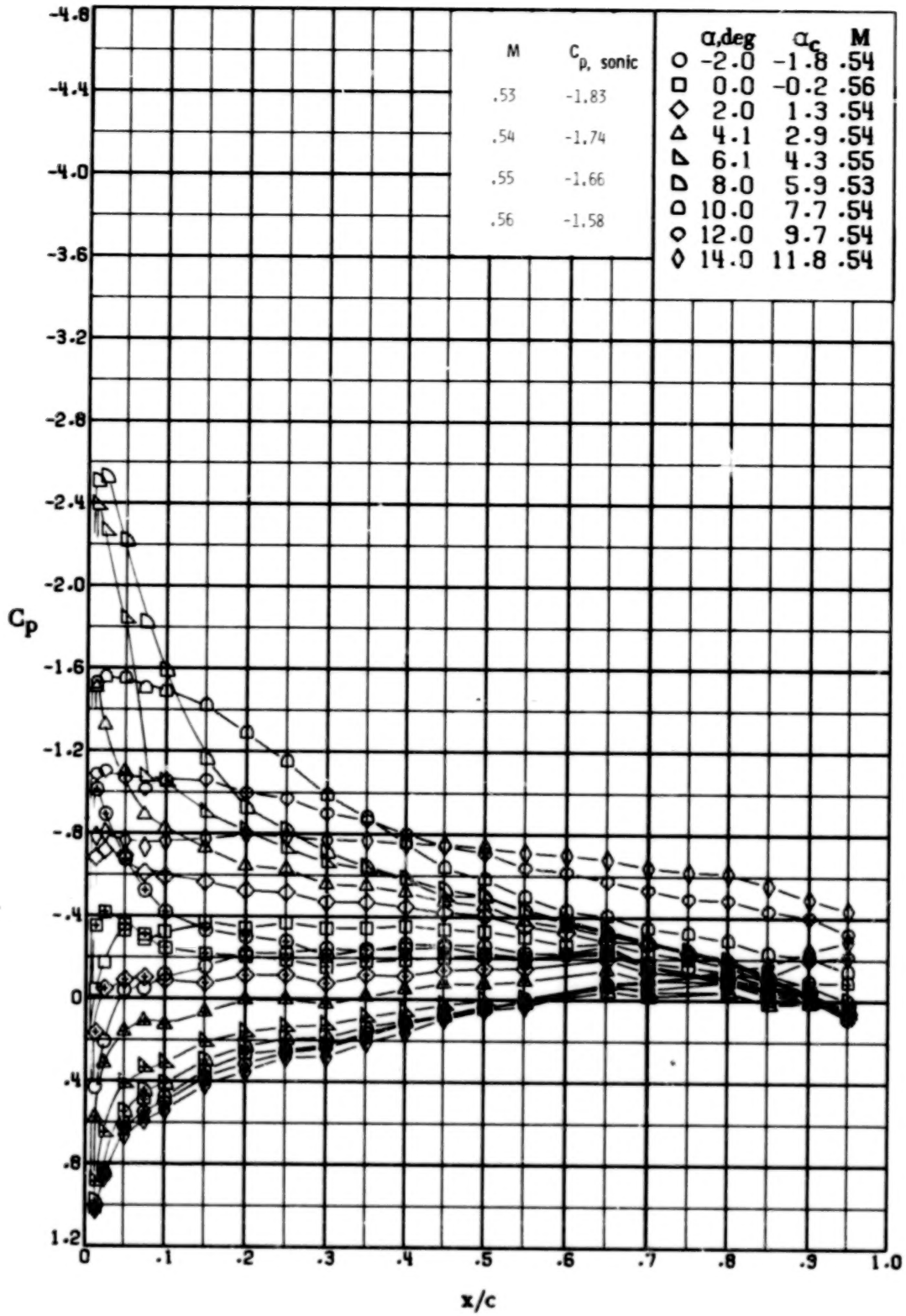

(d) $M \approx 0.54$; $R \approx 1.4 \times 10^6$.

Figure 17.- Continued.

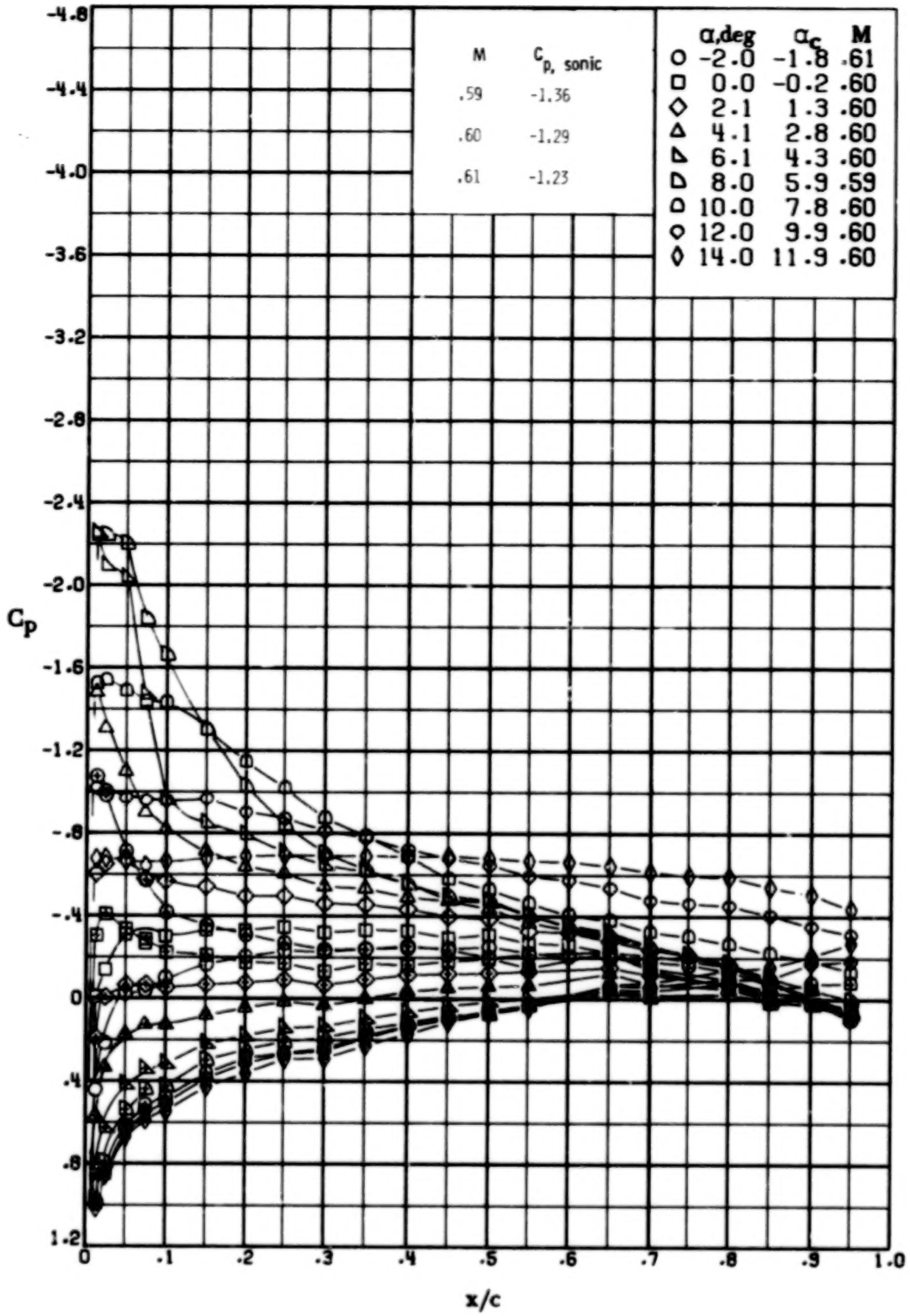

(e) $M \approx 0.60$; $R \approx 1.5 \times 10^6$.

Figure 17.- Continued.

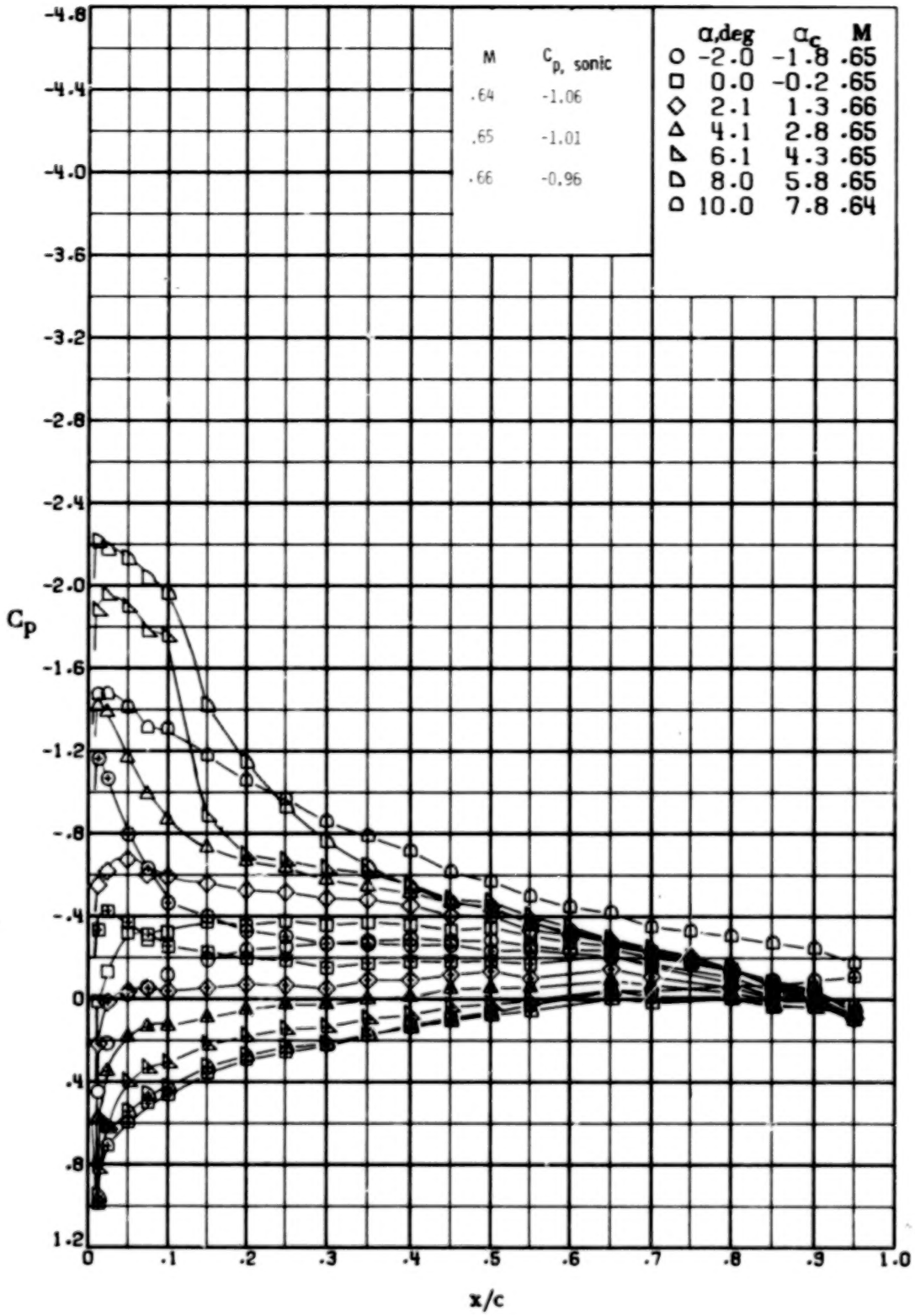

(f) $M \approx 0.65$; $R \approx 1.7 \times 10^6$.

Figure 17.- Continued.

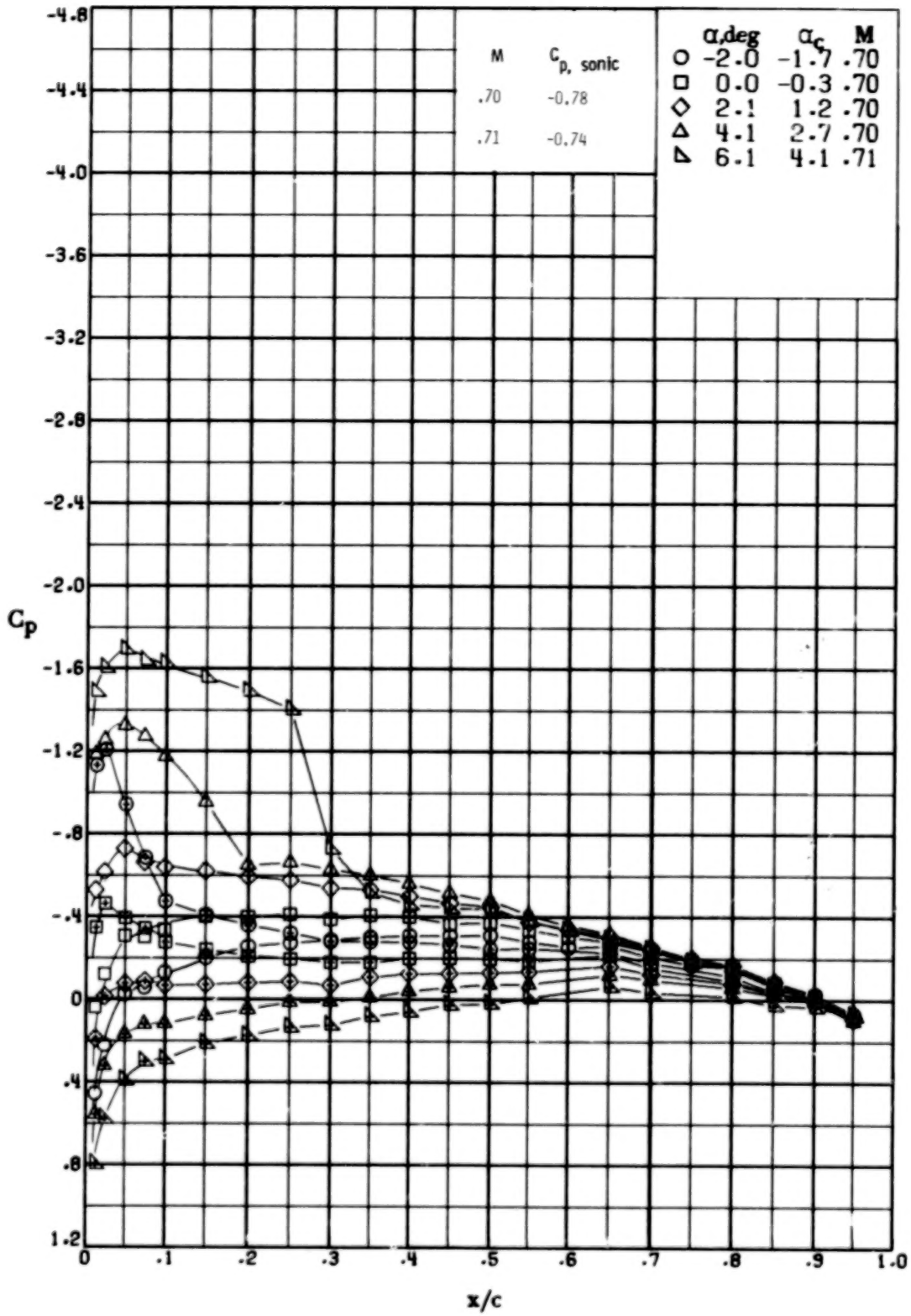

(g) M ≈ 0.70; R ≈ 1.7×10^6.

Figure 17.- Continued.

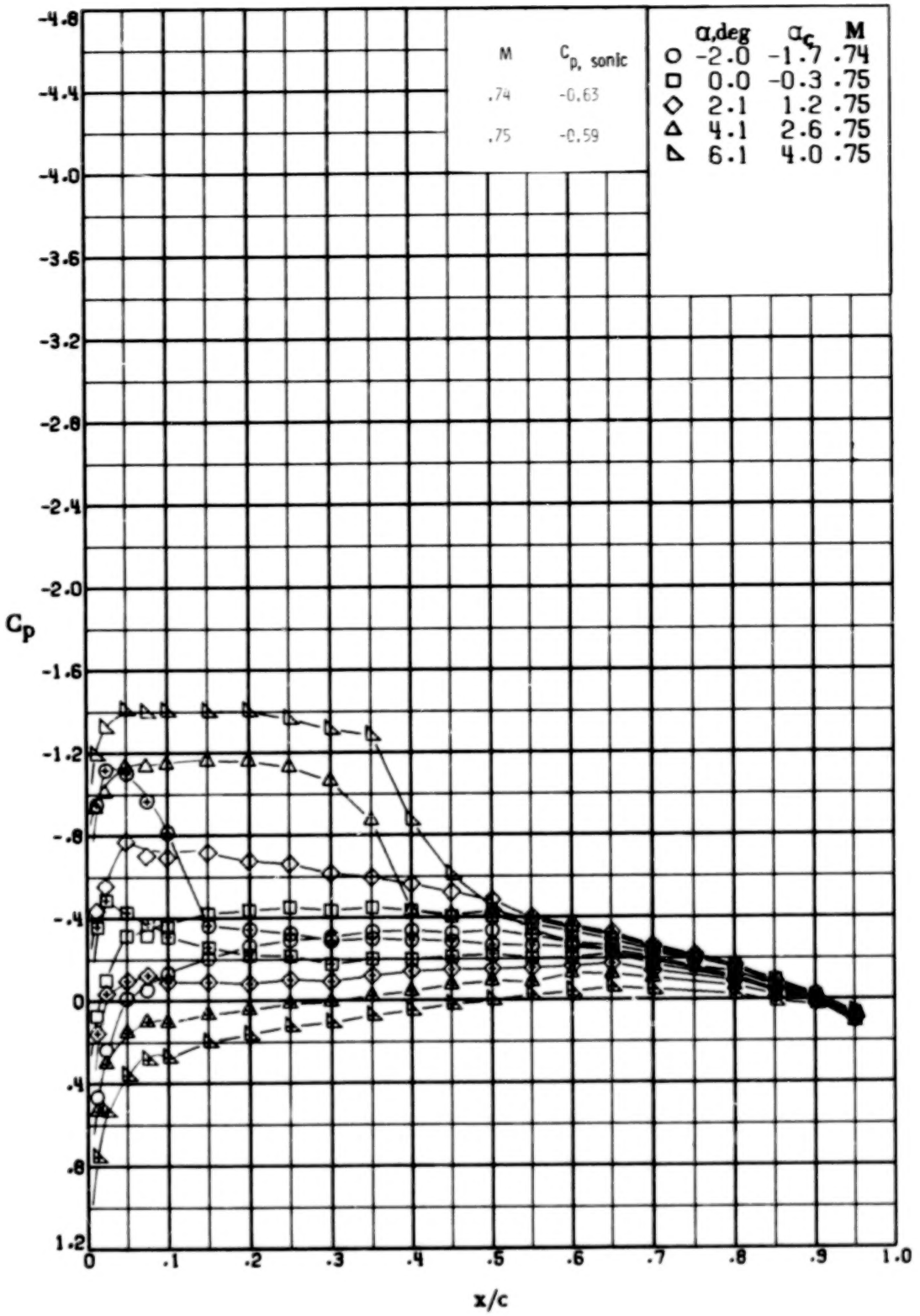

(h) $M \approx 0.75$; $R \approx 1.9 \times 10^6$.

Figure 17.- Continued.

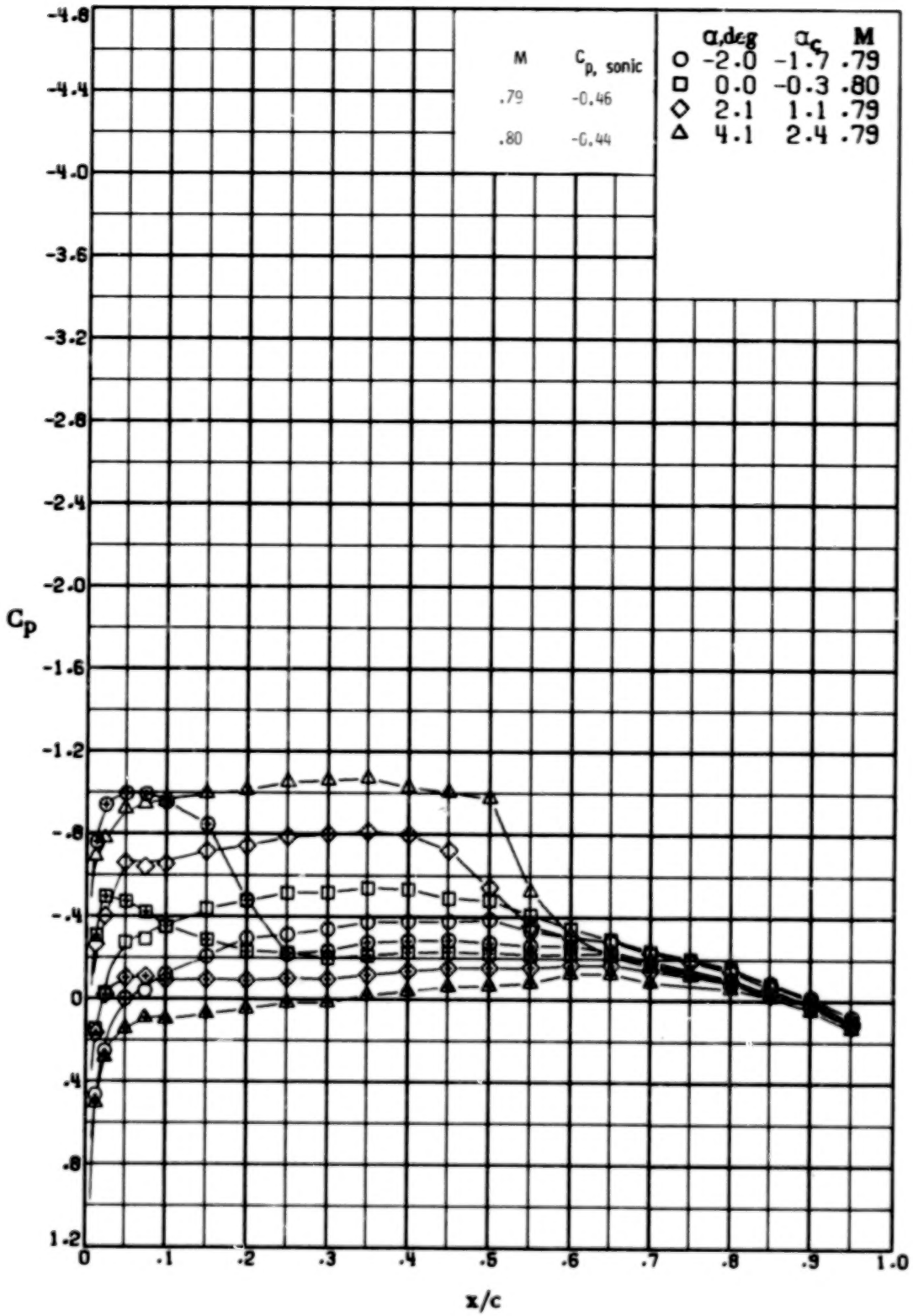

(i) M ≈ 0.79; R ≈ 2.0 × 10^6.

Figure 17.- Continued.

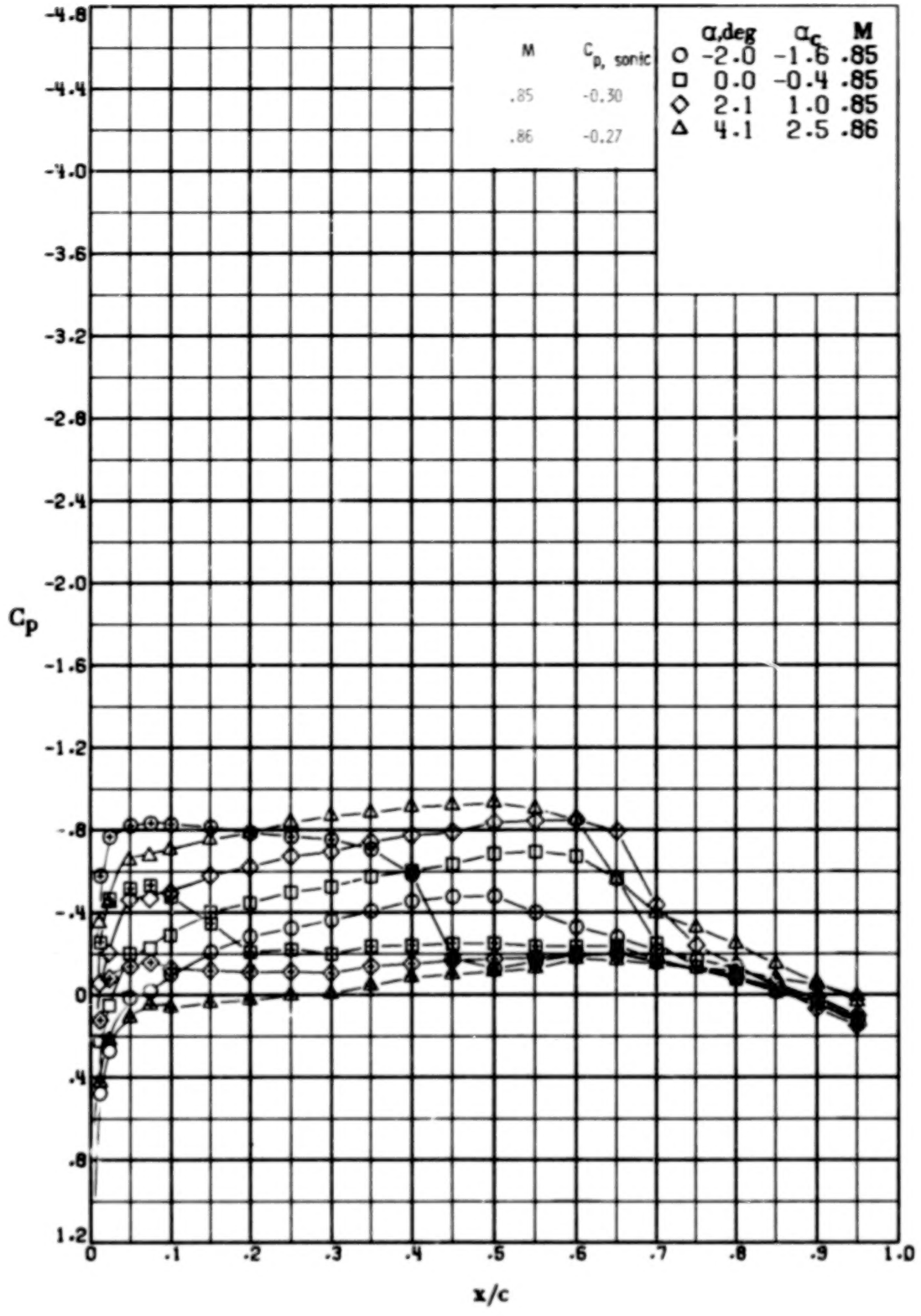

(j) M ≈ 0.85; R ≈ 2.1×10^6.

Figure 17.- Continued.

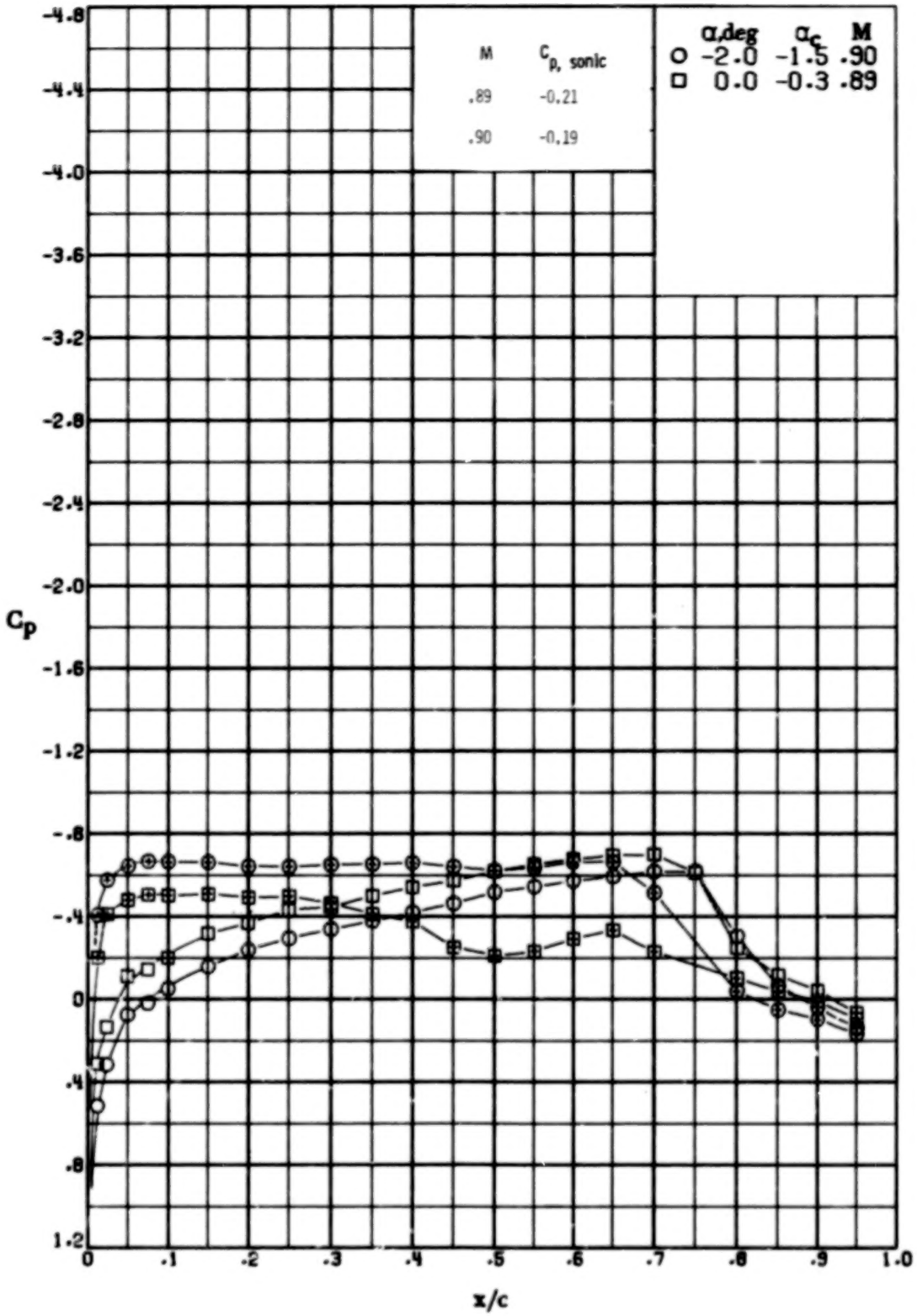

(k) M ≈ 0.90; R ≈ 2.2×10^6.

Figure 17.- Concluded.

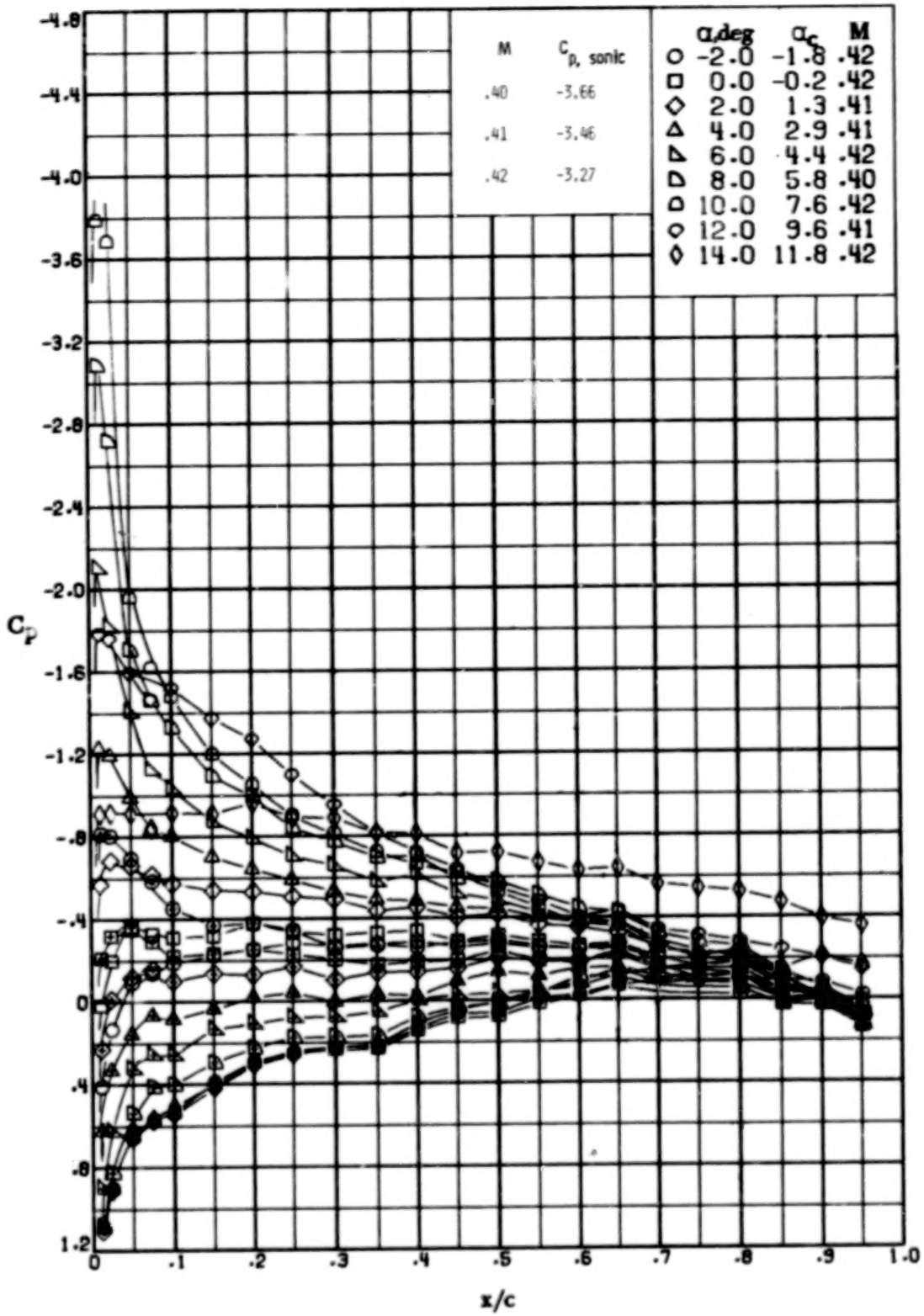

(a) $M \approx 0.42$; $R \approx 1.0 \times 10^6$.

Figure 18.- Pressure distribution over 10-64C airfoil measured in Langley 6- by 19-inch transonic tunnel. Centered symbols indicate lower surface.

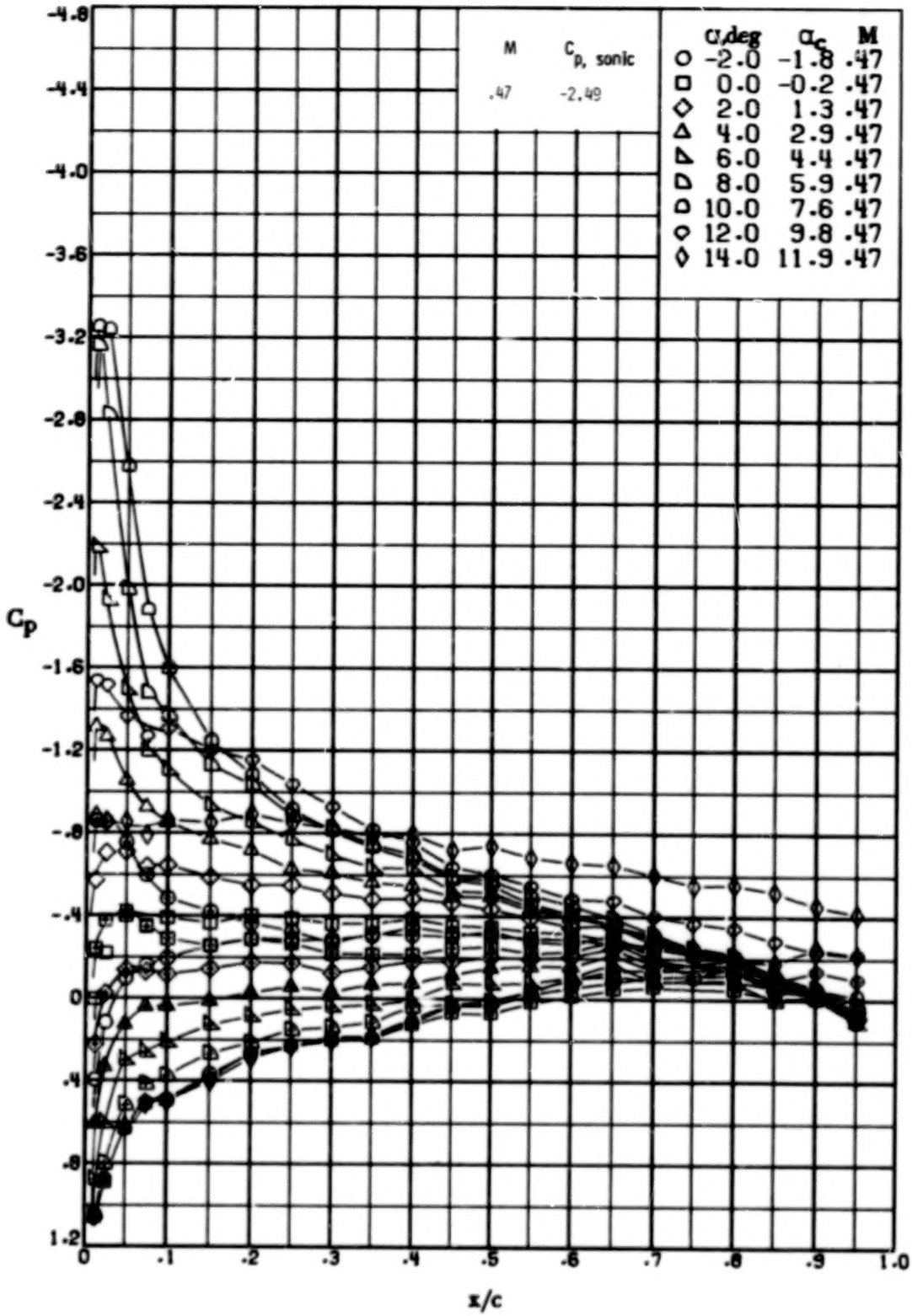

(b) M ~ 0.47; R ~ 1.1×10^6.

Figure 18.- Continued.

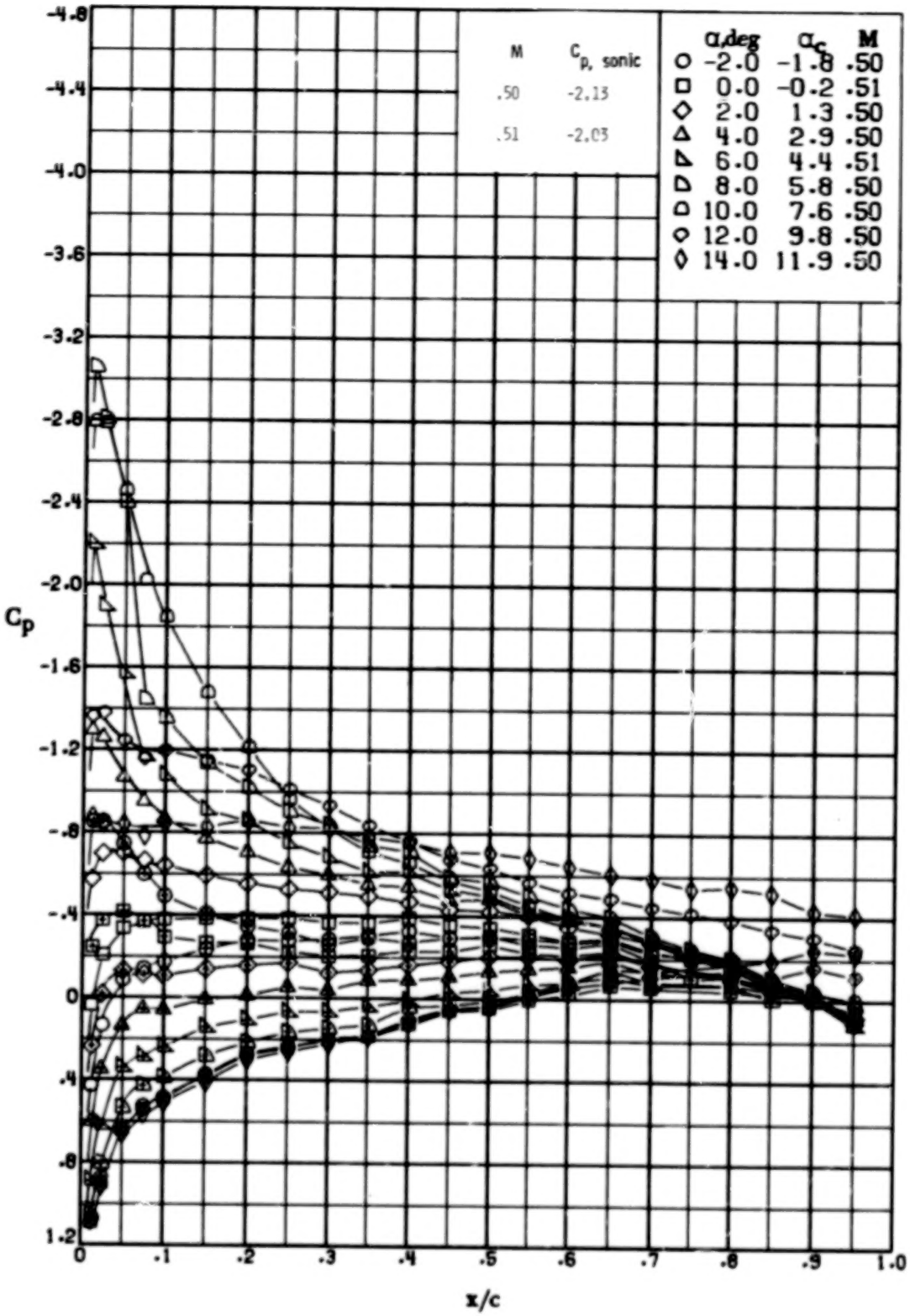

(c) $M \approx 0.50$; $R \approx 1.2 \times 10^6$.

Figure 18.- Continued.

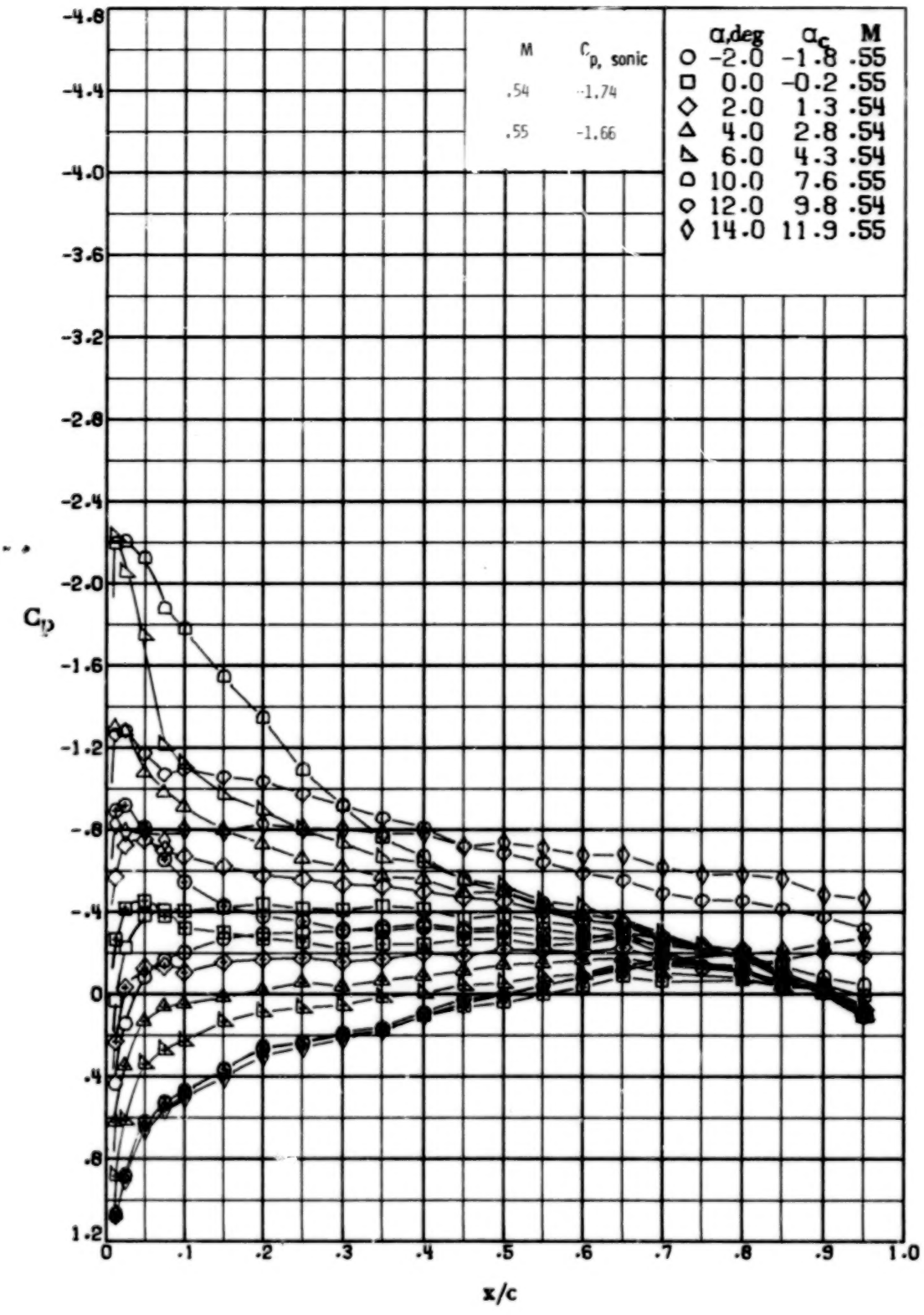

(d) $M \approx 0.55$; $R \approx 1.4 \times 10^6$.

Figure 18.- Continued.

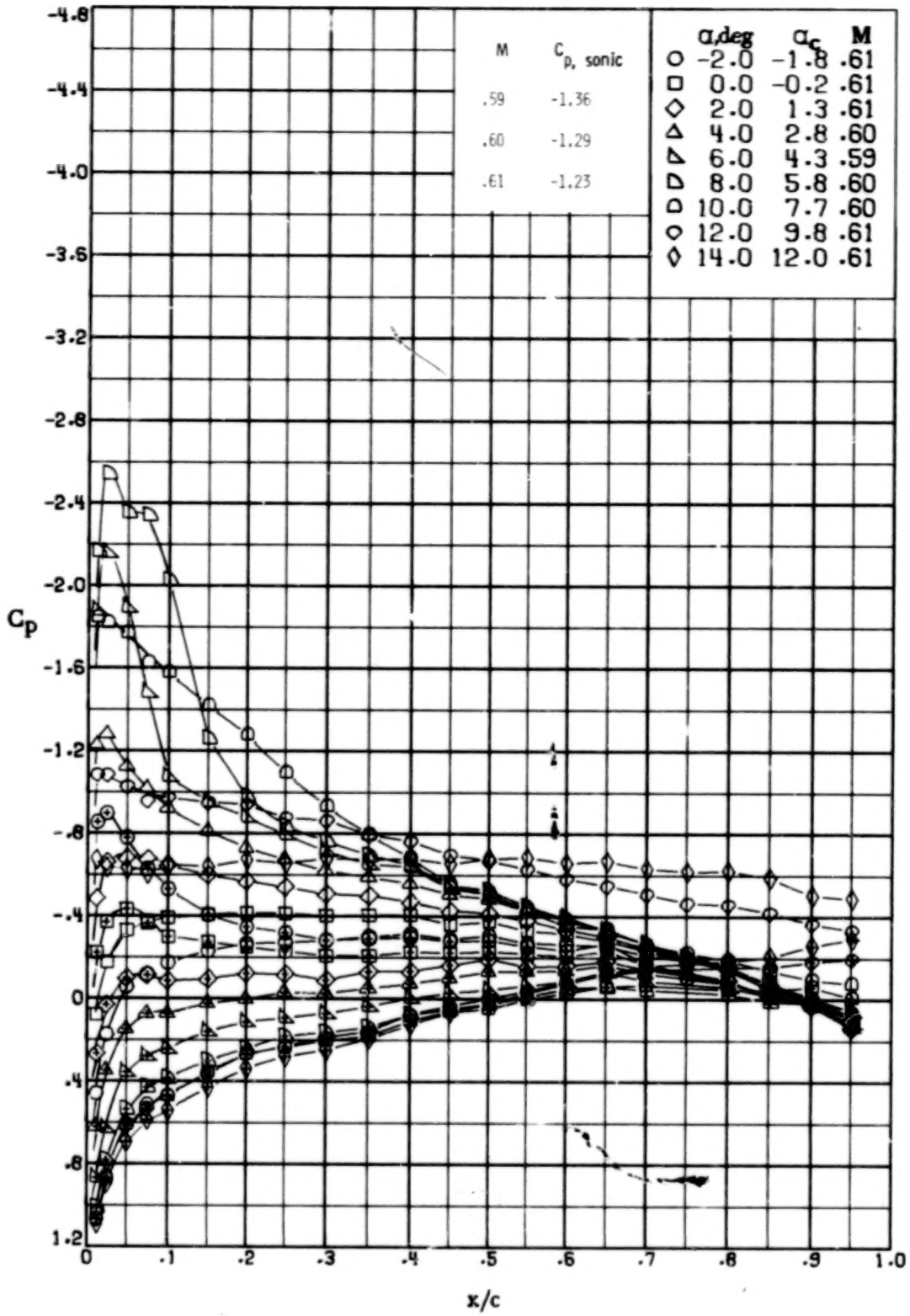

(e) M ≈ 0.60; R ≈ 1.5×10^6.

Figure 18.- Continued.

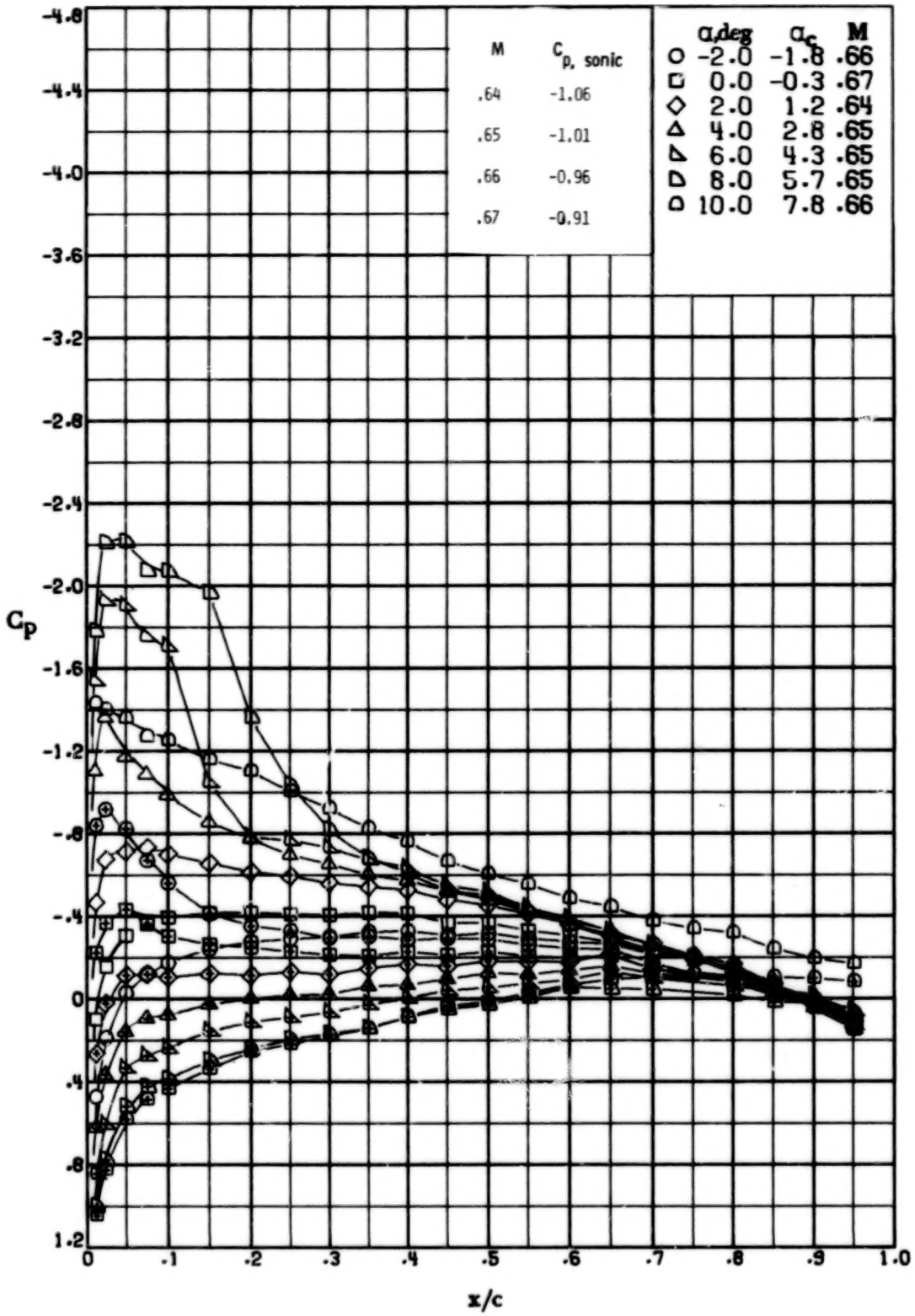

(f) M ≈ 0.65; R ≈ 1.7×10^6.

Figure 18.- Continued.

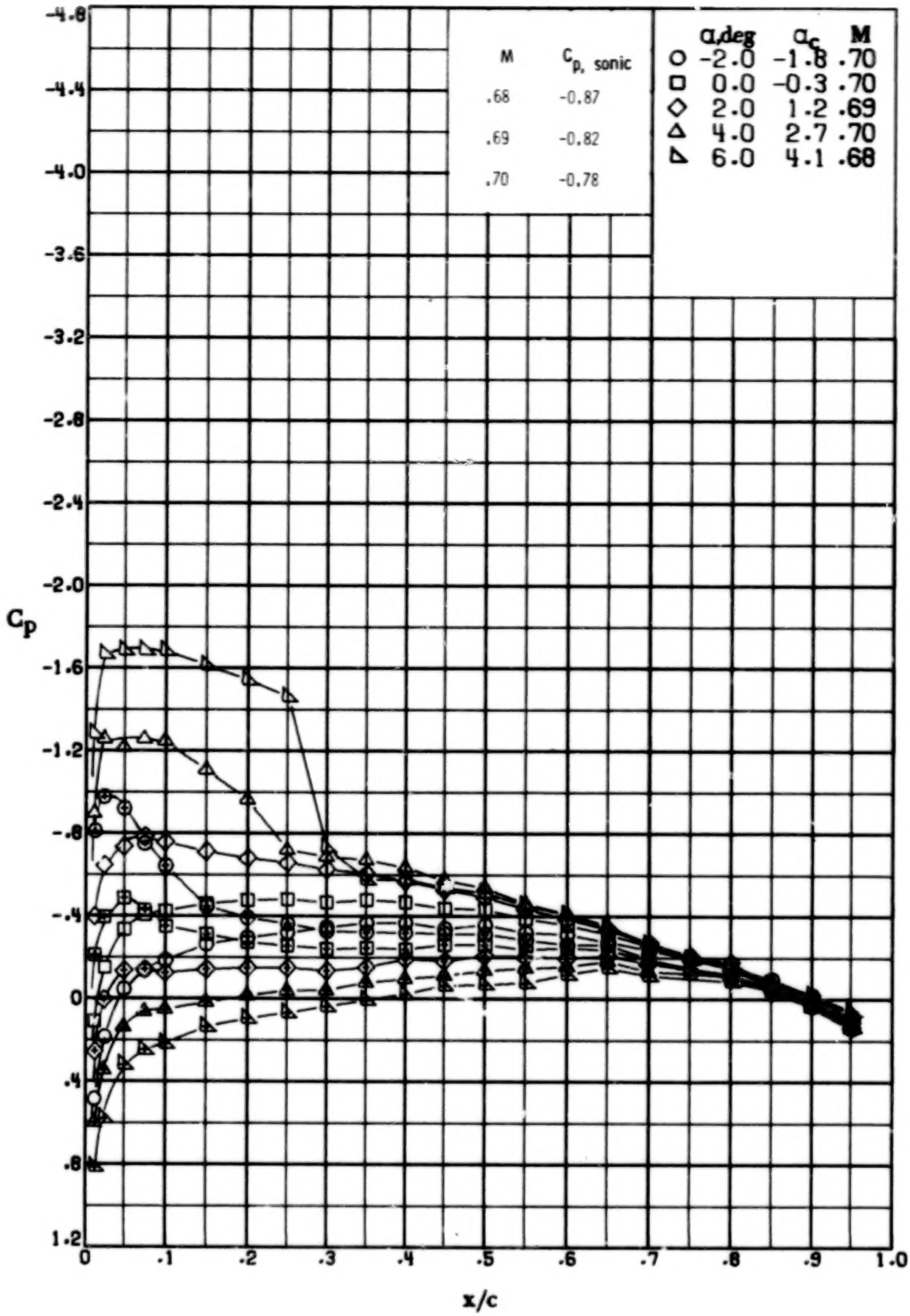

(g) M ≈ 0.69; R ≈ 1.8×10^6.

Figure 18.- Continued.

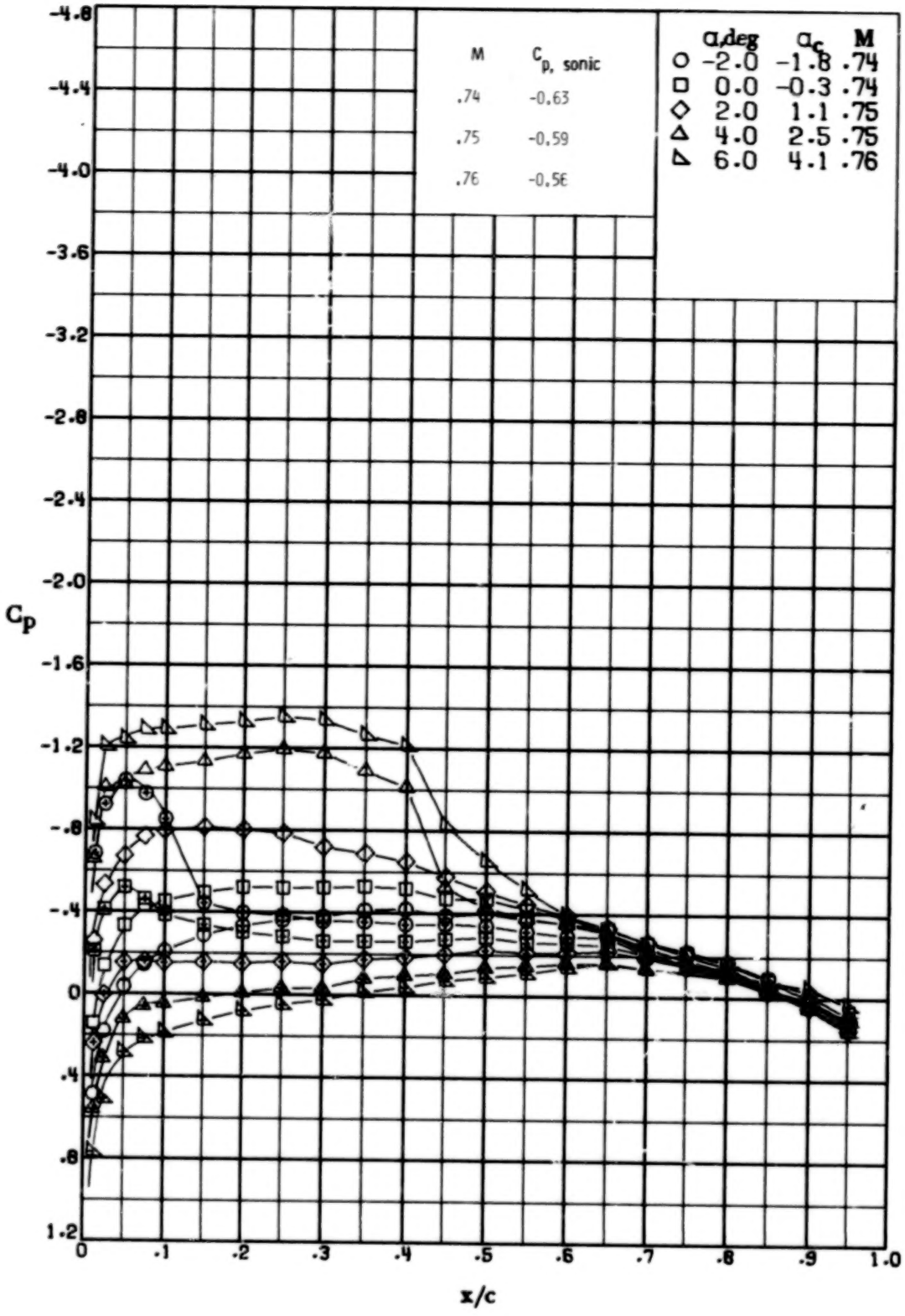

(h) M ≈ 0.75; R ≈ 1.9 × 10^6.

Figure 18.- Continued.

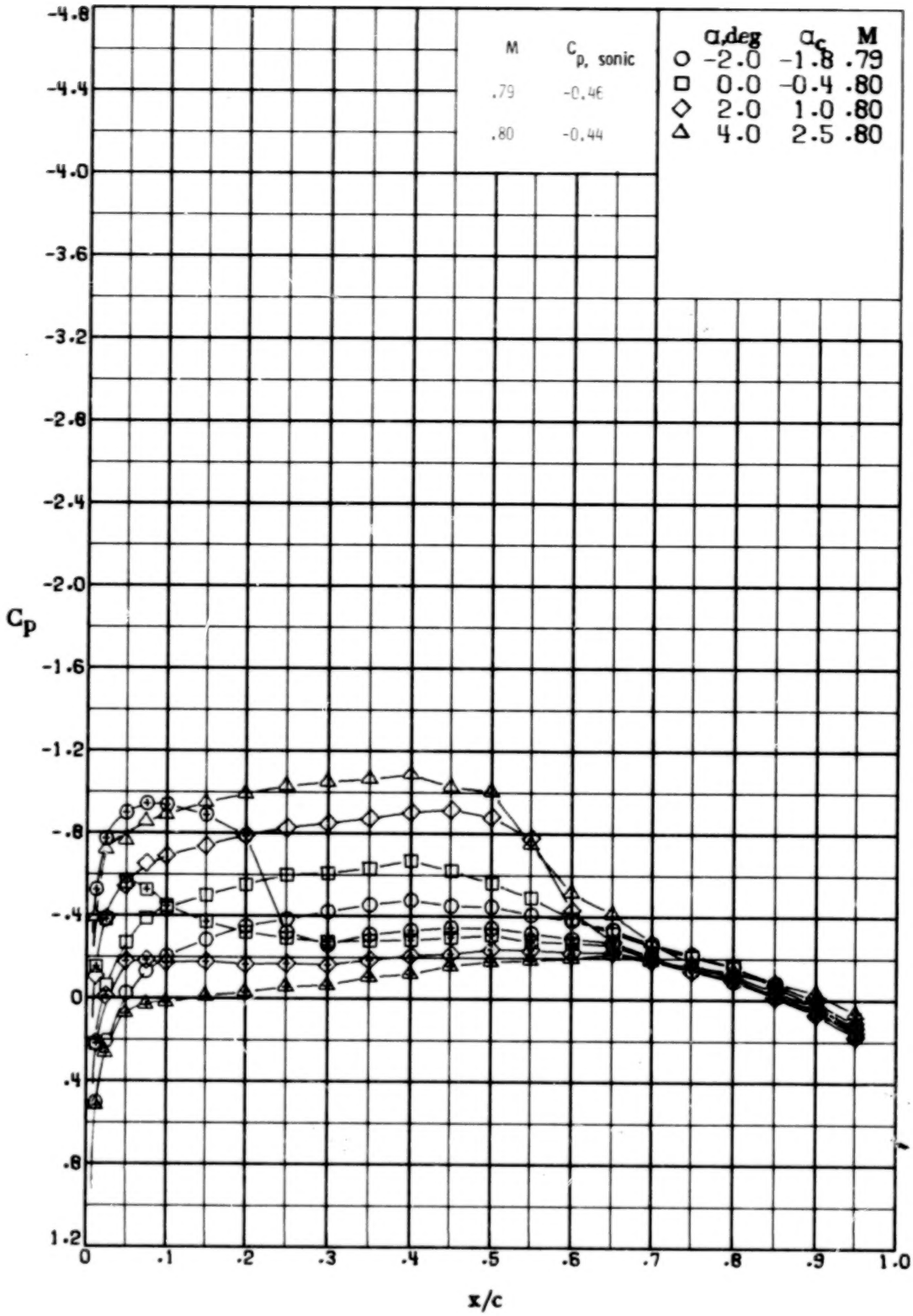

(i) $M \approx 0.80$; $R \approx 2.0 \times 10^6$.

Figure 18.- Continued.

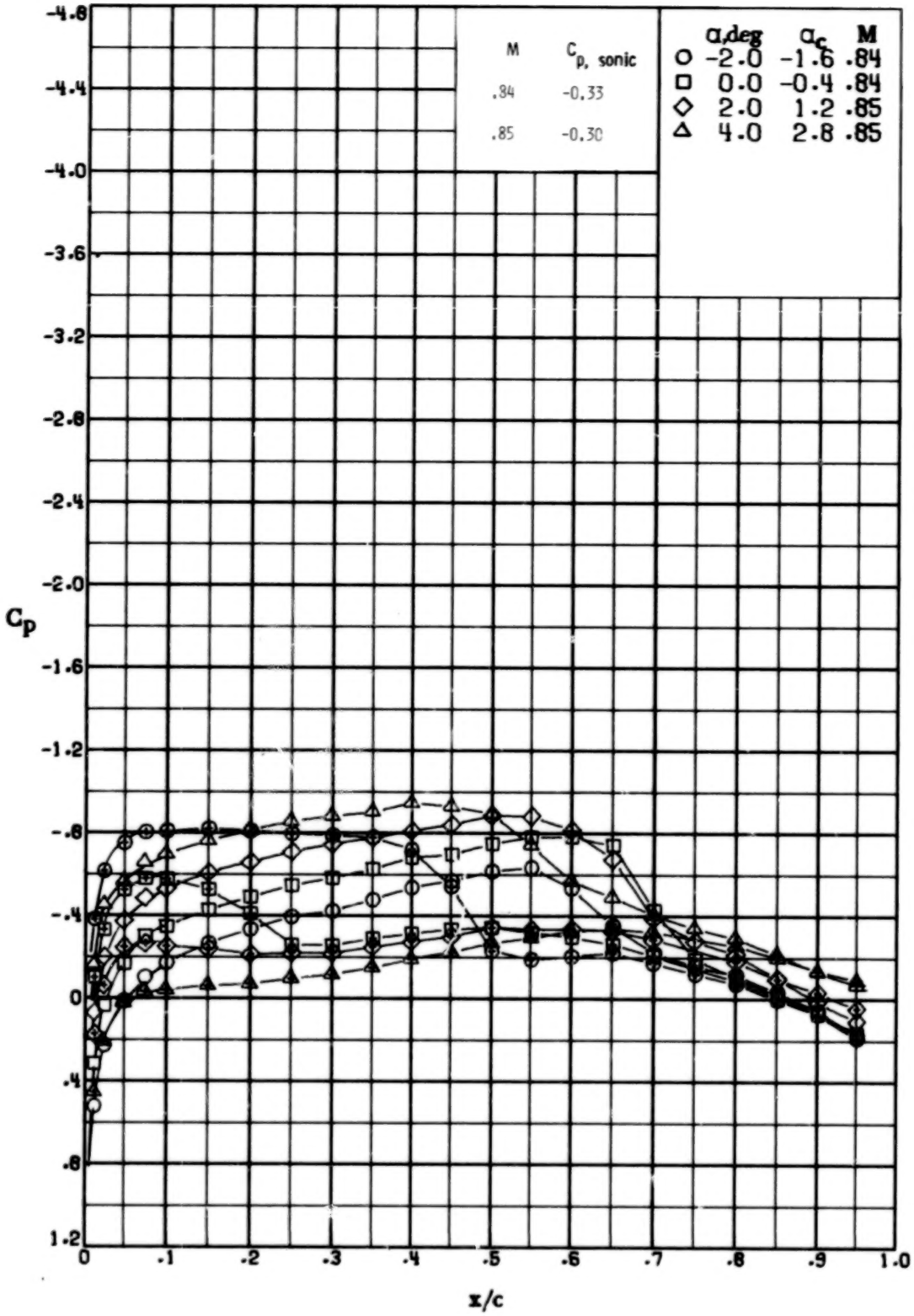

(j) M ≈ 0.85; R ≈ 2.1 × 10^6.

Figure 18.- Continued.

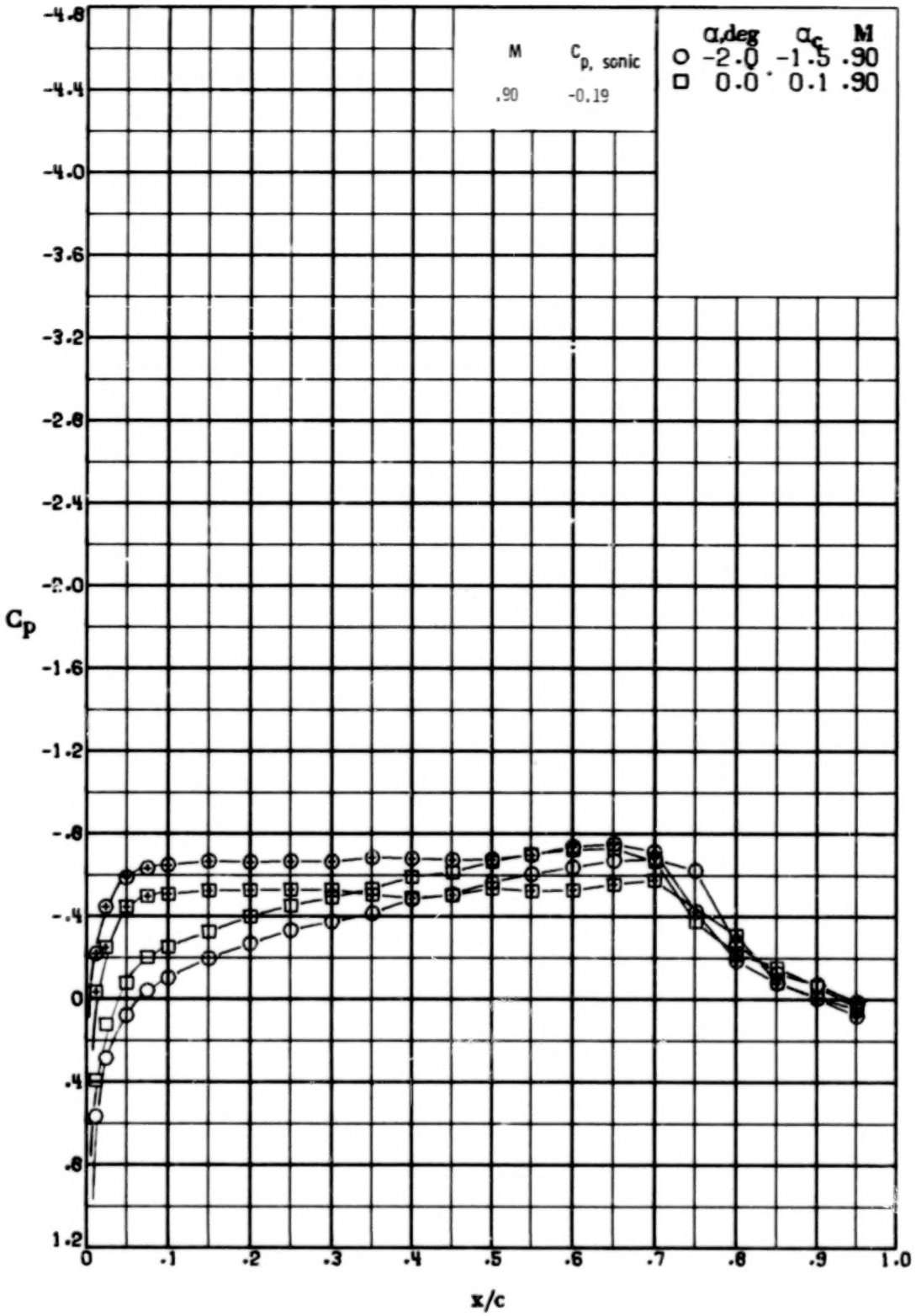

(k) M ≈ 0.90; R ≈ 2.2 × 10^6.

Figure 18.- Concluded.

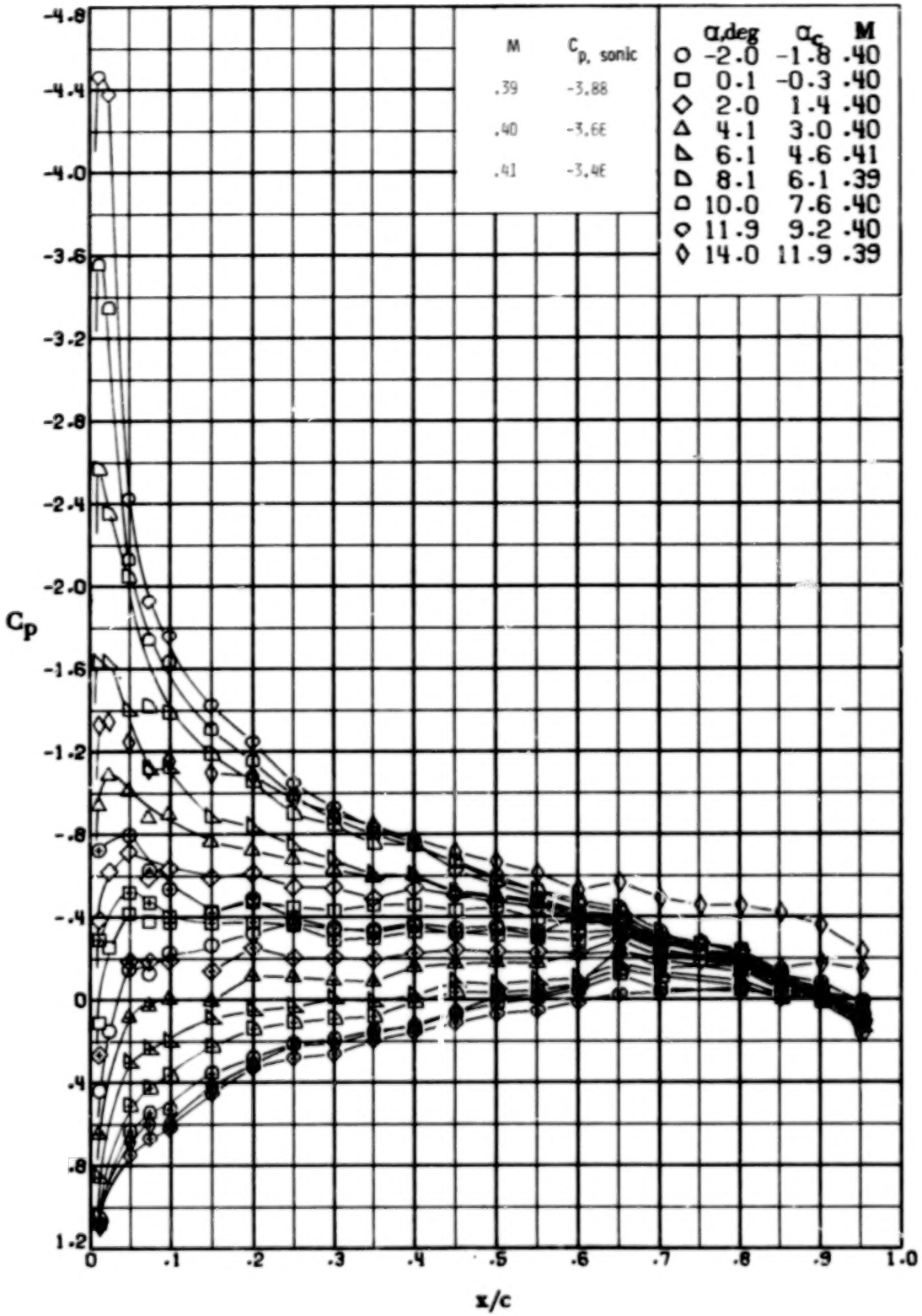

(a) $M \approx 0.40$; $R \approx 1.0 \times 10^6$.

Figure 19.- Pressure distribution over 12-64C airfoil measured in Langley 6- by 19-inch transonic tunnel. Centered symbols indicate lower surface.

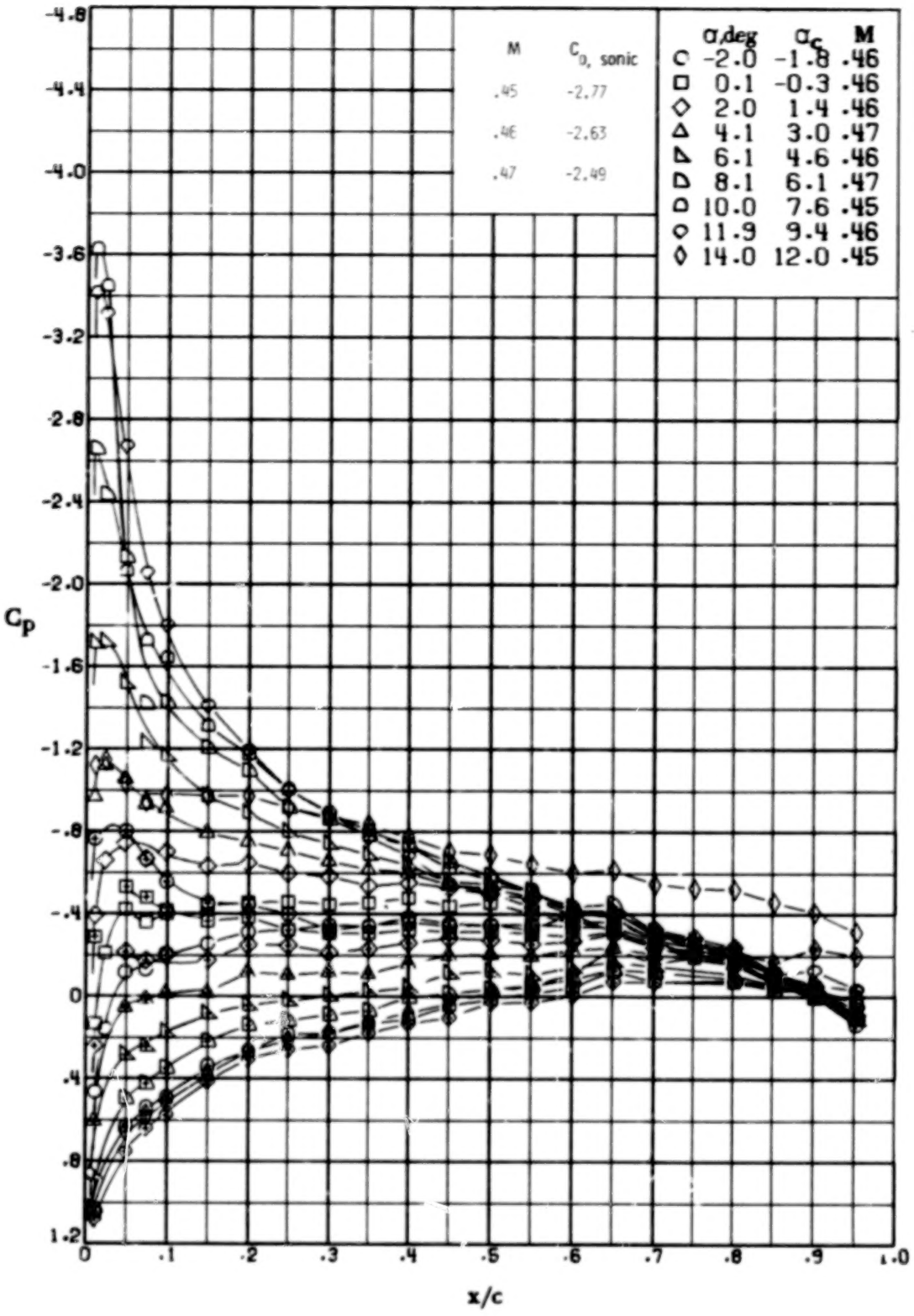

(b) $M \approx 0.46$; $R \approx 1.1 \times 10^6$.

Figure 19.- Continued.

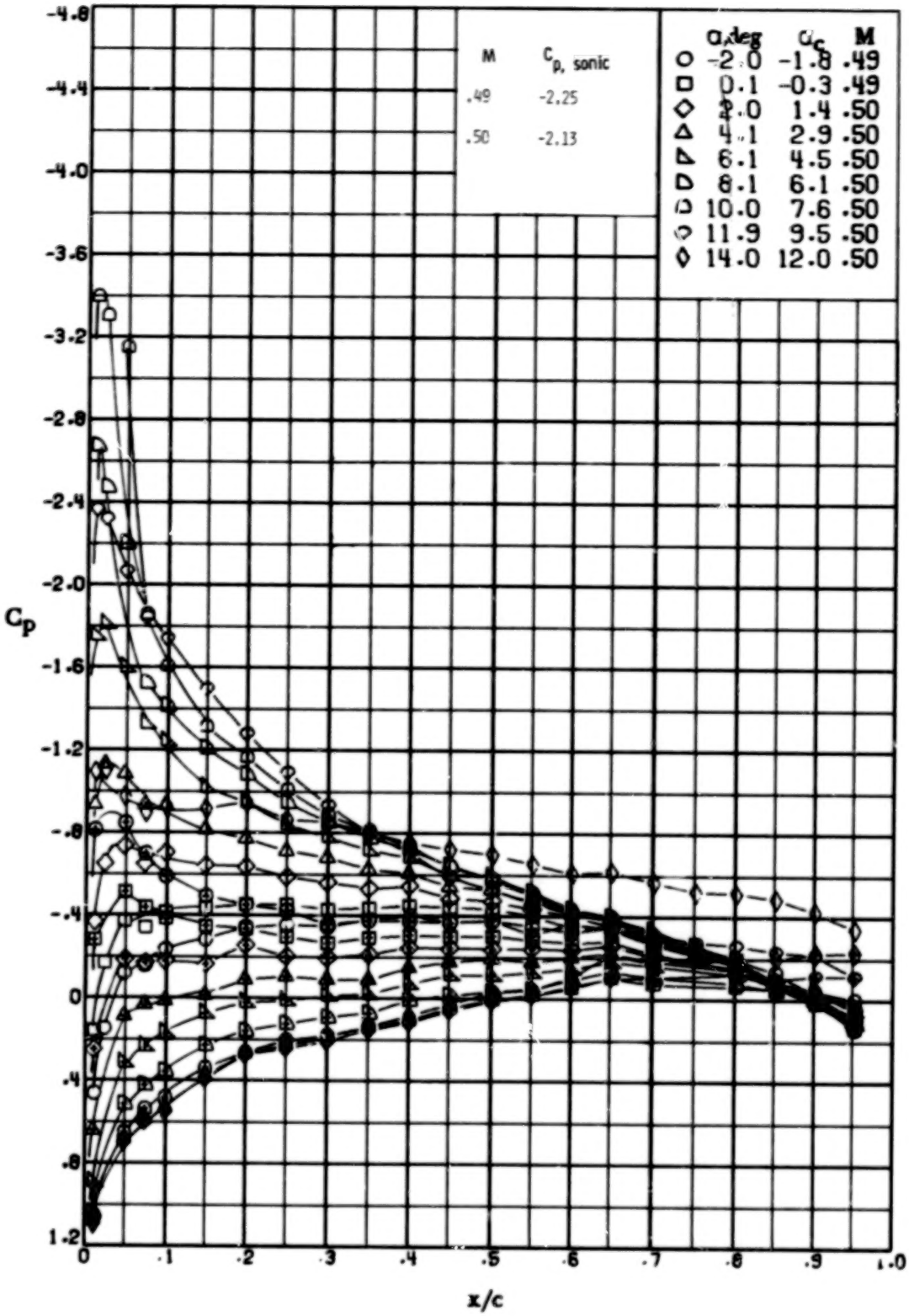

(c) M ≈ 0.50; R ≈ 1.2×10^6.

Figure 19.- Continued.

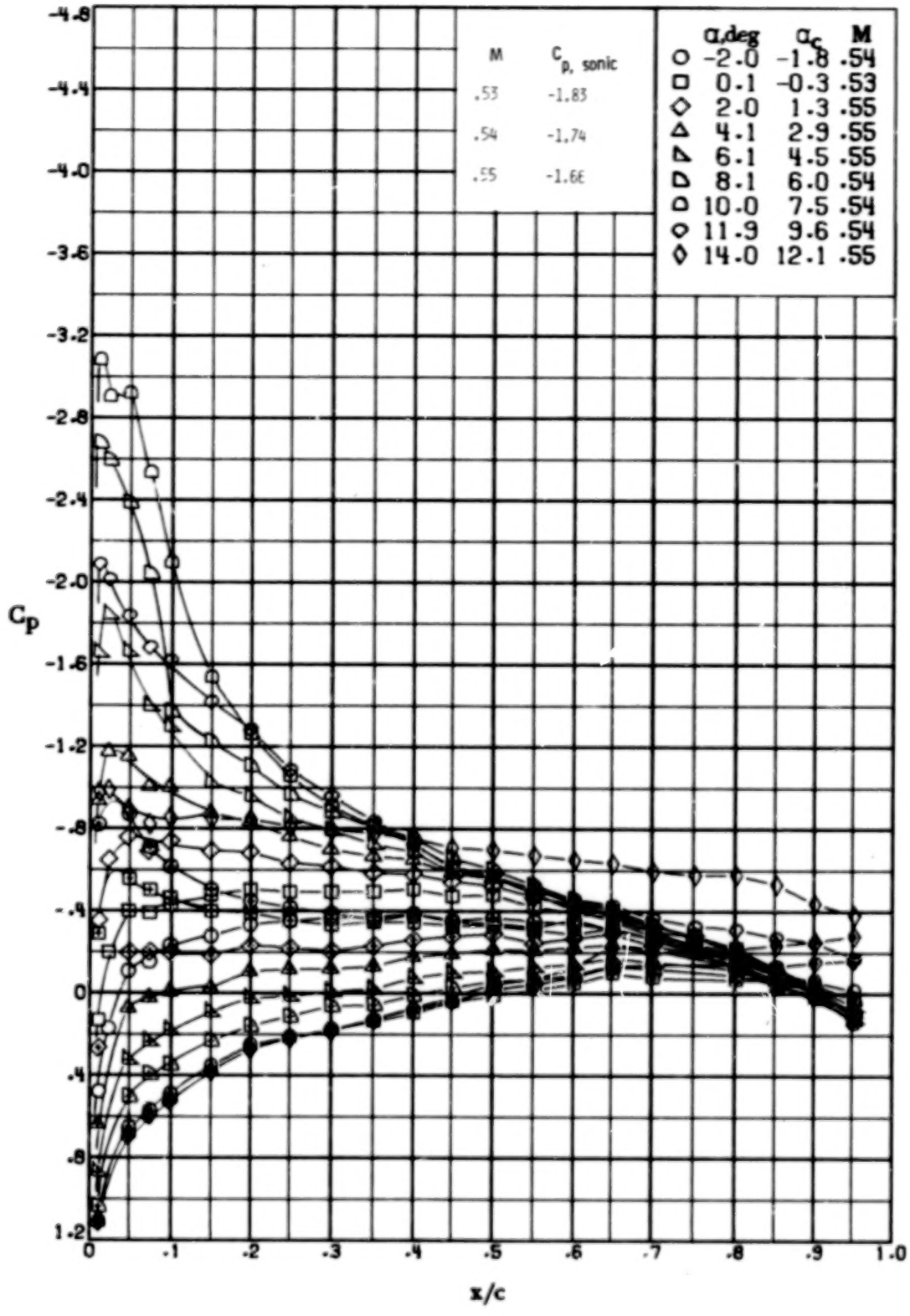

(d) M ~ 0.54; R ~ 1.4×10^6.

Figure 19.- Continued.

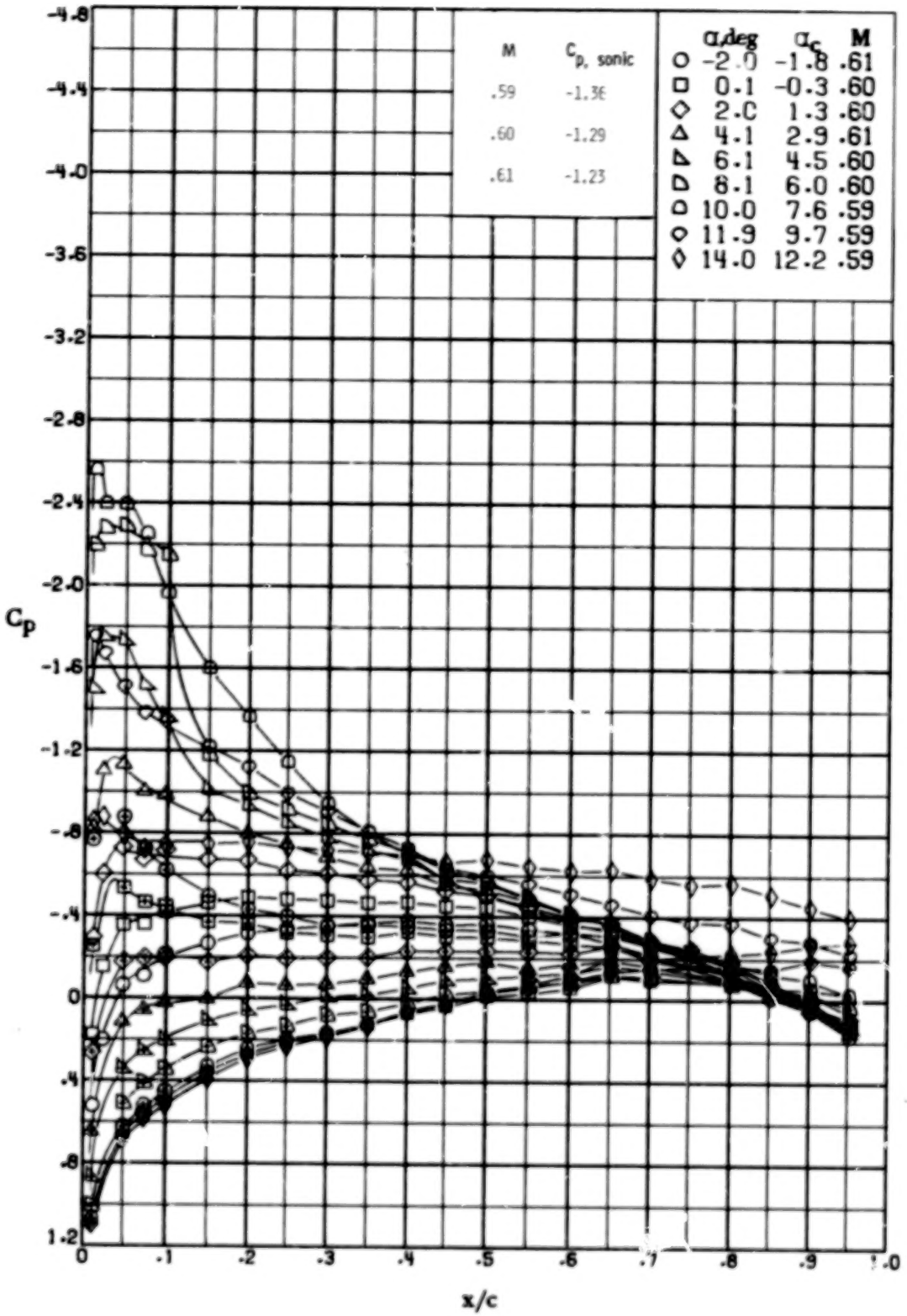

(e) M ≈ 0.60; R ≈ 1.5×10^6.

Figure 19.- Continued.

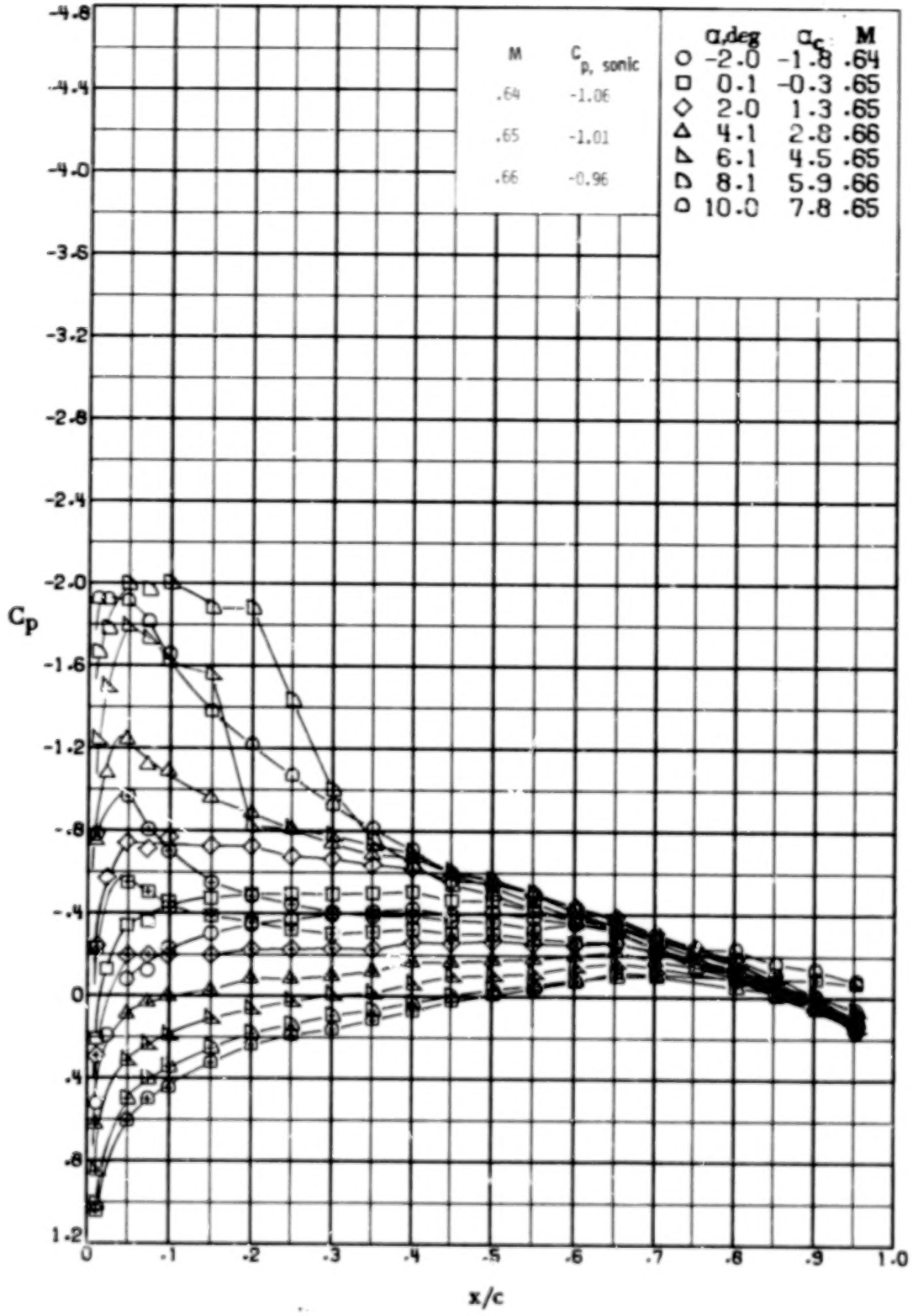

(f) $M \approx 0.65$; $R \approx 1.6 \times 10^6$.

Figure 19.- Continued.

830-H-15

NAS 1.60:1396

MAY 1979

NASA
Technical Paper 1396

AVRADCOM
Technical Report 79-11

COMPLETED
ORIGINAL

Experimental Investigation of Three Helicopter Rotor Airfoils Designed Analytically

Gene J. Bingham and Kevin W. Noonan

APRIL 1979

95

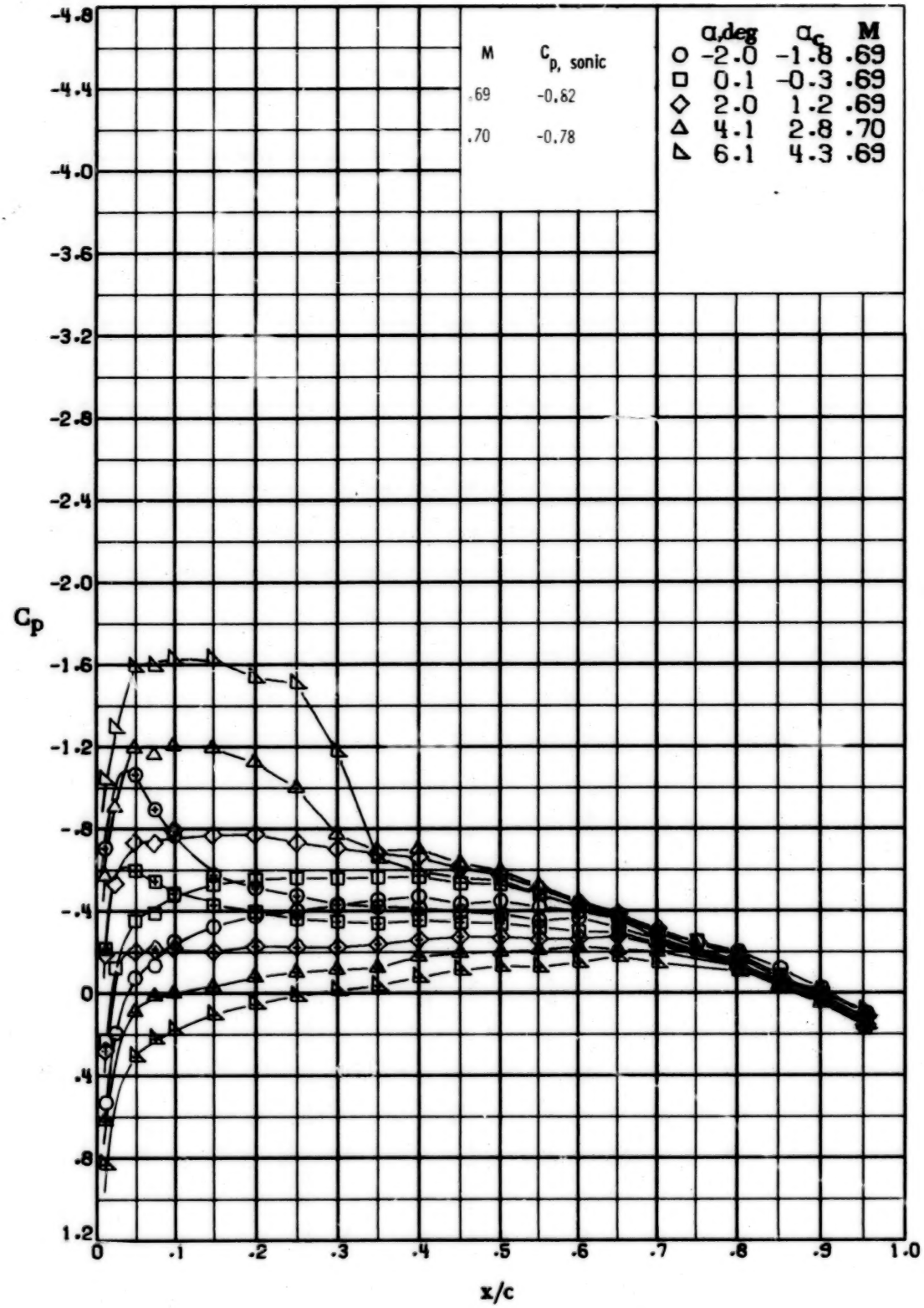

(g) M ≈ 0.69; R ≈ 1.8×10^6.

Figure 19.- Continued.

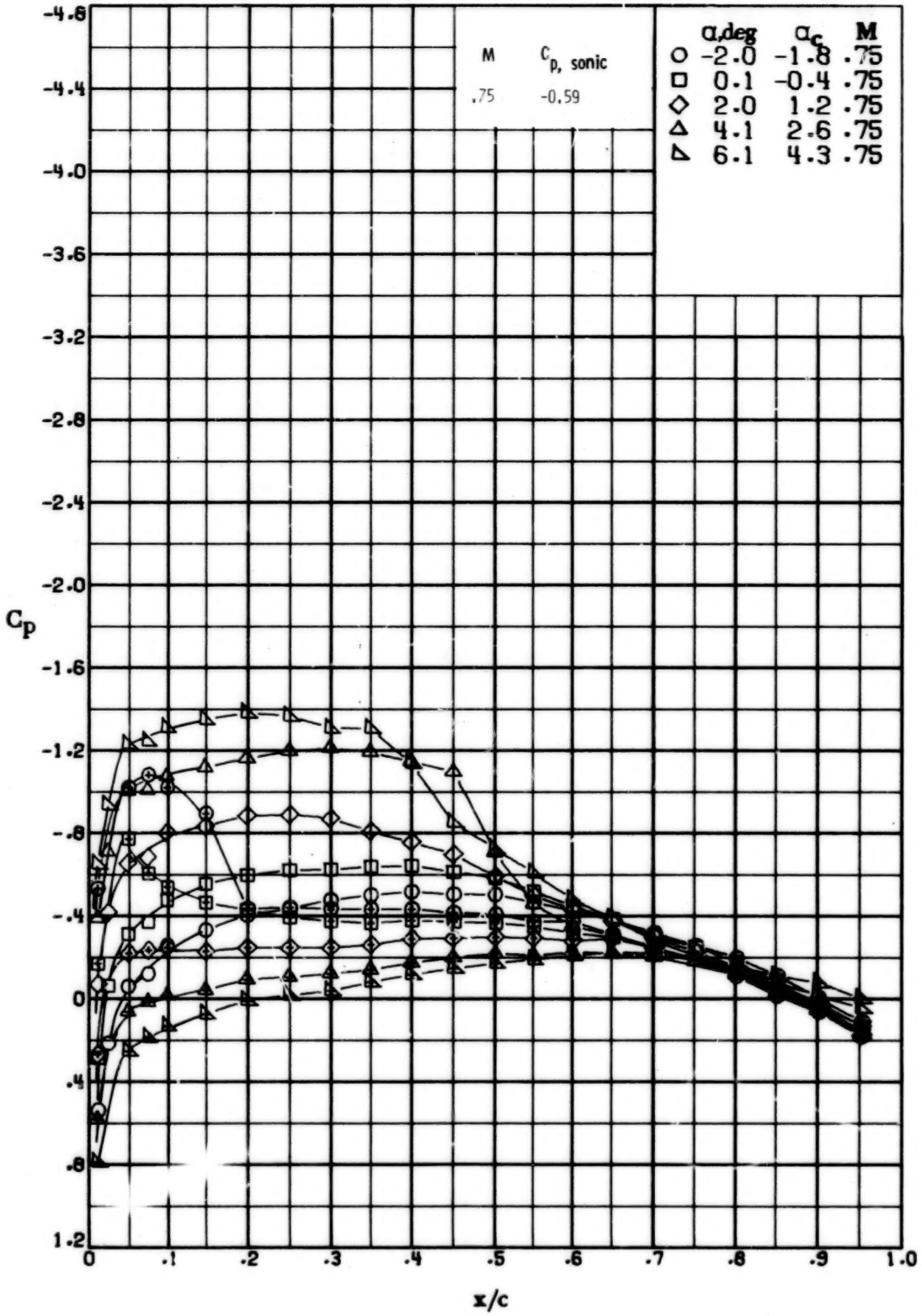

(h) $M \approx 0.75$; $R \approx 1.9 \times 10^6$.

Figure 19.- Continued.

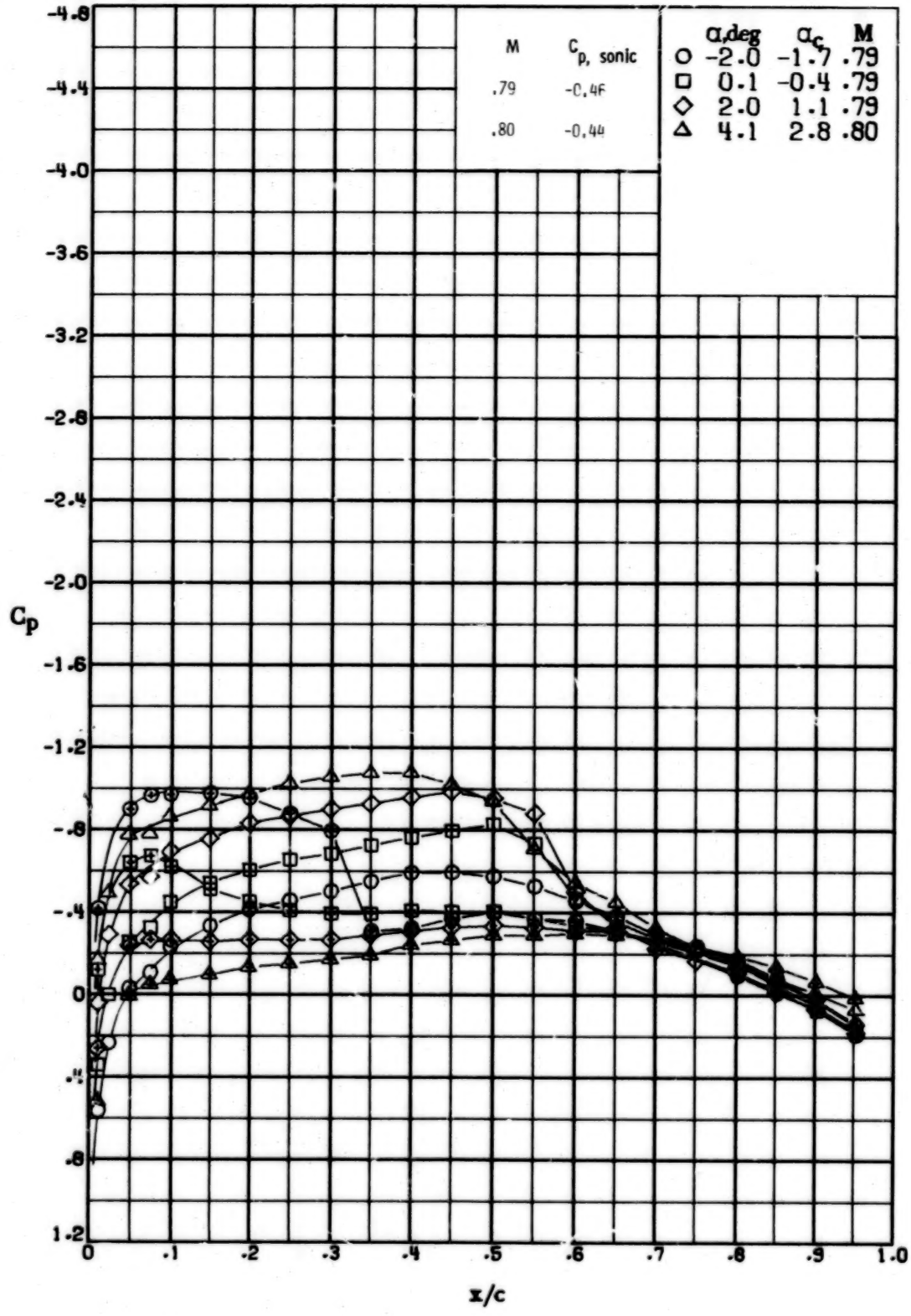

(i) $M \approx 0.79$; $R \approx 2.0 \times 10^6$.

Figure 19.- Continued.

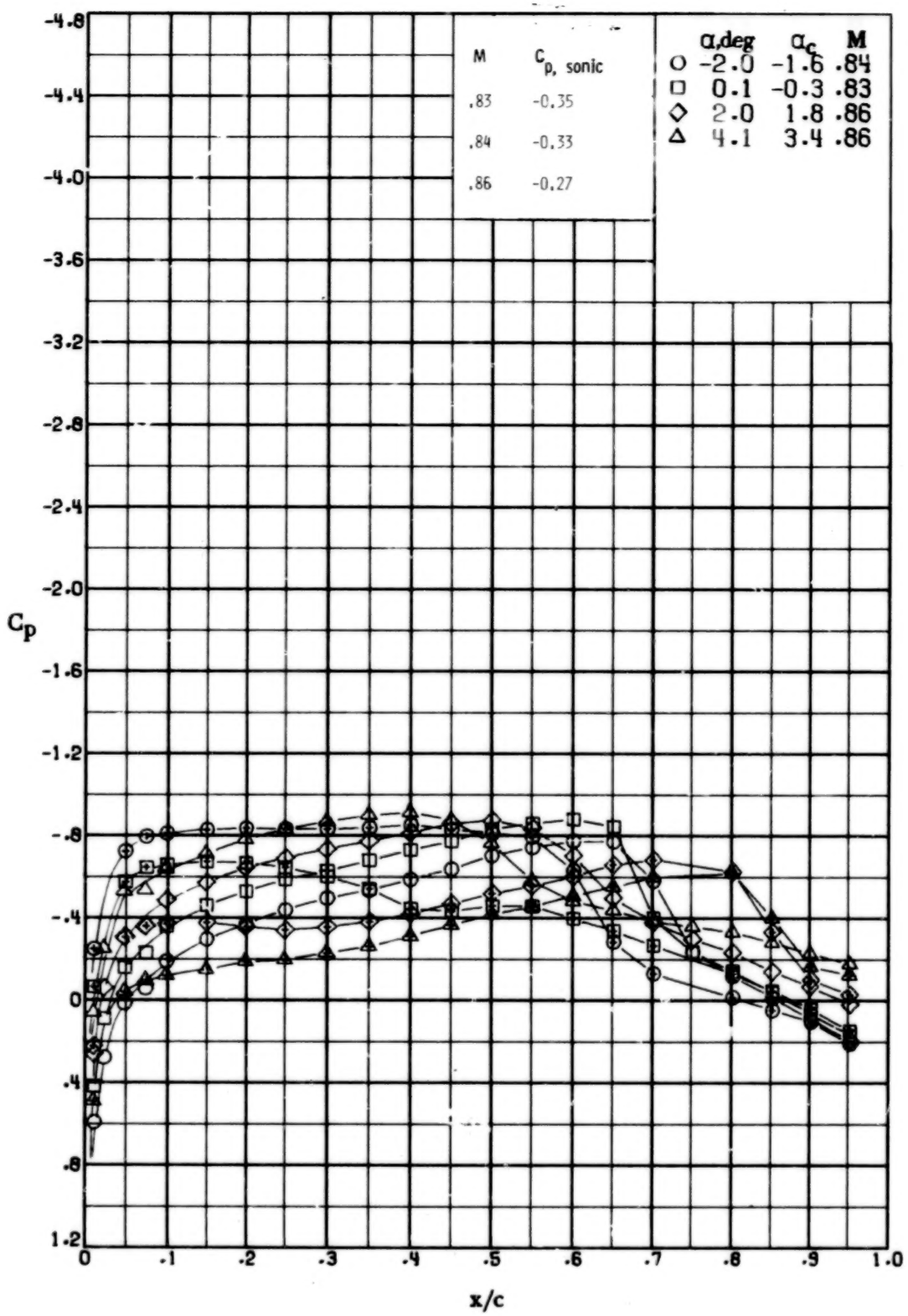

(j) M ≈ 0.85; R ≈ 2.1×10^6.

Figure 19.- Continued.

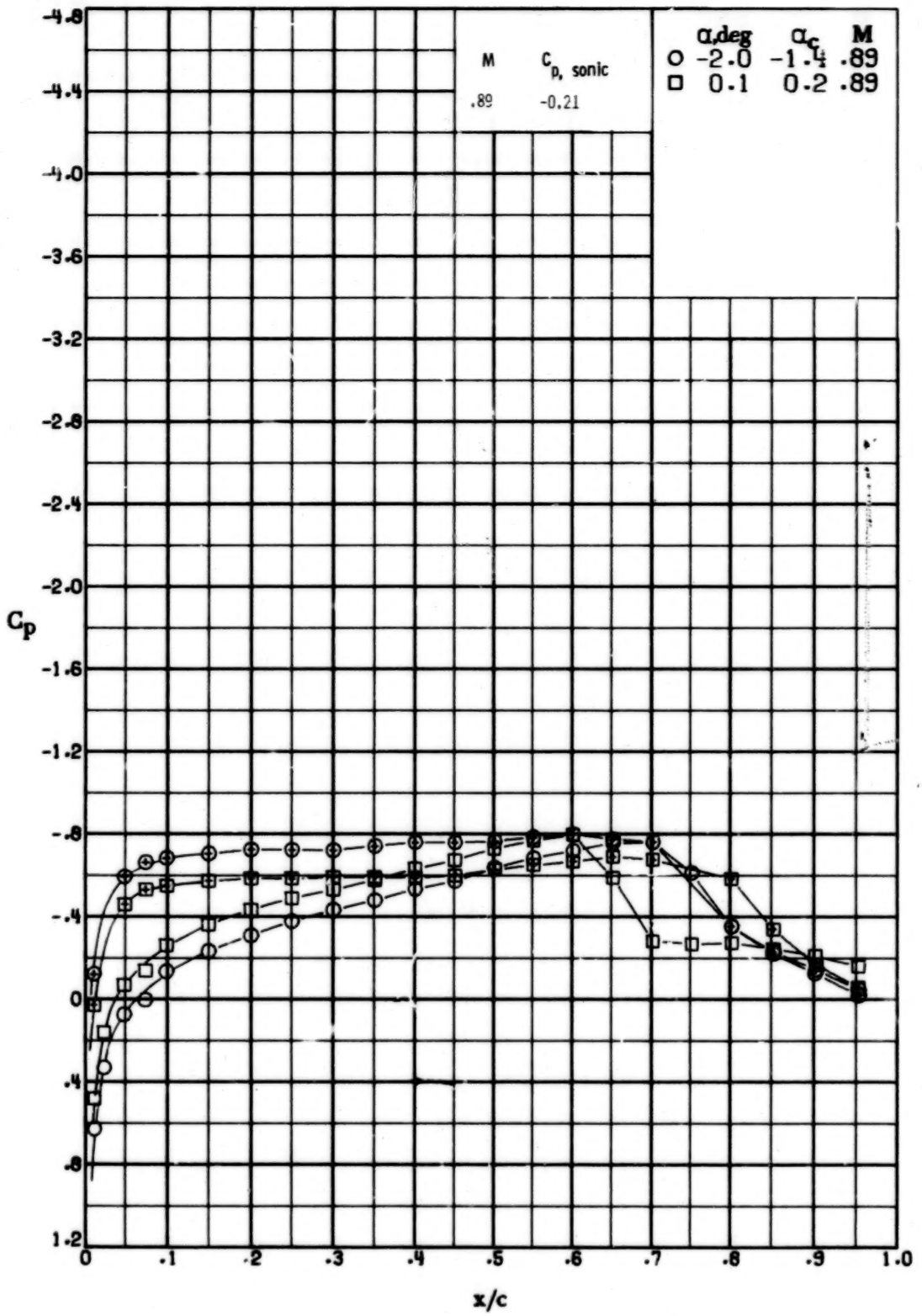

(k) $M \sim 0.89$; $R \sim 2.2 \times 10^6$.

Figure 19.- Concluded.

1. Report No.	2. Government Accession No.	3. Recipient's Catalog No.
NASA TP-1396 AVRADCOM TR-79-11		

4. Title and Subtitle	5. Report Date
EXPERIMENTAL INVESTIGATION OF THREE HELICOPTER ROTOR AIRFOILS DESIGNED ANALYTICALLY	April 1979
	6. Performing Organization Code

7. Author(s)	8. Performing Organization Report No.
Gene J. Bingham and Kevin W. Noonan	L-11703
	10. Work Unit No. 505-06-33-07

9. Performing Organization Name and Address	11. Contract or Grant No.
Structures Laboratory AVRADCOM Research and Technology Laboratories NASA Langley Research Center Hampton, VA 23665	

12. Sponsoring Agency Name and Address	13. Type of Report and Period Covered
National Aeronautics and Space Administration Washington, DC 20546 and U.S. Army Aviation Research and Development Command St. Louis, MO 63166	Technical Paper
	14. Army Project No. 1L161102AH45

15. Supplementary Notes

Gene J. Bingham and Kevin W. Noonan: Structures Laboratory, AVRADCOM Research and Technology Laboratories.

16. Abstract

Three helicopter rotor airfoils designed analytically have been investigated in a wind tunnel at Mach numbers from about 0.30 to 0.90 and Reynolds numbers from about 0.8 to 2.3 × 10^6. The airfoils had thickness-to-chord ratios of 0.08, 0.10, and 0.12 with maximum thickness at 40 percent chord. The camber distribution of each section was the same with maximum camber at 35 percent chord. The 10-percent-thick airfoil was also investigated at Reynolds numbers from 4.8 × 10^6 to 9.4 × 10^6.

The drag divergence Mach number of the 10-percent-thick airfoil is about 0.83 at a normal-force coefficient of 0 and about 0.72 at a normal-force coefficient of 0.6 at Reynolds numbers near 9 × 10^6. The maximum normal-force coefficient is slightly less than that of the NACA 0012 airfoil tested in the same facility.

The results indicate that a qualitative evaluation of the drag divergence can be made at normal-force coefficients up to the onset of boundary-layer separation by analytically predicting the onset of sonic flow at the airfoil crest. The qualitative results are conservative with respect to experimental values with the experimental drag divergence Mach number up to 0.05 higher than that indicated by analysis.

17. Key Words (Suggested by Author(s))	18. Distribution Statement
Airfoils Airfoil design Helicopter airfoils	Unclassified - Unlimited Subject Category 02

19. Security Classif. (of this report)	20. Security Classif. (of this page)	21. No. of Pages	22. Price*
Unclassified	Unclassified	92	$6.00

*For sale by the National Technical Information Service, Springfield, Virginia 22161

NASA-Langley, 1979

END

Sept. 13, 1979